Observed and simulated relationships amongst ENSO, the IPO, and rainfall variability in eastern Australia

by

Sonya Joan Wellby

Submitted in partial fulfilment of the requirements for the degree of
Bachelor of Science with Honours
in the Fenner School of Environment and Society,
Australian National University
November 2015

Australian National University

ARC CENTRE OF EXCELLENCE FOR CLIMATE SYSTEM SCIENCE

Candidate's Declaration

This thesis contains no material which has been accepted for the award of any other degree or diploma in any university. To the best of the author's knowledge, it contains no material previously published or written by another person, except where due reference is made in the text.

Sonya Joan Wellby Date:

Acknowledgements

Whilst this thesis only bares one name, it would certainly not exist without the help of others. Firstly, I would like to thank the Australian Research Council (ARC) for awarding me with the 2015 ARC Centre of Excellence for Climate System Science Honours Scholarship; without this financial support, I could not have wholly dedicated myself to this project. Secondly, I would like to thank the many staff at the Fenner School of Environment and Society who have contributed to this project in many ways, including the information technology and administrative staff; I would especially like to thank Mrs Veenita Vido for her patience, organisational prowess, and cake. I thank my teaching colleagues for respecting my commitment to this thesis—I could not have asked for better support; in particular, I thank Mr Nicholas Engerer. I would like to thank the academics within the Fenner School who have taken an interest in my work and have given me time to discuss various aspects of the project, including Professor Michael Hutchinson and both of my mid-term reviewers. To my fellow students: thank you for your support and friendship.

I thank the CSIRO and Bureau of Meteorology for making the AWAP dataset—one of the key datasets at the heart of this project—publicly available. Likewise, I thank the Earth System Federation Grid for hosting the ACCESS dataset, and the UK Met Office Hadley Centre for making the HadISST dataset available. I also thank the academics from different Australian institutions whom I have met throughout the year, who have taken an interest in my work, shared their own projects with me, and have helped me to acquire the skills I have needed to complete this project. In particular, I thank Dr Benjamin Henley for making the code available that was used to compute the IPO Tripole Index.

I must also thank the dogs at the RSPCA, whom I have walked each weekend and who have kept me silly and human. And of course, I thank you, Bailey, for your unconditional love and boundless delight in life. To Sam Duke, my ever-patient and code-literate partner: you have kept me sane—not a mean feat. Without you, this thesis would most likely be a stapled compilation of variously-sized scraps of paper, covered in exquisite but rather senseless doodles. Thank goodness you were there to ensure this never happened!

Finally, but a long, long way from least, I would like to thank my supervisors, Professor Janette Lindesay and Associate-Professor Frank Mills, for their tireless support throughout the year. Quite simply, without your encouragement and genius, this thesis would not exist.

Abstract

Understanding changes in past and future rainfall variability can improve societal, environmental and economic decision-making. Global climate models (GCMs) are commonly used to improve the understanding of rainfall variability; however, accurately simulating the variability of precipitation is difficult as many processes with different spatial and temporal scales influence precipitation. Interactions between climate drivers, which influence precipitation over wide temporal and spatial scales, often have the greatest impact on rainfall variability. Currently, the ability of GCMs to simulate interactions between climate drivers and their influence on rainfall is not well known. This thesis uses correlation and composite analysis to investigate how the joint interaction between two climate drivers, the El Niño Southern Oscillation (ENSO) and the Interdecadal Pacific Oscillation (IPO), influences eastern Australian rainfall variability, and whether or not this relationship is simulated by a GCM optimised to simulate the Australian climate. To do this, the Australian Water Availability Project (AWAP, run 26j) gridded observational dataset is compared with the Australian Community Climate and Earth-System Simulator (ACCESS1.3) GCM for the years 1900–2005.

The ENSO–rainfall teleconnection is stronger and geographically broader than the IPO–rainfall teleconnection, and ENSO tends to influence lower-latitude rainfall whilst the IPO tends to influence higher-latitude rainfall. The ENSO–rainfall relationship is strongest in austral spring and weakest in austral autumn. The IPO exhibits a strong negative correlation with rainfall in austral summer, but influences rainfall the most in austral autumn, when the ENSO signal weakens. ACCESS1.3 simulates the ENSO teleconnection with rainfall with reasonable accuracy, although its simulation of the seasonality and variability in regional rainfall requires improvement. The model appears to represent the IPO as an ENSO-like phenomenon, and does not simulate the spatial or temporal features that characterise the IPO.

The ENSO–IPO interaction exhibits its strongest influence on eastern Australian rainfall in austral summer and autumn. The influence of the joint ENSO–IPO interaction on rainfall reflects the interplay between the inter-annual and inter-decadal scales of the climate drivers. Stratification of rainfall into the nine combinations of the positive, neutral and negative states of the ENSO and IPO reveals that ENSO has a strong influence on rainfall variability, but that the IPO modifies the relationship between ENSO and rainfall. The IPO negative phase enhances the ENSO–rainfall relationship; the IPO positive phase attenuates this relationship; and the IPO neutral phase results in a slight decrease in rainfall. In the case of moderately extreme ENSO and IPO events, these relationships change somewhat. Rainfall variability is influenced by ENSO, but is modified by the IPO neutral and positive phases, and in the case of the most extreme ENSO and IPO events, only the IPO appears to influence rainfall variability. ACCESS1.3 does not simulate these relationships. If the accuracy of modelled precipitation is to increase, the physical processes through which climate drivers interact should be incorporated into GCMs.

Table of Contents

List of Figures

List of Tables

List of Equations

List of Acronyms and Abbreviations

ACCESS	Australian Community Climate and Earth-System Simulator
ACCESS R1 **ACCESS R2** **ACCESS R3**	The first, second, and third ensemble members in the ACCESS1.3 historical experiment (r1i1p1, r2i1p1, r3i1p1)
AMIP	Atmospheric Model Intercomparison Project
AWAP	Australian Water Availability Project
BoM	Australian Bureau of Meteorology
CDC	Centers for Disease Control and Prevention
CMIP3, CMIP5	Coupled Model Intercomparison Project (phase three/phase five)
CSIRO	Commonwealth Science and Industrial Research Organisation
DJF	December–January–February (austral summer)
ENSO	El Niño Southern Oscillation
ERSST v4	The Extended Reconstructed Sea Surface Temperature dataset (version four)
ESGF	Earth System Grid Federation
GCM	Global climate model
HadISST	Hadley Centre Global Sea Ice and Sea Surface Temperature dataset
IOD	Indian Ocean Dipole
IPCC AR5	The Fifth Assessment Report of the Intergovernmental Panel on Climate Change
IPO	Interdecadal Pacific Oscillation
JJA	June–July–August (austral winter)
MAM	March–April–May (austral autumn)
MJO	Madden-Julian Oscillation
NCAR	National Center for Atmospheric Research
Niño 3.4	The index used to measure ENSO
OISST v2	The Optimally Interpolated Sea Surface Temperature dataset (version two)
PDO	Pacific Decadal Oscillation
SAM	Southern Annual Mode
SOI	Southern Oscillation Index
SON	September–October–November (austral spring)
SST	Sea surface temperatures
SPCZ	South Pacific convergence zone
STR	Subtropical ridge (or the ‘subtropical high’)
TPI	The IPO Tripole Index (the index used to measure the IPO)

Glossary and Terms

Aleutian Low	A semi-permanent region of low pressure present in boreal winter in the north Pacific Ocean, near the Aleutian Islands.
Artificial neural networks	Artificial neural networks (ANN) describe computational models that operate similarly to biological neural networks (e.g. the human brain). ANNs are often used to compute functions that rely on a large number of (sometimes unknown) inputs. Inputs are multiplied by weights, and the resulting value will either activate or not activate an artificial 'neuron' (i.e. an algorithm). ANNs are used in machine learning.
Atmospheric Model Intercomparison Project	This is an international project that aims to determine systematic errors in atmospheric climate models (i.e. climate models that simulate the atmosphere only).
Climate	Climate describes the long-term characteristics of weather variables (e.g. precipitation, temperature) in a given location or region. The World Meteorological Organisation requires a minimum of 30 years to be studied in a climate analysis.
Climate driver	Climate drivers are similar to climate oscillations, although they may exhibit an irregular or limited periodicity.
Climate oscillation	Climate oscillations are reoccurring regional or global climatic phenomena, which typically have two or more states (e.g. positive, negative). The scale of their periodicity ranges from inter-annual to multi-millennial.
Coupled Model Intercomparison Project	This is an international project that aims to determine systematic errors in coupled climate models (i.e. climate models that simulate multiple and interacting components of the earth system that contribute to climate, such as the atmosphere, oceans, and land).
Downscaling	Downscaling involves interpolating data into a finer-scaled dataset (i.e. a dataset with more points). The quality of the finer-resolution dataset depends on the quality of the original dataset.
Ensemble	A group of observational or modelled datasets that are similar (e.g. all simulate global mean rainfall), but that are run independently. Results may or may not be synthesised to produce an 'envelope' showing the range of results in the datasets. In the case of model ensembles, each of the members begins the simulation with slightly different (but realistic) conditions.
Global climate model	Global climate models (GCMs) are numerical models that simulate physical processes in the earth system (e.g. atmosphere, oceans). GCMs depict the earth as a grid with both horizontal and vertical components.
Indian Ocean Dipole	The Indian Ocean Dipole is an inter-annual climate oscillation that involves the east Indian Ocean becoming anomalously warm and the west Indian Ocean becoming anomalously cool, and vice versa. It is a coupled ocean–atmosphere phenomenon.

Interpolation	Interpolation is the process of creating new data points from an original dataset. Interpolation enables estimation of a value at a point where data is not available. 'Downscaling' describes the process of producing a finer-resolution dataset than the original, and 'upscaling' describes the process of producing a coarser-resolution dataset than the original.
Madden–Julian Oscillation	The Madden–Julian oscillation is an inter-seasonal cycle originating from interactions between the ocean and tropical atmosphere. Unlike other oscillations, it is not stationary; rather, it travels eastwards. It is associated with a wet and dry phase, which affects rainfall in the Indian and Pacific Ocean, and may affect monsoon rainfall.
Meridional	Meridional is the north–south direction (i.e. longitude). See 'zonal'.
Milankovitch cycles	The Milankovitch cycles describe oscillations of the Earth's orbit. These oscillations are multi-millennial and influence the total amount of energy in the earth system (i.e. incoming solar radiation).
Parameterisation	This is the process of representing small-scale or complex climatological processes in GCMs as simplified numerical functions. Large scale processes are usually not parameterised as they are resolved within the models.
Phase (of an oscillation)	The period of time throughout which a climate oscillation experiences a particular state (e.g. positive, negative). See 'state (of an oscillation)'.
Precipitation/rainfall	Precipitation (and in this thesis, rainfall) includes rain, drizzle, hail, snow, sleet, and graupel (soft hail).
Reanalysis	Reanalysis datasets are observational, gridded global datasets that incorporate information from multiple observational sources (e.g. weather stations, buoys, satellites). Observational data are incorporated into the model every six to twelve hours. Numerical modelling uses the observational data to 'fill in' areas where no observations are available.
Rossby waves	Rossby waves (or planetary waves) are large-scale, horizontal atmospheric waves that are initiated when the temperature gradient in a rotating fluid (e.g. the atmosphere) breaches a critical threshold. These waves are responsible for creating atmospheric stability or instability, and therefore fuel or supress synoptic processes.
Southern Oscillation Index	The Southern Oscillation Index (SOI) is a commonly used index of ENSO. It is derived from the difference in surface pressure between Darwin and Tahiti.
South Pacific convergence zone	The South Pacific convergence zone is a region of converging low pressure that extends from Indonesia to the Cook Islands. It is associated with cloudiness and precipitation. It is an extra-tropical component of the Intertropical Convergence Zone (ITCZ), a region of low pressure and precipitation ringing the equator.

State (of an oscillation)	A climate oscillation may have several states (e.g. positive, negative). A given state is characterised by particular conditions (e.g. anomalously warm SSTs, a particular physical process) that typically reverse, are subdued, or are amplified in a different state. See 'phase (of an oscillation)'.
Subtropical ridge	The subtropical ridge (or 'subtropical high') is a mid-latitude belt of high pressure encircling the globe, found in both hemispheres (associated with the descending arm of the Hadley cell). It is associated with dry conditions, and moves meridionally with the seasons.
Synoptic-scale	The scale at which synoptic systems (e.g. high pressures systems, cold fronts) operate. Temporally: days to weeks; spatially (horizontally): hundreds to thousands of kilometres.
Teleconnection	A 'teleconnection' refers to a particular characteristic of an oceanic or atmospheric circulation (e.g. anomalously warm equatorial Pacific Ocean SSTs) that encourages further changes either within the same circulation, or in a related circulation. Teleconnections produce changes in weather patterns that may be geographically removed from the location of the original characteristic (e.g. anomalously warm SSTs in the eastern equatorial Pacific Ocean may be associated with reduced rainfall in eastern Australia).
Thermocline (oceanic)	A layer in a body of water (e.g. oceans, lakes) below which the temperature changes more rapidly with depth. This layer 'separates' surface water and non-surface water. Surface water is affected most strongly by day-to-day changes in the rest of the earth system.
Unforced variability	Unforced variability is produced by interactions amongst processes within the climate system (e.g. synoptic features). Forced variability is produced by external processes that act on the system (e.g. such as volcanic eruptions or anthropogenic activities).
Zonal	Describes the east–west direction (i.e. latitude). See 'meridional'.

Chapter 1: Introduction

Australia is the driest inhabited continent on earth, receiving an average of only 461 millimetres of rainfall per year (Davidson 1969; Hennessy *et al.* 1999; Smith 2004). Climates characterised by low annual precipitation averages, such as Australia, tend to experience high rainfall variability (Conrad 1941; Nicholls 1988; Nicholls *et al.* 1997). Australia experiences an even higher degree of rainfall variability, due to the influence of climate drivers such as the El Niño Southern Oscillation (ENSO) (Nicholls *et al.* 1997). Consequently, rainfall variability impacts Australia greatly. Many aspects of society (such as resource management, agriculture, and the emergency services) require a sound understanding of rainfall variability and how it may change in order to conduct current and future activities. This is especially relevant as one of the largest impacts that climate change is expected to have on society is through changes in precipitation patterns and variability (Trenberth *et al.* 2003; IPCC 2014). Commonly, trends and future changes in rainfall variability are simulated and analysed using global climate models (GCMs). However, simulating precipitation and, in particular, aspects of precipitation aside from total average rainfall (such as rainfall frequency or intensity), is particularly difficult (e.g. Sun *et al.* 2006; Perkins *et al.* 2007; Suppiah *et al.* 2007; Alexander and Arblaster 2009; Brown *et al.* 2010). This is because rainfall is influenced by multiple processes with varying temporal and spatial scales. Improving the understanding of interactions between rainfall drivers and their simulation by GCMs has the potential to increase the understanding of possible changes in rainfall variability in the future, which could enhance adaptation policy and management responses.

In order to assess how accurately climate models simulate rainfall variability, one must firstly ascertain how well the processes that drive rainfall variability are simulated. This requires a sound knowledge of the physical processes that drive observed rainfall variability. Rainfall is the result of interactions amongst various atmospheric phenomena with different temporal and spatial scales. Inter-phenomenon interactions and, in particular, interactions between climate drivers have the greatest impact on rainfall variability, due to their broad spatial and temporal influence. Inter-driver interactions not only influence decadal and inter-annual climate variability, but also intra-annual and daily weather-related variability (e.g. Risbey *et al.* 2009a). Consequently, climate drivers are the focus of this thesis.

Australian precipitation is influenced by several long-term (monthly to multi-decadal) regional- and global-scale climate drivers, including ENSO, the Interdecadal Pacific Oscillation (IPO), Indian Ocean Dipole (IOD), Southern Annual Mode (SAM), Madden-Julian Oscillation (MJO), atmospheric blocking, and the subtropical ridge (STR). Figure 1.1 depicts the regions of influence of these drivers. Each operates on a different timescale, has its greatest impact in a different area of the continent, and exerts maximum influence at a particular time of year, as summarised in Table 1.1. In most regions of Australia, each individual climate driver typically accounts for less than 20 per cent of monthly rainfall variability (Risbey *et al.* 2009a),

which, given the complexity of the climate system, is a reasonably strong signal. However, this number highlights that rainfall is typically influenced by more than one phenomenon (Kiem and Verdon-Kidd 2009).

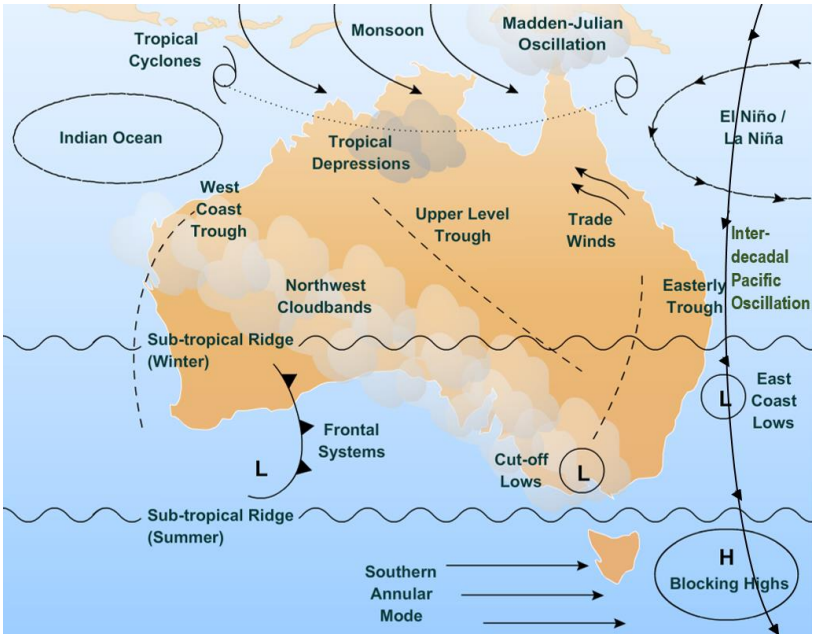

Figure 1.1: The main climate drivers and synoptic features that influence rainfall in Australia. The climate drivers depicted here are the MJO, ENSO ('El Niño/La Niña'), the IPO, the IOD ('Indian Ocean'), the STR, atmospheric blocking ('blocking highs') and the SAM. All other features are synoptic-scale. The image has been modified from the Bureau of Meteorology (Australian Bureau of Meteorology 2010).

Final rainfall amount is largely determined by whether or not one climate driver reinforces, limits, or counter-balances the precipitation tendencies of another climate driver (e.g. Murphy and Timbal 2008; Risbey *et al.* 2009a). This effect is particularly strong in some regions; for example, in south-eastern Australia and South Australia, rainfall variability is influenced more strongly by the interactions amongst climate drivers than by any one single climate driver (Kiem and Verdon-Kidd 2009; Risbey *et al.* 2009a; Mekanik and Imteaz 2012; Tozer 2014). Rainfall that is responding to interactions between climate drivers may occur after the interactions have taken place; for example, during austral autumn and winter, the MJO enhances the development of ENSO, but the rainfall influenced by this interaction occurs in the following spring and summer (Chakraborty and Krishnamurti 2003; Hendon, Wheeler, *et al.* 2007). It would be expected that the climate models which simulate rainfall variability most accurately will account for interactions amongst the phenomena that contribute to rainfall. However, very few studies have yet examined how accurately climate models represent rainfall variability influenced by interacting phenomena, and such analysis has been limited in its depth (e.g. Arblaster *et al.* 2002; Parker *et al.* 2007; Risbey *et al.* 2011; Dai 2013).

The research in this thesis aims to understand the observed relationship between two oscillating climate drivers—ENSO and the IPO—and their influence on eastern Australian rainfall variability, and to determine the degree to which these relationships are presented in a

GCM. The datasets analysed are the Australian Water Availability Project (AWAP) observational dataset, and the model output data from the latest version of the Australian Community Climate and Earth-System Simulator model (ACCESS1.3) (a Coupled Model Intercomparison Project phase 5 (CMIP5) model that contributed to the Fifth Assessment Report of the Intergovernmental Panel on Climate Change (IPCC AR5)). The period of study is 1900–2005, as the accuracy of simulations of past rainfall variability must be determined before the accuracy of future rainfall variability simulations can be assessed. This addresses the need identified by Lewis and Karoly (2014:100) to determine how well the ACCESS1.3 model represents the 'actual climate'. The study focuses on eastern Australia as: (a) ENSO influences rainfall in this region most strongly, and it is where the ENSO–IPO interaction is most apparent; (b) the majority of the Australian population resides in eastern Australia, and so the demand for water resources in this area is large; and (c) industry that is sensitive to rainfall variability (such as agriculture, including the agriculturally significant Murray–Darling Basin) is concentrated in this region (Murphy and Timbal 2008; Murray–Darling Basin Authority 2010).

Is observed rainfall variability attributed to the ENSO–IPO interaction well-represented in simulations? In answering this central question, several sub-issues will be explored:

- What relationships do ENSO and the IPO individually exhibit with rainfall?
    - Does the observed and modelled seasonality and spatial distribution of ENSO align with past studies?
    - What is the seasonality of the IPO–rainfall relationship? What is the extent of its influence in Australia?

- How do ENSO and the IPO jointly affect rainfall variability?
    - Does the observed nature of the ENSO–IPO interaction align with past studies?
    - How does the relationship between ENSO, the IPO, and rainfall variability differ seasonally and spatially?
    - How do interactions between different states of the ENSO and IPO affect rainfall? How does this relationship change with the increasing strength of the ENSO and IPO?
- How well does ACCESS1.3 capture the above relationships?

The thesis unfolds as follows. Chapter 2 examines the factors that influence rainfall variability in eastern Australia, including the ENSO and the IPO; it also discusses GCM simulation of rainfall variability. Chapter 3 introduces the chosen observational and model datasets, and outlines the correlation and composite analysis techniques used in the analysis. Chapter 4 presents the observed relationship between the ENSO, IPO and rainfall variability, whilst Chapter 5 examines how well ACCESS1.3 models this relationship. Chapter 6 synthesises the research findings, discusses their implications, and proposes future research pathways.

Climate driver	*Description*	*Region of influence*	*Impact*	*Period of greatest variability; periodicity (if relevant)*	*Interacts with these global-scale drivers*	*Influence on small-scale rainfall drivers*	*Austral season with most impacted rainfall variability*
ENSO	Anomalous changes exhibited in SSTs, surface pressure, and wind fields. Positive (negative) phase: eastern equatorial SSTs anomalously cool (warm).	Continental; especially eastern and northern Australia[1]	*Positive phase* (La Niña): rainfall increases over eastern Australia. *Negative phase* (El Niño): rainfall decreases over eastern Australia.	Inter-annual; 2–10 years[2]	IPO,[3] IOD,[4] SPCZ,[5] SAM,[6] MJO[7] (interactions are detailed below).	**Tropical cyclones:** increased cyclogenesis in Western Australia in La Niña;[8,9] **cut-off lows**.[10]	Winter, spring
IPO	Anomalous changes exhibited in SSTs in four main regions the Pacific Ocean.[11] Positive (negative) phase: SSTs in the east equatorial Pacific are anomalously warm (cool).	Global (Pacific Ocean, Indian Ocean, and surrounds),[12] including eastern Australia[13-16]	*Positive phase*: rainfall decreases over eastern Australia. *Negative phase*: rainfall increases over eastern Australia.	Inter-decadal; 40–60 years (previous research)[17]	**ENSO**.[3] Interacts to modulate summer rainfall (southeast Queensland). **SPCZ**.[15] Negative phase: SPCZ broadens meridionally and shifts westward, leading to increased southeast Queensland rainfall.	Meridional shift in **storm-tracks** in the north Pacific Ocean.	Summer, autumn (this study)
IOD	Anomalous changes exhibited in SSTs in the east and west equatorial Indian Ocean. Positive (negative) phase: SSTs in the east are anomalously cool (warm).[19,20]	Western and southern Australia	*Positive phase*: anticyclonic conditions prevail over Australia and rainfall decreases. East-coast rainfall is unaffected.[20]	Inter-annual; 18 months to 3 year cycles[21]	**ENSO**. The IOD and ENSO are largely independent; they interact in summer. [22] In southeast Australia, El Niño (La Niña) and the positive (negative) IOD reduce (increase) rainfall.[23]	The ENSO–IOD interaction influences **cut-off lows**.[24] The negative phase is associated with increased **northwest cloud bands**.[25]	Winter
SAM	Positive (negative) phase: the mid-latitude westerlies contract (expand) pole-ward (equator-ward). Observed in pressure and temperature fields.[6,22, 26]	South-west and south-eastern Australia; coastal and mountainous areas.[24]	Positive (negative) phase: decrease (increase) in frontal systems passing over southern Australia, leading to a decrease (increase) in rainfall.	Inter-annual	**ENSO**.[6] The positive phase occurs during El Niño and the negative phase occurs during La Niña. The **polar front jet** (which influences extra-tropical cyclones and cold fronts) moves south (north) during the positive (negative) phase.[6, 27] **MJO.** SAM lags a week behind changes in the MJO pressure field.[28]	Influences **stream synoptic conditions** in mountainous areas.[29] *Positive phase*: enhanced southeast Australian rainfall via intensified **blocking** and **cut-off** systems.[24]	Winter,[2] summer[22]

STR	The STR belt of high pressure moves pole-ward in late winter and spring.	Southern and eastern Australia	Meridional movement of the STR pole-ward increases precipitation, as anticyclonic conditions make way for rain-bringing mid-latitude storms.	Annual[30]	**ENSO**. La Niña is associated with a weakening of the STR. **SAM, IOD.** Changes in SAM lead to changes in the STR.[31, 32]	Dominance of the STR 'blocks' rain-bringing low pressure systems in southern Australia, reducing rainfall.	Winter
MJO	An equatorial, eastward-propagating planetary wave. Expressed in anomalous sea level pressure values in the equatorial Indian and east Pacific Oceans.[33, 34]	Northern Australia	Influences when the 'active' (wet) and 'break' (less wet) phases of the of Australian and Indian monsoons occur.[35, 36]	Inter-seasonal; 30–60 days	**ENSO**.[7, 37] El Niño (La Niña): decreased (increased) rainfall in monsoon 'break'. Enhanced MJO activity typically precedes ENSO by several months. Induces **blocking** features in south-eastern Australia that decrease extra-tropical rainfall.	In winter, the **easterly trade winds** moderate MJO strength.[39]	Summer
Atmo-spheric blocking	Anti-cyclones in the Southern Ocean and Tasman Sea influence the mid-latitude storm track.	Southern Australia	*In Southern Ocean*: storms steered south of Australia, decreasing rainfall. Cut-off lows may form over inland Australia, increasing rainfall. *In Tasman Sea*: increased coastal rainfall.[3]	Inter-annual and inter-decadal[40]	When the **jet-stream** is favourably orientated, blocking strengthens.[24] Possibly links the extra-tropics and tropics through interaction with the **MJO**.[7]	*In Southern Ocean*: Affects **cut-off lows** and **mid-latitude cyclones.** *In Tasman Sea*: Affects **onshore easterlies**.[3]	Non-summer;[24] mainly winter–spring[3, 41]

Table 1.1: This table provides key information relating to the main global-scale climate drivers that impact the Australian region. The drivers are not presented in any particular order. [1] (McBride and Nicholls 1983), [2] (Sturman and Tapper 2009), [3] (Klingaman *et al.* 2013), [4] (Cai *et al.* 2012), [5] (Folland 2002), [6] (Meneghini *et al.* 2007), [7] (Hendon, Wheeler, *et al.* 2007), [8] (Kuleshov *et al.* 2009), [9] (Hastings 1990), [10] (Pook *et al.* 2006), [11] (Henley *et al.* 2015), [12] (Vance *et al.* 2015), [13] (Power *et al.* 1999a), [14] (Kiem and Franks 2004), [15] (Cai and van Rensch 2012), [16] (King *et al.* 2013a), [17] (Dong and Dai 2015), [18] (Trenberth and Hurrell 1994), [19] (Saji and Vinayachandran 1999), [20] (Ashok *et al.* 2003), [21] (Nakamura *et al.* 2009), [22] (Hendon *et al.* 2007), [23] (Meyers *et al.* 2007), [24] (Risbey *et al.* 2009b), [25] (Nicholls 1989), [26] (Hall and Visbeck 2002), [27] (Limpasuvan and Hartmann 2000), [28] (Matthews and Meredith 2004), [29] (Risbey *et al.* 2011), [30] (Murphy and Timbal 2008), [31] (Williams and Stone 2009), [32] (Cai and Cowan 2013), [33] (Krishnamurti *et al.* 2013), [34] (Madden and Julian 1971), [35] (Madden and Julian 1994), [36] (Wheeler and Hendon 2004), [37] (Chakraborty and Krishnamurti 2003), [39] (Wheeler *et al.* 2009), [40] (Trenberth and Mo 1985), [41] (Lejenäs and Økland 1983).

Chapter 2: Literature Review

This chapter discusses the concept of rainfall variability, including changes in variability over time, and the separate and joint roles played by the ENSO and the IPO in influencing eastern Australian rainfall variability. It also presents an overview of current research in rainfall variability modelling. It is suggested that GCM simulations of rainfall variability will likely improve if they are able to capture the interactions amongst the climate drivers that influence rainfall variability.

2.1 Rainfall variability in eastern Australia

2.1.1 What is rainfall variability?

Formally, rainfall variability is a function of how much measured rainfall differs from long-term mean annual rainfall (Conrad 1941; Nicholls 1988); this is presented in Equation 2.1.

Equation 1.1: Rainfall variability, as defined by Conrad (1941), where v_a is the absolute average variability of rainfall and v_r is the relative variability of rainfall. $\bar{p}$ is long-term mean precipitation, p_i is precipitation in the time period of interest, and n is the number of time-steps examined.

$$v_a = \frac{\sum(p_i - \bar{p})}{n}$$

$$v_r = \frac{100\, v_a}{\bar{p}}$$

Average rainfall is distinct from rainfall variability, as demonstrated in Figure 2.1.a. Similarly, changes in average rainfall are distinct from changes in rainfall variability (compare Figure 2.1.b with Figure 2.1.c). For example, a climate may experience a 'step-wise' shift in average rainfall (e.g. average rainfall increases) but rainfall variability may remain the same (see Figure 2.1.b.). In this instance, changes in rainfall variability influence changes in average rainfall. Twentieth century trends in both mean and extreme Australian rainfall are highly correlated (Alexander *et al.* 2007), which suggests that rainfall extremes make a large contribution to mean rainfall (i.e. the Australian climate is more similar to the dark-blue line in Figure 2.1.c, than to the dashed grey line) (Haylock and Nicholls 2000). It is possible for changes in rainfall variability to influence changes in average rainfall. Eastern Australia experienced an increase in rainfall in between 1910–1950, and a decline in rainfall between 1950–2005 (Alexander *et al.* 2007; Gallant *et al.* 2007). Whether or not extreme (dry or wet) rainfall events are experienced is determined by the drivers of inter-annual rainfall variability (e.g. Nicholls 1988; Nicholls and Kariko 1993; Smith 2004), the causes of which are discussed next.

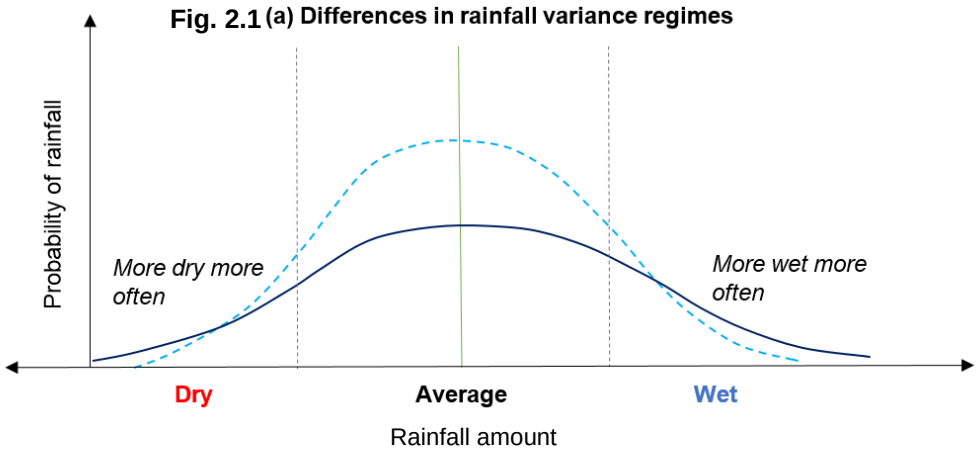

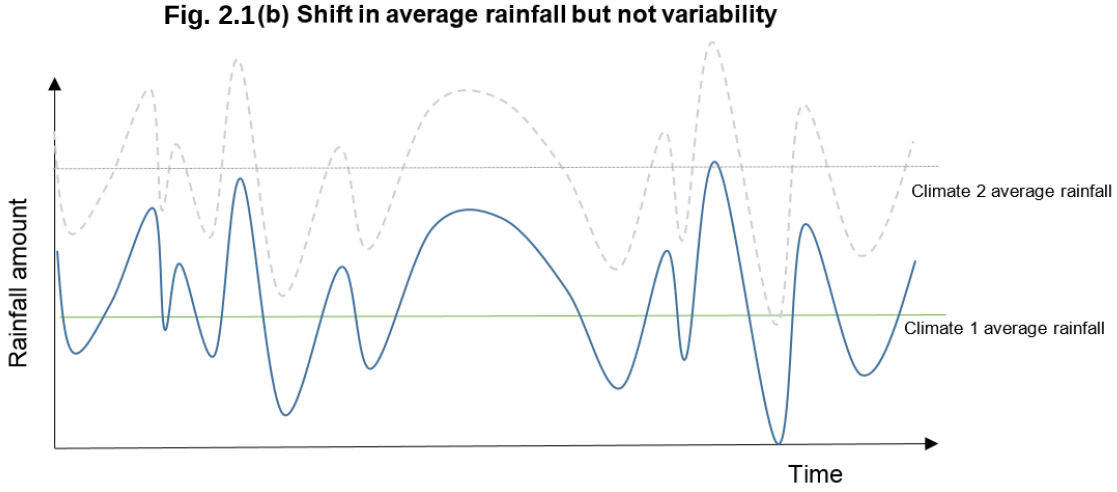

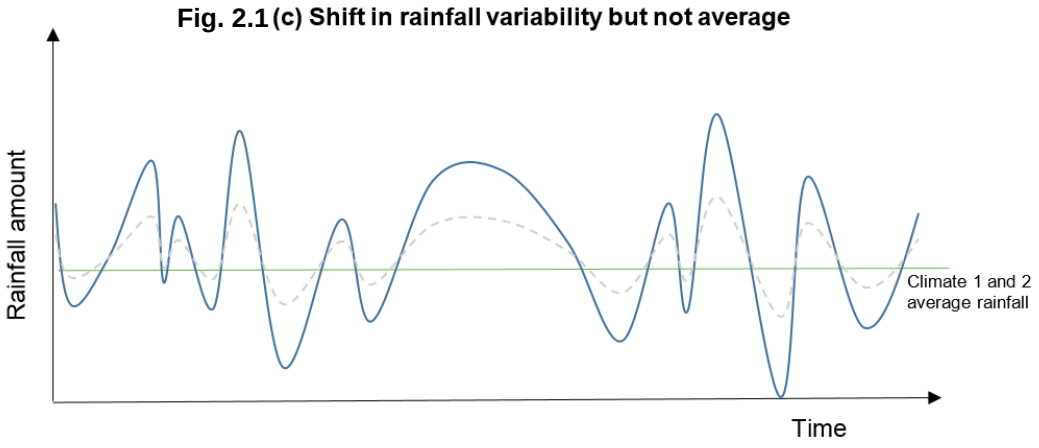

Figure 2.1: Schematic representing differences between average rainfall and rainfall variability. (*2.1.a*) Two different climates (the dashed, light-blue line and the solid, dark-blue line). Both climates receive the same mean rainfall (central green line). The area under both curves is the same (this is not depicted to scale). However, the climate of the dark-blue line is more variable, as the tails of its curve in which dry and wet events occur (to the left and right of the two dashed grey lines, respectively) cover a greater area (i.e. the probability of experiencing a dry or wet event is increased). (*2.1.b*) Two climates, both of which have the same rainfall variability but different rainfall means. (*2.1.c*) Two climates, both of which experience the same mean rainfall, but different rainfall variability.

2.1.2 The study region and climate driver selection

This study focuses on eastern Australia, for two reasons. Firstly, changes in rainfall variability have a significant societal impact in eastern Australia. For example, the majority of the Australian population resides in eastern Australia, and so the demand for water resources in this area is large; additionally, the agriculturally significant Murray–Darling Basin, which contributes to 40 per cent of Australian agriculture, is located in this region (Murray–Darling Basin Authority 2010). Secondly, eastern Australia is an ideal location to observe how interactions between climate drivers impact rainfall variability. For much of the year, ENSO is the dominant modulator of rainfall over most of Australia (Risbey *et al.* 2009a). Its influence is felt most strongly in the eastern two-thirds of the continent, and, in particular, in south-eastern Australia, where inter-annual rainfall variability is especially high (McBride and Nicholls 1983; Ropelewski and Halpert 1987; Nicholls 1989; Murphy and Timbal 2008; Risbey *et al.* 2009a). This suggests that changes in rainfall variability are likely to be related to changes in ENSO; for this reason, this thesis focuses (a) on ENSO, and (b) on the region in which its impact is strongest.

As discussed in Chapter 1, Australian rainfall is modulated by other climate drivers in addition to ENSO that would all need to be considered to derive a complete picture of rainfall variability. Since the analysis of the interactions amongst all of these drivers is an immense undertaking beyond the scope of this thesis, one climate driver known to strongly affect rainfall variability in addition to ENSO has been selected. The ENSO–IPO interaction modulates rainfall in parts of eastern Australia, although no studies have yet comprehensively documented the extent and characteristics of that influence (Power *et al.* 1999a; Kiem *et al.* 2003; Verdon *et al.* 2004; Cai *et al.* 2010; King *et al.* 2013a). The influence of the IPO is geographically broader than that of the SAM, which predominantly influences southern Australian mountainous and coastal rainfall (Risbey *et al.* 2011); the MJO, which influences northern Australia (Wheeler and Hendon 2004; Wheeler *et al.* 2009); and the IOD, which influences western and southern Australia (Ashok *et al.* 2003). Additionally, unlike inter-seasonal or inter-annual drivers, the IPO is more likely to modulate ENSO on inter-decadal timescales (Power *et al.* 1999a). Inter-decadal changes affect long-term rainfall variability trends more profoundly, and therefore have a high socio-economic impact (e.g. long-term droughts), which increases the value of studying the ENSO–IPO interaction.

2.1.3 The El Niño Southern Oscillation (ENSO)

The ENSO is a coupled ocean–atmosphere system that is influenced by changes in sea surface temperatures (SSTs) in the tropical Pacific Ocean. Anomalies in SSTs are linked to changes in atmospheric patterns; during positive ENSO states (La Niña) these changes are associated with above average rainfall in eastern Australia, and during negative ENSO states (El Niño) these changes are associated with below average rainfall in eastern Australia (see Figure 2.2). ENSO has a 2–10 year periodicity, and the individual states (positive, neutral, or negative) of the ENSO

may persist for 18–24 months (Trenberth 1997). Multiple phases of the ENSO have been observed throughout the twentieth century (e.g. Meyers *et al.* 2007).

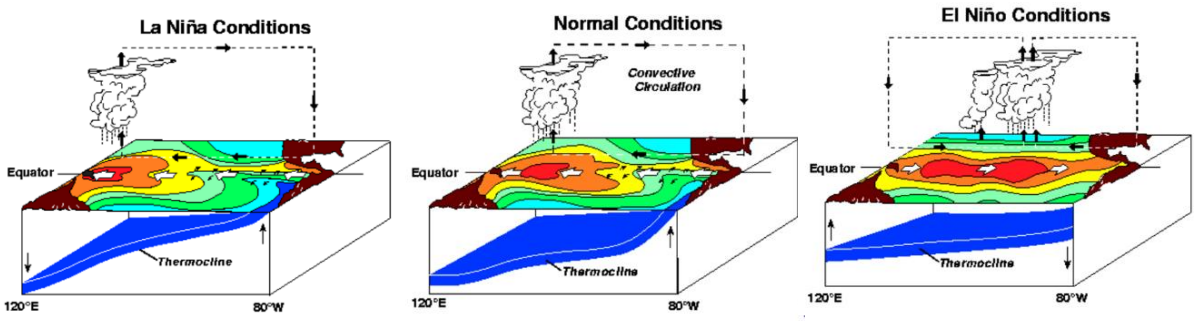

Figure 2.2: The three states of ENSO: positive (La Niña—left), neutral (middle), and negative (El Niño—right). When La Niña conditions prevail, the easterly winds increase in strength, producing a strengthened thermocline (the lower blue 'sheet'). This shifts the region of warm SSTs west, along with the centre of convection, which moves closer to Australia (the brown landmass to the bottom-left). Consequently, rainfall increases. When El Niño conditions prevail, the easterly wind weakens, and circulation in the equatorial waters becomes eastward. The thermocline weakens, and the region of warm SSTs moves towards the middle of the Pacific Ocean, along with the centre of convection. Consequently, Australia receives less rainfall. Image from TOA/NOAA/PMEL (n.d.).

Several aspects of ENSO's interaction with other climate drivers are nonlinear. For example, nonlinearities have been identified between ENSO and the IOD: different precipitation mechanisms contribute to rainfall during different states of ENSO (Cai *et al.* 2012). ENSO's relationship with Australian rainfall itself (including extreme rainfall) is nonlinear: a strong positive state is more likely to result in intense and longer-duration rainfall, whereas a strong negative state may or may not produce extremely dry conditions (Suppiah 2004; Power *et al.* 2006; Cai *et al.* 2010; King *et al.* 2013a). As ENSO and its teleconnections vary on inter-decadal timescales (e.g. Power *et al.* 2006; King *et al.* 2013a), the question arises of whether the ENSO nonlinearity is related to ENSO interactions with other climate drivers. Since the ENSO and IPO are *not* independent modes of variability (Newman *et al.* 2003; Power *et al.* 2006; Cai *et al.* 2010; King *et al.* 2013a), and it is uncertain how much of the ENSO nonlinearity can be attributed to the ENSO–IPO interaction, there is a strong incentive to investigate the joint influence of ENSO–IPO interaction on rainfall variability, rather than separately (and potentially erroneously) attributing rainfall variability to either ENSO or the IPO.

In Australia ENSO influences winter and spring rainfall most strongly; the correlation with rainfall is strongest in spring (McBride and Nicholls 1983). In some regions rainfall in a particular season responds most strongly to the previous season's ENSO values, or, sometimes, those of two seasons before. Any analysis of ENSO and rainfall needs to account for lagged correlations and the potential for correlations to differ geographically.

2.1.4 The Interdecadal Pacific Oscillation (IPO)

The Interdecadal Pacific Oscillation (IPO) is a mode of inter-decadal climate variability expressed as changes in SST anomalies in four main regions in the Pacific Ocean (Power *et al.* 1999a; Henley *et al.* 2015) (see Figure 2.3). The IPO is closely related to the Pacific Decadal Oscillation, which is a decadal mode of climate variability in the northern Pacific Ocean (Mantua *et al.* 1997). The PDO is considered to be the northern-most node of the IPO (box '1' in Figure 2.3). The mechanisms that drive the IPO remain unclear, although it appears that, in addition to SSTs, the oscillation is associated with changes in sea level pressure, upper-level oceanic heat content, and wind patterns. It is thought that changes in these parameters are influenced by processes of different timescales and origins, such as sea level pressure in the Aleutian Low, variability within ENSO, broader oceanic circulations, and Rossby waves (Schneider and Cornuelle 2005; Meehl and Hu 2006; Power and Colman 2006).

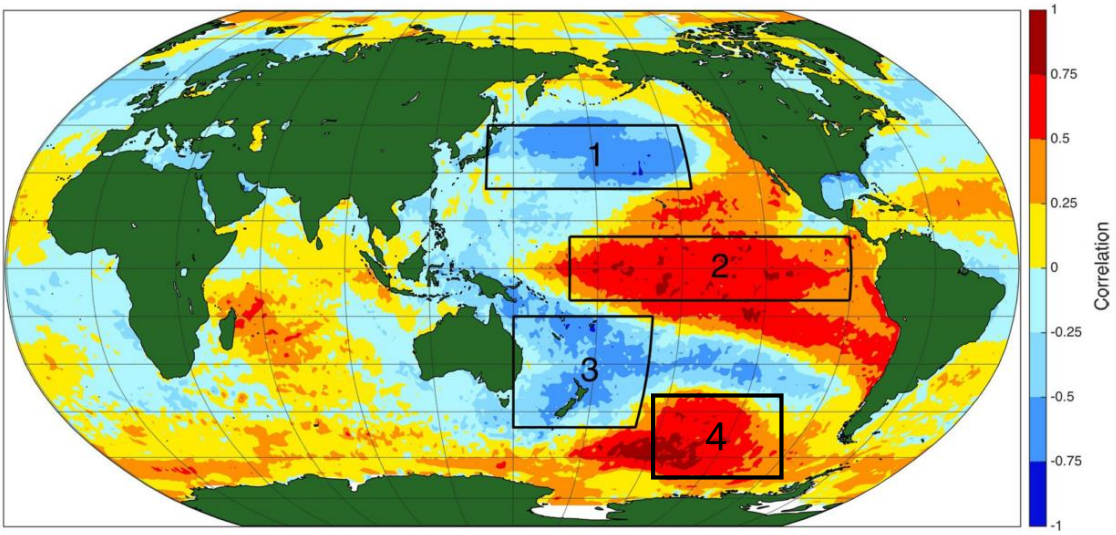

Figure 2.3: The four regions in the Pacific Ocean in which SST anomalies contribute to the IPO (as shown and numbered in the boxes). The PDO corresponds with box '1'. This figure shows the IPO positive phase; opposite correlations for the four boxed regions would be expected in the negative phase. Correlation coefficients (*r*) are presented for the relationship between SST and the IPO_{UKMO}, as defined in Henley *et al.* (2015). Image modified from Henley *et al.* (2015).

Figure 2.3 shows conditions in the positive phase of the IPO, in which the east Pacific warms and the west Pacific cools. Conditions are reversed in the negative phase of the IPO, and the east Pacific cools whilst the west Pacific warms. Although the IPO has a neutral phase (Power *et al.* 1999a), it has only rarely been included in studies of the IPO, and its characteristics remain largely undescribed—although Kiem and Franks (2004) suggest that El Niño years that correspond with IPO positive years are less dry than El Niño years in IPO neutral or negative states. Currently, the IPO is thought to have a cycle of 40–60 years, exhibiting a shift between positive and negative phases every 20–30 years. During the twentieth century three phases were observed—two

positive (1924–1941 and 1979–1997) and one negative (1947–1975) (e.g. Power *et al.* 1999a; Dong and Dai 2015; Vance *et al.* 2015). It has been proposed that the IPO resumed its negative phase in 2011 (Cai and van Rensch 2012).

During a positive (negative) phase of the IPO—when tropical SSTs are warm (cool)—rainfall typically decreases (increases) in Australia (e.g. Power *et al.* 2006). For example, Kiem and Franks (2004) found that the risk of falling below the critical threshold of 30 per cent water storage in New South Wales is almost twenty times higher during the positive state of the IPO. As an IPO phase may persist for several decades, there are many opportunities for the states of other, shorter drivers (e.g. ENSO) to occur within one phase of the IPO (as shown in Figure 2.4), either attenuating or strengthening rainfall. This is the case with the IPO and ENSO (e.g. Power *et al.* 2006).

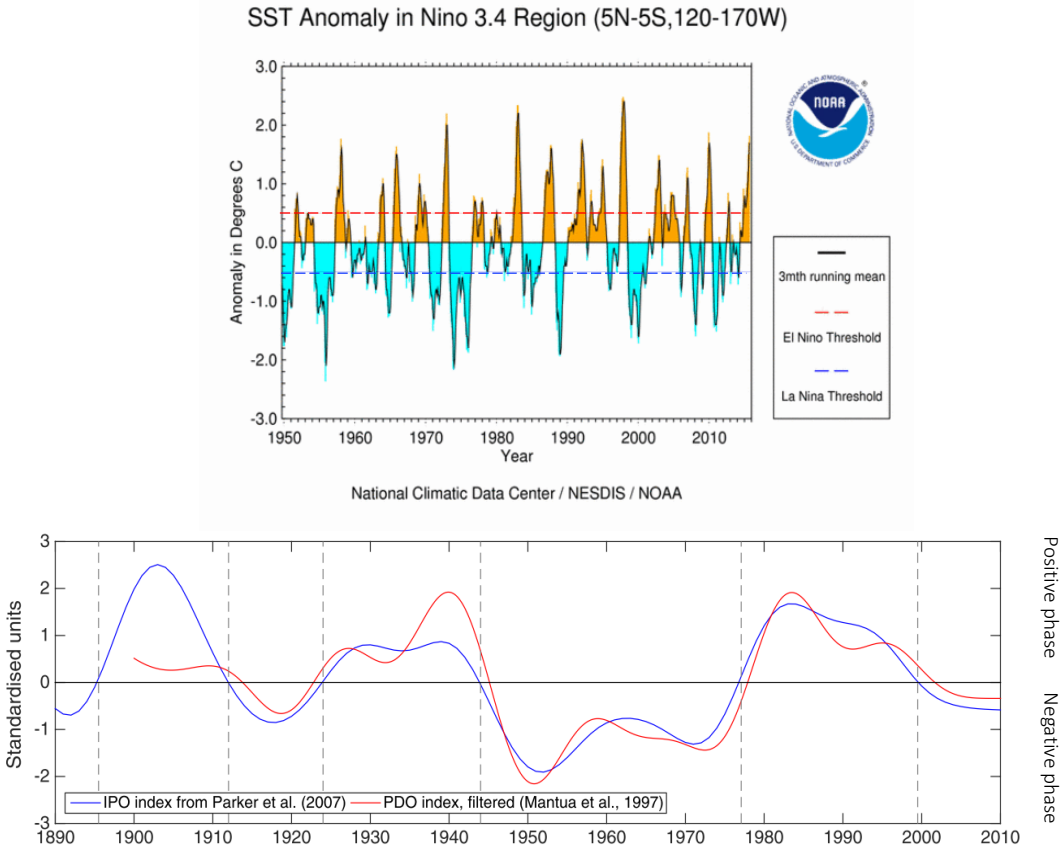

Figure 2.4: Phases of (*upper*) ENSO and (*lower*) the IPO in the twentieth century. ENSO exhibits inter-annual variability (i.e. higher frequency phase changes), whilst the IPO exhibits inter-decadal variability (i.e. lower frequency phase changes). It is clear that within one phase of the IPO, multiple phases of ENSO occur. In the ENSO image (NOAA n.d.), ENSO phases are defined according to the Niño 3.4 index (values are only available from 1950 onwards). Negative SST anomalies below the blue line show La Niña events, and positive SST anomalies above the red line show El Niño events. The IPO image (Henley *et al.* 2015) shows phases as defined by Parker *et al.* (2007) and Mantua *et al.* (1997), for the period 1890–2010. Positive values correspond with positive phases, and negative values correspond with negative phases. Note that the threshold lines for the neutral phases are not shown.

2.1.5 The joint influence of ENSO and the IPO on rainfall variability

The IPO influences rainfall volume in El Niño and La Niña events (e.g. Power *et al.* 1999a). This relationship is nonlinear: during the negative phase of the IPO, La Niña events have occurred more frequently, and have tended to result in increased mean and extreme Australian precipitation, whilst during the positive phase of the IPO, La Niña rainfall is thought to be unaffected (Kiem and Franks 2004; Verdon *et al.* 2004; Power and Colman 2006; Cai *et al.* 2010; King *et al.* 2013a). For example, a high volume of La Niña-related rainfall in south-east Queensland was recorded in 2011 during the negative, rain-producing phase of the IPO (Cai *et al.* 2010; Cai and van Rensch 2012). It is possible that the nonlinear relationship between ENSO and the IPO explains why some particularly strong El Niño events were not associated with drought (e.g. the 1997 El Niño), whilst some moderate El Niño events have been linked with drought, such as the 2002–3 El Niño (Suppiah 2004; Wang and Hendon 2007; Brown *et al.* 2009).

Not only does the IPO modulate ENSO, but ENSO also influences the IPO. Several studies have suggested that variance within ENSO (in combination with other mechanisms) contributes to the overall inter-decadal periodicity of the IPO (Newman *et al.* 2003; Schneider and Cornuelle 2005; Power and Colman 2006; Westra *et al.* 2015). These inter-dependencies suggest that the relationships between (a) ENSO and precipitation, (b) the IPO and precipitation, and (c) the joint interaction between ENSO–IPO and precipitation are likely to be linked in some way.

Additionally, the relationship between ENSO, the IPO and rainfall varies across eastern Australia. The joint influence of the IPO negative–ENSO positive state on rainfall is strongest in the north (Queensland) and weakest in the south (Victoria) (Verdon *et al.* 2004). These latitudinal changes may reflect a difference in which process (inter-annual/ENSO or inter-decadal/IPO) affects rainfall the most. Power and Colman (2006) note that, with increased latitude, variability in multi-decadal processes (e.g. the IPO) tends to impact internal atmospheric variability (e.g. Rossby waves), and thus oceanic variability (e.g. SSTs), more strongly.

2.2 Modelling rainfall variability

Mathematical models are a useful tool for analysing precipitation, as the numerous processes that contribute to precipitation have varying temporal and spatial scales. The most widely used tool is the GCM. This thesis examines how well the latest version of one GCM, ACCESS1.3, simulates rainfall variability attributed to ENSO and the IPO and their interactions in eastern Australia.

2.2.1 Difficulties associated with modelling rainfall variability

Because rainfall and rainfall variability are produced by many interacting phenomena with different temporal and spatial scales, realistically simulating rainfall variability is one of the greatest challenges for GCMs (e.g. Randall *et al.* 2007). Simulating mean annual precipitation is

simpler and generally more accurate than simulating precipitation extremes (which inform rainfall variability) (e.g. Eden *et al.* 2012), but simulations of both means and extremes have tended to be relatively poor (e.g. Alexander and Arblaster 2009, Rocheta *et al.* 2014, McMahon *et al.* 2015, Perkins *et al.* 2014).

Because simulating rainfall is so complex, most research has focused on correctly simulating average annual rainfall volume, rather than the processes that drive rainfall (and, hence, rainfall variability). However, even though a model may accurately simulate rainfall volume, this does not necessarily mean that it captures the processes that determine rainfall volume (Brown *et al.* 2010; Lewis and Karoly 2014). Additionally, GCMs that do account for the phenomena that influence rainfall variability typically focus on successfully modelling one primary contributor to rainfall variability (e.g. ENSO), which affects the accuracy of simulations as other modulating phenomena are not accounted for (such as the IPO) (Kiem and Verdon-Kidd 2009). This approach has resulted in the tendency of models, including the ACCESS model, to overestimate the frequency of light rainfall and underestimate the intensity of heavy rainfall—two key characteristics of rainfall variability (Sun *et al.* 2006; Brown *et al.* 2010).

2.2.2 Capturing the influence of single climate drivers and joint interactions amongst climate drivers on rainfall variability

Until recently, GCM simulations of single climate drivers affecting the Australian region have produced mixed results. For example, whilst Mark 3 (and subsequent versions) of the Commonwealth Science and Industrial Research Organisation (CSIRO) GCM[1] was able to simulate the amplitude of twentieth-century ENSO events (Cai *et al.* 2003), simulation of ENSO-related rainfall variability was poor (Rotstayn *et al.* 2007; Shi *et al.* 2008). Poor simulation of individual climate drivers has led to poor simulation of rainfall and cloudiness (Rotstayn *et al.* 2007). GCMs have only recently begun to simulate rainfall variability attributed to individual climate drivers with some degree of accuracy, due to the addition of key elements of the earth system, such as interactive aerosol schemes (Rotstayn *et al.* 2010). The ACCESS1.3 model captures the main features of the ENSO–rainfall teleconnection, although the signal over eastern Australia is relatively weak (Rashid *et al.* 2013). Although it has not been directly discussed in the literature, it is possible that this is due to the inability of ACCESS1.3 to model ENSO interactions with other climate drivers (e.g. the IPO). The ability of the ACCESS model to capture the rainfall teleconnection associated with the IPO has not been analysed previously.

Most recently, Risbey *et al.* (2011) assessed the ability of a (pre-ACCESS1.0) ACCESS Atmospheric Model Intercomparison Project (AMIP) run to capture historical rainfall teleconnections with particular climatic drivers, with mixed results. The ENSO teleconnection

[1] The CSIRO GCM was the primary model used for Australia-focused modelling prior to the development of ACCESS. The CSIRO GCM continues to be used and developed; the latest version is CSIRO Mk3.6.0 (CSIRO 2014).

was apparent in eastern Australia in spring but not winter; the model captured the rainfall teleconnection with atmospheric blocking well; and the IOD teleconnection was poorly represented. Small-scale, topographically-induced rainfall responses to the SAM were also poorly simulated. Overall, the modelled rainfall teleconnections are weaker than those in the observations, and the influence of some climate-producing phenomena is captured only during particular seasons or at particular spatial scales. Although several studies have examined the observed relationship between climate drivers (e.g. Meyers *et al.* 2007; Murphy and Timbal 2008), examination of the ability of GCMs in the Australian region to represent rainfall produced by joint drivers has been limited (Cai *et al.* 2010; Risbey *et al.* 2011). Only two studies have compared observations and model simulations of the ENSO–IPO interaction in the Australian region so far, neither of which have assessed the ACCESS model. In one, observations were compared with reanalysis data (which differ from GCM output), and only extremes were examined (King *et al.* 2013a). In the other, the analysis was restricted to south-east Queensland (Cai *et al.* 2010).

It seems likely that poor simulations of rainfall variability are influenced by their inability to capture the interactions between the phenomena contributing to rainfall variability; Cai *et al.* (2010) suggest that this is a result of failing to capture multi-decadal variability (such as that produced by the ENSO–IPO interaction). Understanding how well GCMs model rainfall variability, then, requires an understanding of how well GCMs model the interactions between rainfall-producing phenomena, such as ENSO and the IPO.

2.3 Chapter summary

The ENSO relationship with Australian rainfall has been well studied. ENSO impacts Australian rainfall more than other climate drivers, and influences rainfall in the eastern two-thirds of the continent. The relationship between ENSO and rainfall is lagged and nonlinear; it is uncertain how much of this nonlinearity is influenced by interactions with other climate drivers. Although it is known that the IPO influences rainfall in eastern Australia, many aspects of this relationship remain unstudied (e.g. seasonality, regional variations). The mechanisms underlying the IPO are unclear, although the IPO appears to be influenced by ENSO. The interactions between ENSO and the IPO have been studied to a limited extent and a nonlinear relationship between the ENSO–IPO interaction and rainfall (and rainfall extremes) has been detected; however, the nature and cause of this nonlinearity is unclear.

The ability of ACCESS1.3 to simulate the ENSO relationship with rainfall has been studied, but its ability to simulate the IPO–rainfall relationship has not. A limited number of studies have assessed GCMs for their representation of interactions amongst climate drivers that impact rainfall variability, and a smaller number have assessed how well GCMs simulate the influence of the ENSO–IPO interaction on rainfall. This will be the first study to assess how well ACCESS1.3 simulates this relationship.

Chapter 3: Data and Methods

As shown in Chapter 2, the broad effect of the ENSO–IPO interaction on rainfall variability in Australia is understood but the nuances of this relationship remain unknown. The ENSO–IPO influence on rainfall at both global and regional scales has not been well studied. Additionally, the accuracy of GCM simulations of the ENSO–IPO interaction with rainfall is largely unknown, and the ability of ACCESS1.3 to simulate this relationship has not yet been examined. This chapter describes the data and methods used to study the relationship between the ENSO–IPO interaction and Australian precipitation, and its representation in ACCESS1.3.

3.1 Data

3.1.1 The observational dataset (AWAP)

An observational precipitation dataset is required to identify and quantify the impact of the ENSO–IPO interaction on rainfall variability, as well as to act as a comparison dataset for examining how well the ACCESS1.3 model simulates the observed relationship. The Australian Water Availability Project (AWAP) dataset is used in this analysis (Jones *et al.* 2009; Raupach *et al.* 2009; Raupach *et al.* 2012). In AWAP, daily and monthly observed rainfall values (1900–present) from land-based Australian Bureau of Meteorology (BoM) weather-station rain-gauges are interpolated onto a $0.05^{o} \times 0.05^{o}$ grid (approximately 5 km × 5 km) using the Barnes successive-correction method (Koch *et al.* 1983) and three-dimensional thin plate smoothing splines (Hutchinson 1995). This study uses the latest version of the data, Run26j.[2]

Gridded datasets like AWAP are preferred for this study to other types of datasets. Satellite datasets are too short to examine the IPO, and can be subject to errors of quality, resolution, and calibration (Jeffrey *et al.* 2001; Jones *et al.* 2009). Reanalysis datasets incorporate a mix of observations (e.g. rain-gauge observations, satellite observations) and use numerical modelling to 'fill in' any observational gaps (e.g. Kalnay *et al.* 1996). They incorporate any biases present in observational or modelled datasets (e.g. Hanson *et al.* 2007). Gridded datasets like AWAP are also subject to error. For example, if weather-station density is low (e.g. central Australia) the interpolated precipitation values can be unreliable. However, the robustness of the AWAP dataset has been scrutinised and concluded fit for use (King *et al.* 2013b), and it is considered a good choice as it captures the nonlinear relationship between ENSO and extreme rainfall events (King *et al.* 2013a). Additionally, other gridded datasets do not capture extreme rainfall as well as AWAP (Contractor *et al.* 2015). AWAP does tend to underestimate the intensity of extremely heavy rainfall events, and to overestimate the frequency and intensity of very low rainfall events

[2] The AWAP dataset can be publicly accessed via the CSIRO FTP site: ftp.eoc.csiro.au/pub/awap/Australia_historical/Run26j/Precip/

(King *et al.* 2013a), but overall, the high quality of the AWAP dataset eliminates the need to use an ensemble of observational datasets.

3.1.2 The global climate model dataset (ACCESS1.3)

The best GCMs to analyse in this study are those which capture the processes that drive rainfall in Australia particularly well. The Australian Community Climate and Earth-System Simulator (ACCESS) coupled climate model simulates Australian and global climates with greater accuracy than another main GCM commonly used in the Australian region, the CSIRO GCM (Bi *et al.* 2013). The CSIRO Mk3A GCM did not simulate rainfall variability attributed to the ENSO–IPO interaction in south-east Queensland (Cai *et al.* 2010), casting doubt on its suitability for this study. Additionally, ACCESS was found to better simulate ENSO than many Coupled Model Intercomparison Project (phase three) (CMIP3) models (Rashid *et al.* 2013); ACCESS is considered a good choice for this study.

ACCESS comprises modules from existing GCMs deemed to best simulate the Australian climate (see Table 3.1 and Bi *et al.* (2013)).[3] The ACCESS model is a medium-resolution GCM, with a horizontal grid resolution of 1.25° × 1.875° (approximately 139.2 km × 208.7 km at latitude 0°S) (Bi *et al.* 2013; Chen *et al.* 2014). To date, simulations from two versions of the ACCESS model—ACCESS1.0 and ACCESS1.3 (the latest version of ACCESS)—have been submitted to CMIP5 for use in the IPCC AR5.[4] The latest version, ACCESS1.3, is used in this study.[5] The CMIP5 experimental configuration of ACCESS1.3 is presented in (Taylor *et al.* 2012; Dix *et al.* 2013). CMIP5 submissions were subjected to rigorous quality control processes (Collier and Uhe 2012), so no further action of this type is required in this thesis. The capability of ACCESS1.3 to simulate rainfall is discussed in Section 5.1. All three ensemble members (r1i1p1, r2i1p1 and r3i1p1) of the ACCESS1.3 historical experiment, which spans 1850–2005, are examined in this thesis. Unlike other CMIP5 experiments that simulate past conditions (e.g. AMIP), the historical experiment spans a period of time sufficient in length to examine the IPO's multi-decadal shifts.

[3] ACCESS was developed by the Centre for Australian Weather and Climate Research (CAWCR), a joint initiative of the CSIRO and the Australian Bureau of Meteorology.
[4] The CSIRO maintains a website with information on the ACCESS GCM: https://wiki.csiro.au/display/ACCESS/Home
[5] ACCESS1.3 model output was obtained freely from the German node of the Earth System Grid Federation (ESGF): http://esgf-data.dkrz.de. Further information on accessing CMIP5 data is available at: http://cmip-pcmdi.llnl.gov/cmip5/data_getting_started.html

Table 3.1: The components of two versions of ACCESS submitted to CMIP5, ACCESS1.0 and ACCESS1.3. The atmospheric modules of ACCESS were taken from the UK Met Office's Unified Model (UM); ACCESS1.3 uses UM 7.3. The GA1.0 suite of model implementations includes the atmospheric component of the UK Met Office's HadGEM3 (r1.1) coupled model, and includes the prognostic cloud fraction and prognostic condensate scheme (PC2). The PC2 scheme improves simulations of Australian precipitation (Wilson *et al.* 2007; Hirsch 2010). Together, MOM4p1 and CICE4.1 form the ACCESS ocean model (ACCESS-OM). This table has been produced with information from in Bi *et al.* (2013) and Puri *et al.* (2013).

Model component	*Ocean*	*Sea ice*	*Coupler*	*Atmosphere*	*Land surface*	*Chemistry and aerosols*
ACCESS1.0	MOM4p1	CICE4.1	OASIS3.2-5	HadGEM2(r1.1)	MOSES2	
ACCESS1.3	MOM4p1	CICE4.1	OASIS3.2-5	GA1.0 (includes the P2C cloud scheme)	CABLE1.8	UKCA

3.1.3 Other datasets

The strength of ENSO and the IPO and the positive, neutral and negative states in the observed and modelled datasets is determined using indices derived from key variables. Several different indices exist for measuring ENSO and the IPO; it is beyond the scope of this project to use index ensembles (e.g. Risbey *et al.* 2009a), and so this study uses the Niño 3.4 index[6] for measuring ENSO, and the IPO Tripole Index (TPI) (Henley *et al.* 2015) for measuring the IPO, both of which are calculated from SST data in key regions of the Pacific Ocean. Table 3.2 presents the relationship amongst the index states, the oscillation states, and precipitation.

Table 3.2: The states of the IPO (*upper*) and ENSO (*lower*), and how these relate to values of the TPI and Niño 3.4 indices, SST anomalies in the eastern equatorial Pacific Ocean, and rainfall in eastern Australia. '–' indicates negative values, whilst '+' indicates positive values.

	IPO positive	**IPO negative**
TPI state	–	+
SST anomalies	+	–
Eastern Aus. rainfall	–	+

	ENSO positive (La Niña)	**ENSO negative (El Niño)**
Niño 3.4 state	+	–
SST anomalies	–	+
Eastern Aus. rainfall	+	–

[6] National Centers for Environmental Prediction Climate Prediction Center of the National Oceanic and Atmospheric Administration (NOAA) introduced the Niño 3.4 index in the April 1996 edition of the *Climate Diagnostics Bulletin* (as explained in Trenberth *et al.* (1997)). However, this edition cannot be accessed online as digital archives only begin in 1999.

Although observed values of Niño 3.4 and the TPI are available and could be used to stratify observed precipitation data into the different states of each oscillation, these datasets cannot be used in the same way for modelled precipitation. This is because the ACCESS historical experiment is initiated from an arbitrary point of a quasi-equilibrium control run; consequently, the timing of unforced climate events (e.g. ENSO, the IPO) is different (a) to those occurring in twentieth century observations and (b) amongst ACCESS1.3 ensemble members (Taylor *et al.* 2012). Consequently, index algorithms were used to derive ENSO and IPO strength and phases, following the methods of Trenberth (1997) and Henley *et al.* (2015).

The SST data used to calculate the Niño 3.4 and TPI indices are from the latest publicly available version of the Hadley Centre Global Sea Ice and Sea Surface Temperature (HadISST1.1) gridded dataset (Rayner *et al.* 2003),[7] which has a resolution of $1^o \times 1^o$. The performance of HadISST is comparable with other observational SST datasets, and it produces SST fields that better match observed variance and month-to-month persistence of SSTs (Rayner *et al.* 2003). Previous studies have also used the HadISST dataset to derive SST-based indices for Australia, and it is considered a robust dataset for index derivation (e.g. Cai *et al.* 2009; Risbey *et al.* 2009a; Bi *et al.* 2013; Klingaman *et al.* 2013).

The Niño 3.4 index has been chosen as the ENSO index for several reasons. Firstly, it is a univariate index, which makes computing index values more efficient as it only requires one dataset (i.e. SSTs). It is also derived from many points (unlike the commonly used Southern Oscillation Index, which is calculated from two pressure values alone), and so robustly represents the atmosphere–ocean teleconnection. Figure 3.1 depicts several SST indices for ENSO that are obtained by averaging SSTs within different regions of the Pacific Ocean. The Niño 3.4 index was selected as its region (5°N–5°S, 120°–170°W) represents ENSO events better than other regions (Trenberth 1997), and Australian rainfall is most sensitive to changes in Niño 3.4 (e.g. Wang and Hendon 2007; Risbey *et al.* 2009a). Niño 3.4 values and ENSO states were obtained using the methods of Trenberth (1997). Five-month running means of SST anomalies in the Niño 3.4 region were computed (using the 1961–1990 base period).[8] An El Niño event is defined if SST anomalies exceed 0.4°C for 6 months or more, and a La Niña is defined if SST anomalies exceed –0.4°C for 6 months or more. The observational Niño 3.4 index calculated in this study is strongly correlated with existing observational Niño 3.4 indices (r = 0.97–0.99),[9] and therefore the index algorithm can be used to determine ACCESS1.3 Niño 3.4 values from modelled SSTs.

[7] The HadISST1.1 dataset was freely obtained online (http://www.metoffice.gov.uk/hadobs/hadisst/).
[8] Before commencing the main analysis, both Niño 3.4 and TPI indices were derived using multiple base periods; correlations did not differ between base periods, indicating that any base period could be chosen (see the file '1. Index generation' in Appendix 3). The 1961–1990 base period was chosen because of its widespread use in climate science (increasing the comparability of this study with others) and because this thirty-year period straddles both positive and negative states of the IPO.
[9] The observational Niño 3.4 values derived in this study agreed with the Niño 3.4 values in OISST v2, ERSST v4 and NCAR CDC datasets (NWS CPC 2015; NCAR CDC 2012). See '1. Index Generation' in Appendix 3.

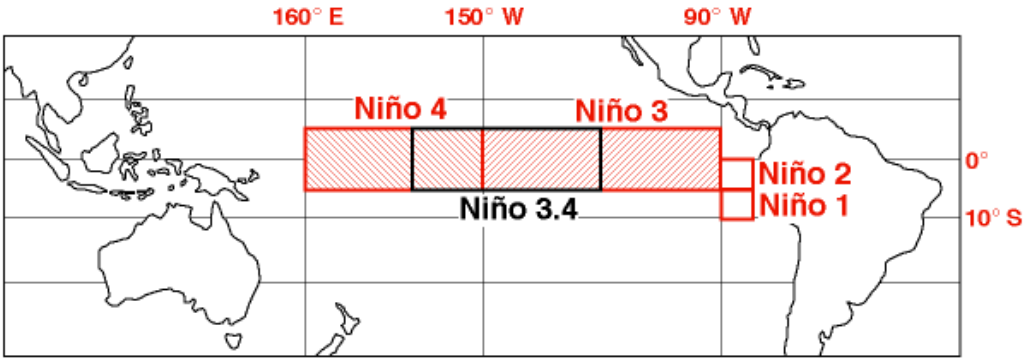

Figure 3.1: Five regions in the Pacific Ocean used to derive indices for ENSO: Niño 1, Niño 2, Niño 3, Niño 3.4 (which straddles the Niño 3 and Niño 4 regions), and Niño 4 (image from Pielke Jr. and Landsea (1999)). The Niño 3.4 region is used in this study.

The TPI is used to measure the IPO. It is a new IPO index (Henley *et al.* 2015), and is the first to be derived from box-averaged SSTs. Previous indices were based on principal component analysis (PCA) (e.g. Power *et al.* 1999a; Parker *et al.* 2007). The TPI is preferred because it avoids inconsistencies arising from misinterpretation of PCA results (see Henley *et al.* (2015) for further discussion), and box-averaging is a simple and efficient calculation method which is consistent with the derivation of Niño 3.4. The TPI was calculated using the methods outlined in Section 6 of Henley *et al.* (2015). Firstly, the seasonal cycle was removed from SST observations by subtracting the monthly climatology from each grid cell in three TPI regions (boxes 1–3 in Figure 2.3), and the monthly mean SST anomalies in the three TPI regions were calculated using the base period 1961–1990.[8] Secondly, unfiltered values of the TPI were computed with Equation 3.1. Finally, a 13-year Chebyshev low-pass filter was applied to remove high-frequency (inter-annual) signals and produce the final TPI index.

Equation 3.1: The equation for calculating the unfiltered TPI (Henley *et al.* 2015). $SSTA_1$ are the SST anomalies for the area 25°N–45°N, 140°E–145°W; $SSTA_2$ are the SST anomalies for the area 10°S–10°N, 170°E–90°W; and $SSTA_3$ are the SST anomalies for the area 50°S–15°S, 150°E–160°W.

$$TPI_{unfiltered} = SSTA_2 - \frac{SSTA_1 + SSTA_3}{2}$$

The observational TPI computed in this study is strongly correlated with the TPI index produced by Henley *et al.* (2015) (r = 0.91),[10] which indicates that this index can be used to derive values of the TPI from the modelled datasets. Additionally, the TPI may be more appropriate than previous indices for exploring the inter-decadal nature of the IPO; the

[10] Differences between the TPI computed in this study and in the study by Henley *et al.* (2015) appear to be due to different study lengths (1900–2005 and 1870–2013). Because the Henley *et al.* (2015) study period is longer, the filtering algorithm can produce TPI values close to observations for the 2000–2005 period (see Figure A in Appendix 2).

unfiltered (i.e. higher-frequency) TPI displays higher correlations with previous indices than those indices do with each other (see Table 3.3), showing that the TPI successfully captures the IPO signal as it has been derived in past studies. The relatively low correlation between the filtered (i.e. lower-frequency) TPI and previous indices suggests that those indices may capture the inter-decadal nature of the IPO less clearly.

Table 3.3: Correlation coefficients (*r*) between observed historical values of various IPO indices. UF = unfiltered; F = filtered. 'Henley' = the TPI, published by Henley *et al.* (2015). 'Wellby' = the TPI as calculated in this study, derived according to Henley *et al.* (2015). 'Parker' = an index of the IPO, published by Parker *et al.* (2007). 'Mantua' = an index of the PDO, published by Mantua *et al.* (1997). Grey cells are used to avoid correlating indices with themselves, unnecessarily repeating correlation values, or avoid entering correlations with no practical relevance.

	Correlation coefficients between various IPO indices					
	Henley (UF)	Henley (F)	Wellby (UF)	Wellby (F)	Parker IPO	Mantua PDO
Henley (UF)		0.46	0.69		0.95	0.57
Henley (F)				0.91	0.52	0.37
Wellby (UF)				0.42	0.70	0.42
Wellby (F)					0.48	0.38
Parker IPO						0.69
Mantua PDO						

3.1.4 A common grid for analysing precipitation datasets

As the spatial resolution of the AWAP dataset ($0.05^o \times 0.05^o$) and the ACCESS1.3 dataset ($1.25^o \times 1.875^o$) are different, the AWAP data were re-gridded onto the ACCESS1.3 grid so that the two datasets could be directly compared; a similar approach was adopted by King *et al.* (2013a). The common grid, depicted in Figure 3.2, has the dimensions 43.75^o to 10.0^o south (latitude) and 114.375^o to 155.625^o east (longitude). Interpolating the AWAP dataset onto a lower spatial resolution is preferred to interpolating the ACCESS1.3 dataset onto a higher resolution grid, as this reduces errors associated with downscaling (e.g. erroneous attribution of climatic characteristics to localised geographic locations). The spatial averaging process used to re-grid the AWAP dataset is discussed in Appendix 1.

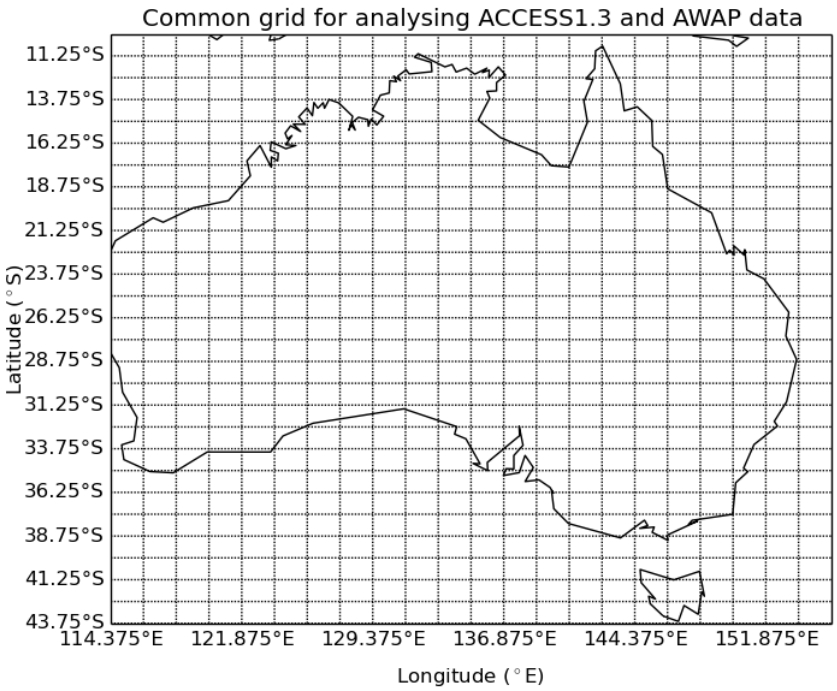

Figure 3.2: The common grid (1.25º × 1.875º—approximately 139 km × 208 km at latitude 0º south) used to compare ACCESS1.3 and AWAP datasets. The grid spans the latitudes 43.75º–10.0º south and the longitudes 114.375º–155.625º east.

3.2 Methods

Investigation of the relationship between ENSO, the IPO, and Australian rainfall variability should begin with an analysis of the relationships the individual oscillations and rainfall, to show how the joint ENSO–IPO interaction influences rainfall differently. Once this has been analysed, the influence of the joint interaction on rainfall can be investigated. Identifying and quantifying the fraction of rainfall variability associated with the ENSO–IPO interaction is challenging, particularly as techniques that can account for the nonlinear nature of ENSO and the ENSO–IPO interaction are required. This difficulty has contributed to the lack of studies investigating interactions between climate drivers and their joint influence on rainfall variability.

Studies examining the relationship between a single climate driver and rainfall, or between the indices of two climate drivers, have tended to use correlation analysis (e.g. Risbey *et al.* 2011); nonlinearities are typically accounted for with piecewise linear analysis, in which data are stratified according to an oscillation's states prior to undergoing correlation analysis (e.g. King *et al.* 2013a; Westra *et al.* 2015). Composite analysis is an extension of this technique, in which the relationship between two climate drivers and a variable of interest (e.g. precipitation) is explored by stratifying data of the investigated variable firstly into the states of one climate driver, and then further stratifying these data by the states of the second climate driver (e.g. Meyers *et al.* 2007; Risbey *et al.* 2009a). This technique accommodates nonlinear relationships within and between the climate drivers (Storch and Zwiers 1999). However, it does not isolate instances of the variable that are *only* influenced by the chosen climate drivers. Techniques such as multiple linear

regression aim to identify this portion of influence (e.g. Mekanik and Imteaz 2012), but do not account for nonlinearities. It seems that the solution to this problem likely lies in computational techniques based on artificial neural networks, which can account for nonlinearities (e.g. Mekanik and Imteaz 2012). Several such approaches, such as self-organising maps (Brown *et al.* 2010), classification and regression trees (Whan *et al.* 2014), and partial mutual information (Tozer 2014) have been applied in climate studies, but there are relatively few examples. Whilst exploration of these techniques seems desirable, their computationally-intensive nature makes them less suited for this project. Composite analysis is preferred as the initial method of exploring the relationships amongst ENSO, the IPO, and rainfall variability; future work can build on this foundational study.

The analysis in this thesis consists of two main parts. Firstly, the observed relationship amongst ENSO, the IPO and rainfall is investigated. Correlation analysis is used to examine relationships between the individual oscillations and rainfall (i.e. ENSO–rainfall and IPO–rainfall). This serves the joint purpose of revealing whether the relationships found are similar to those identified in previous research and filling in knowledge gaps (particularly in the case of the IPO–rainfall relationship). A mix of correlation and composite analyses is then used to examine the joint relationship amongst ENSO, the IPO and observed rainfall variability. In the second part of the analysis, this approach is applied to the three ACCESS1.3 ensemble members. The observational and modelled results are then compared to assess the degree to which ACCESS1.3 captures the observed relationships. All analyses were performed on annual, seasonal, and monthly timescales. Years commenced in June and ended in May, as this coincides with the inter-annual cycle of ENSO (Spencer and Slingo 2003); therefore, the study period is from June 1900 to May 2005.

Analysis code was written in Python and is available both on GitHub[11] and in Appendix 3. Statistical analyses were performed at the 95 per cent confidence level. Analyses were performed individually on the three ACCESS1.3 ensemble members, as the small sample size makes ensemble averaging inappropriate. All figures and tables produced as part of this analysis are available in Appendix 3; selected figures are presented in Chapters 4 and 5, and in Appendix 2.

3.2.1 Correlation analysis

For each land-based grid point, Pearson's correlation coefficient (r; see Equation 3.2) was calculated between: (a) ENSO and rainfall, and (b) the IPO and rainfall. Grid points that showed significant correlations were mapped. Cross correlations were also calculated using Equation 3.3 to determine if the relationship between rainfall and an index is lagged. Although underlying lagged relationships were apparent in the observational data, strong correlations occurred at zero

[11] Code written to analyse the datasets can be accessed publicly at https://github.com/sonyawellby/anu_honours. The code is designed to be able to be run by any user with access to these files and the original datasets.

lag (i.e. the simultaneous correlations were strongest) (e.g. Figures 4.2 and 5.4.a). Consequently, and following the approach in past research (Risbey *et al.* 2009a; King *et al.* 2013a), the analyses below show results for simultaneous correlations only. Partial correlations, which remove the influence of other climate drivers from the correlations between each climate driver and rainfall (e.g. Risbey *et al.* 2009a), were not used in this study due to the strongly inter-dependent nature of ENSO and the IPO. Similarly, filters were not applied to remove underlying trends in indices, as it is possible that this may remove characteristics linking ENSO and the IPO. Although detrending may improve the correlation between indices and rainfall (e.g. Risbey *et al.* 2009a), it seems unlikely in the case of the ENSO–rainfall relationship, at least, as King *et al.* (2013a) found that detrending extreme ENSO-related rainfall had little influence on results.

Equation 3.2: Pearson's correlation coefficient (*r*) (Storch and Zwiers 1999). The first dataset is $\{x_1 \dots x_n\}$ and the second dataset is $\{y_1 \dots y_n\}$, where $\bar{x}$ and $\bar{y}$ are the means of these datasets. n is the number of values in each dataset.

$$r = r_{x,y} = \frac{\sum_{i=1}^{n}(x_i - \bar{x})(y_i - \bar{y})}{\sqrt{(\sum_{i=1}^{n}(x_i - \bar{x})^2)(\sum_{i=1}^{n}(y_i - \bar{y})^2)}}$$

Equation 3.3: Cross correlation function ($\rho_{xy}(\tau)$) (Storch and Zwiers 1999), where (X_t, Y_t) are a pair of stochastic processes (t is the time-step) that are jointly weakly stationary (e.g. the Niño 3.4 and TPI indices). E is the expected value, τ is the lag (e.g. one month, one year), $\bar{x}$ and $\bar{y}$ are vectors containing the means of X and Y, and σ_X and σ_Y are the standard deviations of X_t and Y_t.

$$\rho_{xy}(\tau) = \frac{E[(X_t - \bar{x})(Y_{t+\tau} - \bar{y})']}{\sigma_X \sigma_Y}$$

The correlation between each index and rainfall was further examined at the regional scale. Both the eastern Australian region, as well as the basic Köppen climate classification zones[12] within eastern Australia, were examined (see Figure 3.3). Precipitation values were averaged across each region for each point in time, and correlated with each index, using Equation 3.2.

The relationship between the ENSO and IPO indices was examined. Time series plots and scatterplots were generated as a preliminary analysis. Pearson's correlation coefficients (Equation 3.2) were then calculated between the indices of ENSO and the IPO. For both this analysis and the analysis of index–rainfall correlations based on the Köppen climate zones, an independent two-sided Student's *t* test was used to determine if the correlation coefficients produced between the ACCESS1.3 ensemble members and observations, and within the ACCESS1.3 ensemble members, differed. The ENSO and IPO indices were also tested for cross correlation (Equation 3.3), but again, the observed correlation appears strongest with zero lag (Figure C in Appendix 2). Therefore, no adjustments to account for lags were made.

[12] The Köppen classification scheme (1923) divides the globe into climate zones based on precipitation and temperature; the scheme is therefore likely to reflect the influence of different climate drivers in particular locations.

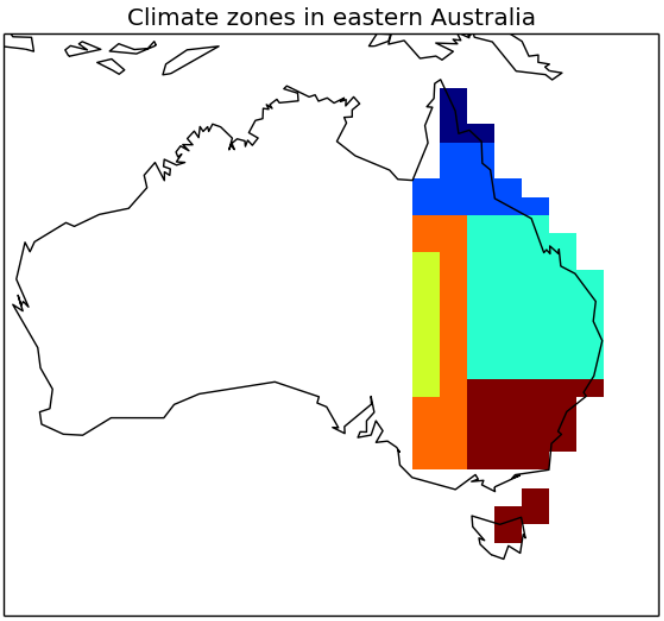

Figure 3.3: The regional areas investigated in addition to the Australia-wide analysis. The eastern Australian region is the region east of 140.625° east. The Köppen climate zones examined are equatorial (navy blue), tropical (medium blue), subtropical (light blue), grassland (orange), desert (yellow), and temperate (brown).

3.2.2 Composite analysis

The second part of the overall analysis explores the interaction between ENSO and the IPO, and their joint influence on rainfall variability. Rainfall was stratified according to the three states (positive, neutral and negative) of the ENSO and the IPO. Kiem and Franks (2001:716) note that 'significant subjectivity' exists when classifying ENSO states. In order to reduce subjectivity, this thesis defines ENSO events according to Trenberth *et al.* (1997), who propose that ENSO events occur when 5-month running mean SST anomalies in the Niño 3.4 region exceed ± 0.4°C for 6 months or more (see Section 3.1.3). As Henley *et al.* (2015) do not stratify the IPO into its three states (i.e. SST thresholds are not specified), states are delineated by the thresholds ± 0.5σ above the mean of the chosen IPO index (as suggested by Power *et al.* (1999a)), to allow for comparison with existing studies.

Prior to undertaking the composite analysis, a preliminary analysis of the relationship between rainfall and the positive and negative states of each oscillation was conducted. Rainfall datasets were stratified into the positive and negative states of each index, and the difference in precipitation between the states was mapped for each index. This was repeated for the three ACCESS1.3 ensemble members.

Next, the composite analysis (formally described in Equation 3.4) was then performed. The dataset was stratified according to the three IPO states. Each phase was further stratified according to ENSO states (producing nine subsets of the precipitation data). Precipitation data

were mapped in three formats, each presenting an average value for each land-based grid point, for the period 1900–2005. Firstly, mean rainfall (mm day^{-1}) was mapped, which shows the distribution of actual rainfall across Australia. Secondly, precipitation data are presented as mean rainfall anomalies (mm day^{-1}) (Equation 3.5.a), which shows how, on average, the volume of measured rainfall in the investigated time period (e.g. June) differs from the climatological average of the same investigated time period (e.g. June precipitation values in the 1961–1990 base period). Thirdly, precipitation data are presented as standardised mean rainfall anomalies (σ), where mean rainfall anomaly data in the investigated time period (e.g. summer) are divided by the climatological (i.e. 1961–1990) standard deviation of the investigated time period (e.g. summer) (Equations 3.5.b). This shows precipitation variability compared with rainfall in the base period. To provide a sense of how the ENSO–IPO interaction affects extreme rainfall variability this procedure was repeated using different definitions of oscillation states. The positive and negative states of both the IPO and ENSO indices were defined as ± 2σ and ± 3σ above the respective index means.

Equation 3.4: The formal definition of the composite, $\vec{V}_{\Theta}$ (Storch and Zwiers 1999). Sets Θ are formed of the index $\vec{z}$ (e.g. Niño 3.4) to estimate the expected value of $\vec{V}$ (e.g. precipitation) conditional on $\vec{z}_t \in \Theta$.

$$\vec{V}_{\Theta} = E(\vec{V}_t \,|\, \vec{z}_t \in \Theta)$$

Equations 3.5: *3.5.a* shows the equation for computing rainfall anomalies, where x is the dataset of interest (e.g. June 1900–2005), n is the number of elements in x, and $\bar{x}$ is the climatological average (e.g. June 1961–1990). *3.5.b* shows the equation for computing standardised rainfall anomalies, where x is as defined above, and $\sigma_{\bar{x}}$ is the standard deviation of the climatological average (e.g. June 1961–1990).

$$anomaly_x = \frac{\sum_{i=1}^{n}(x_i - \bar{x})}{n} \qquad \textbf{Equ. 3.5.a}$$

$$standardised\ anomaly_x = \frac{anomaly}{\sigma_{\bar{x}}} \qquad \textbf{Equ. 3.5.b}$$

In the final analysis, precipitation data were stratified according to the three states of ENSO (firstly as defined by Trenberth (1997) and Henley *et al.* (2015), and secondly defined as ± 2σ and ± 3σ above the Niño 3.4 and TPI means). The three stratifications of precipitation data were then correlated with the IPO. This process was repeated to account for any noncommutative aspects of the correlations between rainfall and ENSO or the IPO (which are possible given the nonlinear nature of the ENSO–IPO interaction); this time the precipitation data were initially stratified according to the three states of the IPO, and then correlated with ENSO.

3.3 Chapter summary

A small body of work has previously investigated the influence of joint interactions between climate drivers and rainfall variability. This thesis builds on that work by investigating the influence of the ENSO–IPO interaction on rainfall variability, both in observations and

simulations. Correlation and composite analyses are used to investigate (a) the ENSO–rainfall and IPO–rainfall relationships, and (b) the relationship amongst the indices of ENSO and the IPO and rainfall. This permits comparison of the results of this thesis with those of previous studies. These analyses may also reveal aspects of the oscillations' interactions with rainfall that have so far not been studied (e.g. the IPO and rainfall variability).

Chapter 4: Observations of ENSO, the IPO, and Rainfall Variability

This chapter explores how ENSO and the IPO, as expressed through the Nino 3.4 and TPI indices (see Chapter 3), influence the variability of observed (AWAP) rainfall. This provides insights into the role these oscillations play in modulating rainfall (the focus of this chapter), and enables the observational analysis to be compared with the ACCESS1.3 analysis in Chapter 5. This chapter begins by discussing the relationships between rainfall and the individual oscillations, providing a foundation for the discussion that follows on the joint impacts of ENSO and the IPO on rainfall variability. In order to minimise confusion relating to differences between the signs of the indices and the oscillation states, it is suggested Table 3.2 (in Chapter 3) is consulted prior to reading this chapter.

4.1 Observations of ENSO and rainfall

Overall, the observed relationship between Niño 3.4 and rainfall confirms the findings of previous studies. As Niño 3.4 decreases (and conditions tend towards La Niña) rainfall increases, and as Niño 3.4 increases (and conditions tend towards El Niño) rainfall decreases. The season in which Niño 3.4 influences rainfall most strongly is spring (r = –0.54); the weakest relationship is in autumn (r = –0.25) (Figure 4.1 and Table A1 in Appendix 2). The magnitude and seasonality of the relationships are similar to those identified in past studies (e.g. McBride and Nicholls 1983; Murphy and Timbal 2008; Mekanik and Imteaz 2012); minor discrepancies likely reflect the use of different indices between studies. The region of correlation is broad and encompasses eastern and central-northern Australia (McBride and Nicholls 1983; Ropelewski and Halpert 1987; Nicholls 1988). As expected, the relationship averaged across eastern Australia (annual: r = –0.60) is stronger than that for continental Australia (annual: r = –0.53). Rainfall on the eastern seaboard and lower-latitude areas (e.g. Queensland) exhibits the strongest relationship with Niño 3.4.

A clearer picture of how the Niño 3.4–rainfall varies spatially is formed by analysing rainfall in climate zones based on the Köppen climate classification scheme (1923), which builds on existing work (e.g. McBride and Nicholls 1983). Lower-latitude regions (equatorial, sub-tropical and tropical) exhibit the strongest relationship between mean rainfall and Niño 3.4, particularly in spring (equatorial zone, spring: r = –0.56) (see Table A1 in Appendix 2). Higher-latitude and inland regions (e.g. desert, grassland) also exhibit a statistically significant relationship between Niño 3.4 and rainfall, although these relationships weaken as latitude increases (e.g. Figure 4.1). Variation within the climate zones reflects the increasing influence of other rainfall-producing phenomena at the regional scale, and the various ways in which ENSO interacts with them (e.g. ENSO influences the number of synoptic-scale cut-off lows that occur in north-west Victoria in winter (Pook *et al.* 2006)). For example, the seasonality of the Niño

3.4–rainfall correlations in temperate zones follows the same pattern as the Australia-wide region, although the correlations are weaker, and some seasons have vastly different correlation coefficients (e.g. Australian autumn: r = –0.25; temperate autumn: r = –0.06) (see Table A1 in Appendix 2).

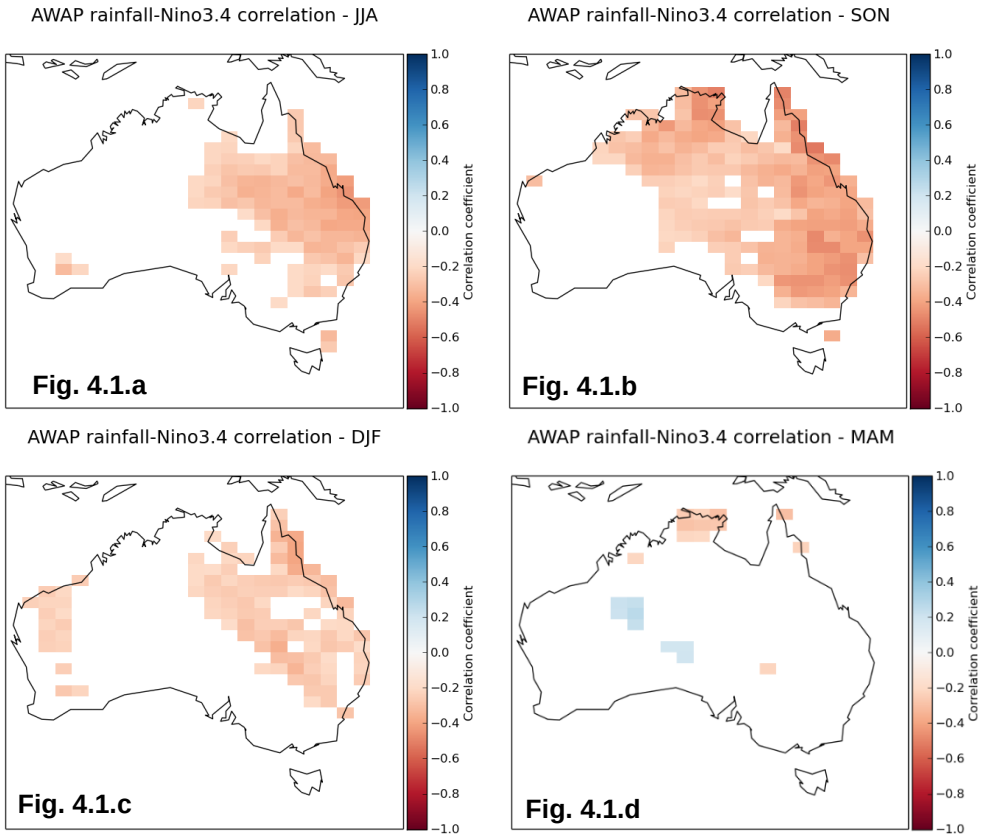

Figure 4.1: Correlation coefficients (r) between observed Australian mean seasonal rainfall and Niño 3.4, for winter (*Fig. 4.1.a*), spring (*Fig. 4.1.b*), summer (*Fig. 4.1.c*), and autumn (*Fig. 4.1.d*). Only grid-points where a significant relationship is observed are shown.

4.2 Observations of the IPO and rainfall

Observations of the relationship between the TPI and rainfall largely align with existing knowledge, although new insights have emerged concerning the cyclical nature, seasonality, regional nuances, and extremes behaviour (the last of which will be explored in Section 4.3).

The three distinct phase shifts since 1920 that have been identified in the literature (positive: 1924–1944, 1977–1998; negative: 1945–1976) (Dai 2013; Dong and Dai 2015; Henley *et al.* 2015) are apparent in the observed dataset (see Table 4.1). The notable difference in the results presented here is that the most recent phase extends from 1978–2004 (rather than 1978–1998), which likely reflects the use of the low-pass filter when calculating the TPI and may not be physically meaningful (see the discussion in Footnote 10 in Chapter 3). Other differences between the phases identified in this study and those previously identified occur because, whilst Power *et al.* (1999a) defined the IPO as having three states (positive, neutral and negative), studies

Table 4.1: The years in the twentieth century identified in existing studies as IPO positive (bold, red—this state tends to cause drying in eastern Australia), neutral (black), and negative (bold, blue—this state tends to cause drying in eastern Australia). 'Henley *et al.* (2015)' is presented as a representative study of those which investigate the early-twentieth century, and 'Dong and Dai (2015)' is selected as the representative study of those which investigate the IPO from the 1920s onwards (i.e. most existing studies). Henley *et al.* (2015) note that the 1911–1923 period exhibits weak negative or neutral TPI values, yet class this period as a positive phase. This highlights the loss of nuances in the IPO that can occur it is not stratified into its three states; the re-assignment of this period to the positive state masks the underlying 'drying' tendency of the IPO neutral state.

Years in twentieth century observations identified as IPO positive, neutral, and negative	
Wellby 2015 (this study)	**1900–1906**, 1907–1912, **1913–1919**, 1920–1921, **1922–1942**, 1943–1945, ***1946–1959***, 1960–1968, ***1969–1976***, 1977, **1978–2004**
Henley *et al.* 2015	**1896–1910**, ***1911–1923***, **1924–1944**, ***1945–1976***, **1977–1999**, ***2000–2007***
Dong and Dai 2015	**1924–1944**, ***1945–1976***, **1977–1998**, ***1999–***

frequently ignore the neutral state and divide the record into IPO positive and negative categories only (e.g. Verdon and Franks 2006; King *et al.* 2013a; Dong and Dai 2015; Henley *et al.* 2015; Vance *et al.* 2015; Westra *et al.* 2015). This can result in an incomplete understanding of the nature of the IPO, including its extremes (see Section 4.3). When the IPO neutral state is accounted for, the length of each phase decreases, and the total number of phases observed increases (e.g. this study identifies 11 phases in the study period, whilst Dong and Dai (2015) identify four phases—see Table 4.1). In this study, the multi-decadal nature of the IPO is retained but an intra-decadal component of the IPO emerges. This is observed in the cross correlation between the TPI and rainfall (Figure 4.2). The strongest correlation occurs at time zero (i.e. rainfall responds simultaneously to changes in the TPI), but that a statistically significant correlation between the TPI and rainfall also occurs approximately eight years into the future. It is possible that this is the same as the 9–13 year decadal signal identified by Meinke *et al.* (2005), who suggest that this signal could be different to—but modulated by—the IPO, and that it could be a key driver of inter-annual ENSO events. This relationship could be a mechanism through which the ENSO and the IPO interact; this is discussed further in Section 4.3. The widespread use of 11- or 13-year filters for computing the IPO (e.g. Mantua *et al.* 1997; Power *et al.* 1999a; Henley *et al.* 2015) is applicable for identifying the *inter-decadal* influence of the IPO, but not its intra-decadal influence. The six-year filter of Zhang *et al.* (1997) is more appropriate for identifying the intra-decadal effect (particularly if the role this eight-year oscillation plays in the ENSO–IPO interaction is to be assessed). In addition to this intra-decadal phenomenon, the inter-decadal relationship between the TPI and rainfall is observed at 60–80 years (the second mode in Figure 4.2). This cycle-length is longer than previously estimated (e.g. Dong and Dai 2015).

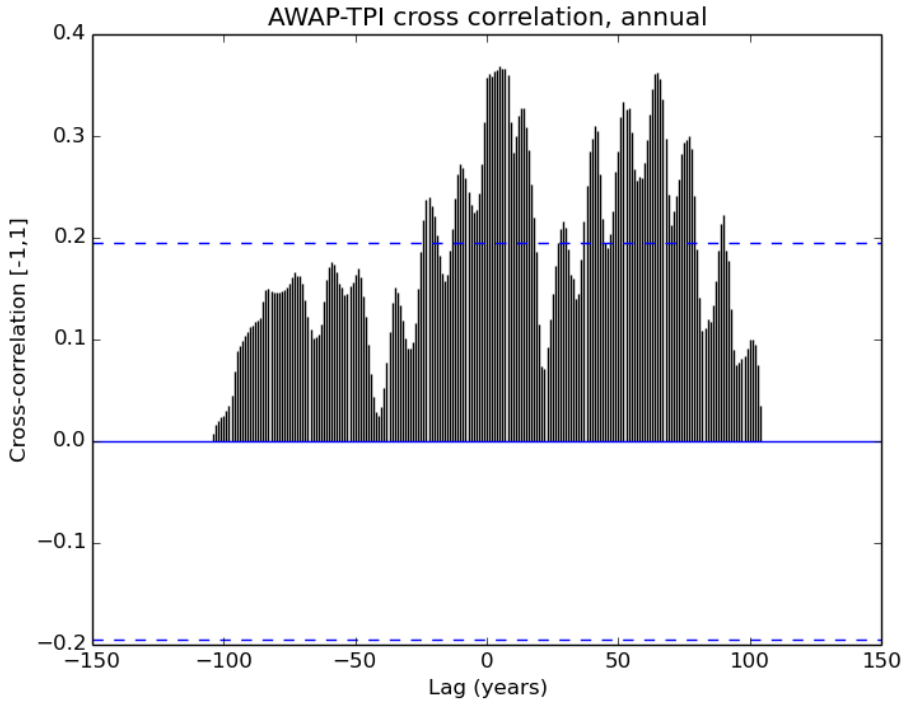

Figure 4.2: Cross correlation values between observed Australia-wide average annual rainfall and the TPI, for all 105 years in the study. The 95 per cent confidence interval is indicated by the dashed blue lines.

The TPI exhibits a weak–moderate relationship with rainfall; when TPI values increase in an IPO negative phase rainfall decreases, and when the TPI values decrease in the IPO positive phase rainfall increases. The relationship between the TPI and rainfall at annual, seasonal and monthly timescales is weaker than that exhibited by Niño 3.4 (e.g. TPI annual: r = –0.19 (not statistically significant at the 95 per cent level); Niño 3.4 annual: r = –0.53). Whilst Dai (2013) identified the IPO–rainfall correlation as significant at the 90 per cent level over north-eastern Australia, this study identifies a significant relationship (at the 95 per cent level) over a broader area of Australia (see Figure 4.3). It is likely that this is because this study uses a gridded dataset based entirely on Australian rainfall observations (avoiding errors incorporated into reanalysis datasets used by Dai (2013)).

There is spatial variation in the TPI–rainfall relationship, which is limited geographically to eastern Australia and is less broad than the extent of the Niño 3.4–rainfall relationship (compare Figures 4.3 (TPI) and 4.1 (Niño 3.4)). The correlation between the TPI and rainfall increases in eastern Australia (Australia: r = –0.19; eastern Australia: r = –0.35) (Table A2 of Appendix 2). Unlike Niño 3.4, the TPI has its greatest impact on higher-latitude, coastal areas (e.g. sub-tropical and grassland), and the correlation between the TPI and rainfall does not extend as far inland as the Niño 3.4–rainfall relationship. This aligns with prior research, which suggests that the influence of ENSO decreases with increasing latitude (Verdon *et al.* 2004) and the influence of multi-decadal climate drivers increases with latitude (Power and Colman 2006), and is likely

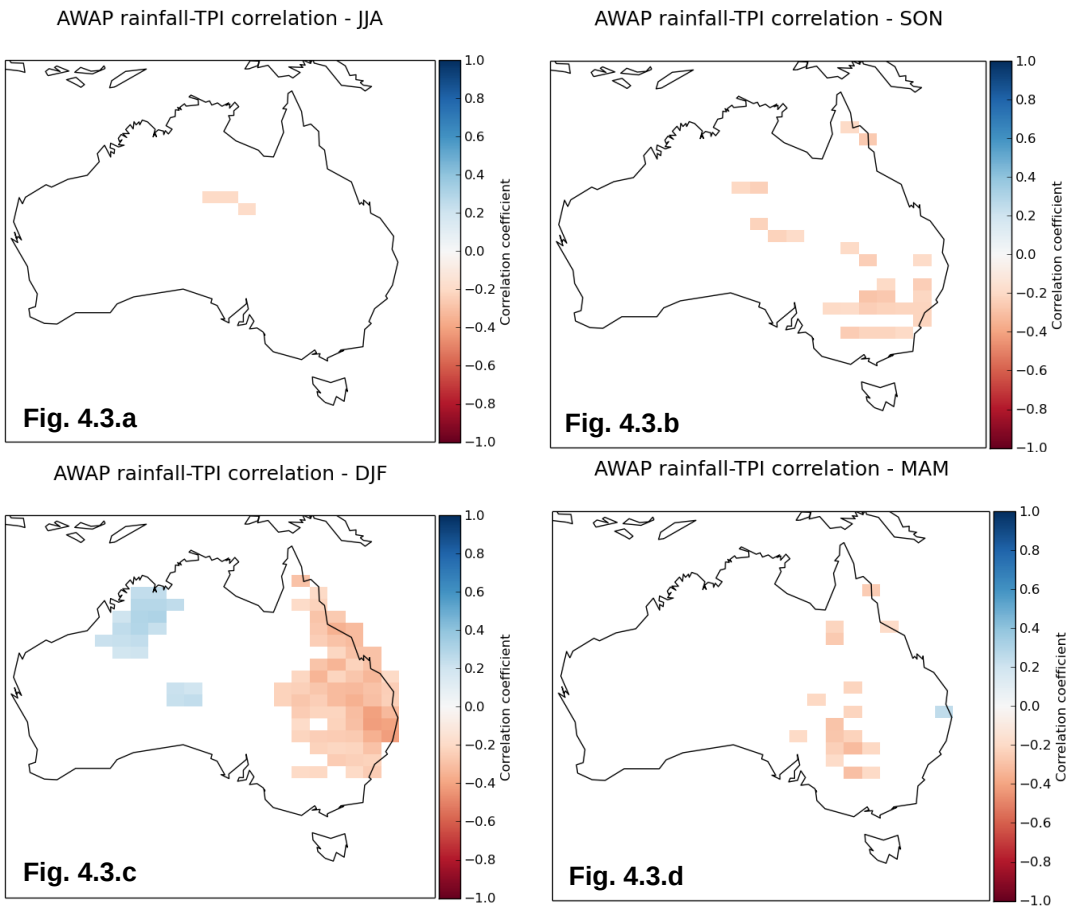

Figure 4.3: Correlation coefficients (*r*) between observed mean seasonal Australian rainfall and the TPI, for winter (*4.5.a*), spring (*4.5.b*), summer (*4.5.c*), and autumn (*4.5.d*). Only grid-points where a significant relationship is observed are shown.

to be a response to the fact that the IPO ocean–atmosphere teleconnection is influenced by a much greater area of the Pacific Ocean than the ENSO ocean–atmosphere teleconnection.

It appears that the IPO may interact with the northern Australian monsoon (e.g. Figure 4.3.c). Latif *et al.* (1997) identified a relationship between decadal variation in SSTs and the rainfall fluctuations in north-east Australia; this decadal variation may be contributing to the apparent relationship between IPO and monsoon rainfall, although research is yet to confirm this. Aside from the work of Latif *et al.* (1997), the possible relationship between the IPO and the monsoon remains largely unstudied (Winderlich 2010), and is an avenue for future research.

Seasonally, the average Australia-wide TPI–rainfall relationship is strongest in in spring (r = –0.17), although this correlation is not statistically significant (Table A2 in Appendix 2). When only eastern Australia is considered, the season with the strongest relationship is summer (r = –0.36). This is reflected in Figure 4.3, which shows that the strongest relationship between the TPI and rainfall occurs in summer. This seasonality matches that observed globally; Dai (2013) identified the strongest correlation between the IPO and boreal winter (austral summer) rainfall in for US precipitation. This suggests that the same processes (i.e. SST changes across

the entire Pacific Ocean) affecting the US IPO–rainfall teleconnection may also influence the IPO–rainfall teleconnection in eastern Australia. Unlike ENSO, the TPI–rainfall teleconnection is only statistically significant in summer and autumn, which suggests that winter and spring rainfall is most heavily influenced by another phenomenon or phenomena. It is possible that this could include ENSO, as Niño 3.4 exhibits its strongest seasonal correlation with spring rainfall, and its second-strongest seasonal correlation with winter rainfall (Table A1 in Appendix 2), although other climate drivers could be involved.

In autumn, the influence of the IPO on rainfall is equal with that of ENSO; in other seasons the IPO influence is weaker than the ENSO influence. In autumn, the ENSO teleconnection is weakest, leading to the increased importance of the IPO on rainfall (e.g. eastern Australia, autumn: Niño 3.4–rainfall, $r = –0.18$; TPI–rainfall, $r = –0.12$).[13] This is observed in the March rainfall difference charts in Figure 4.4.

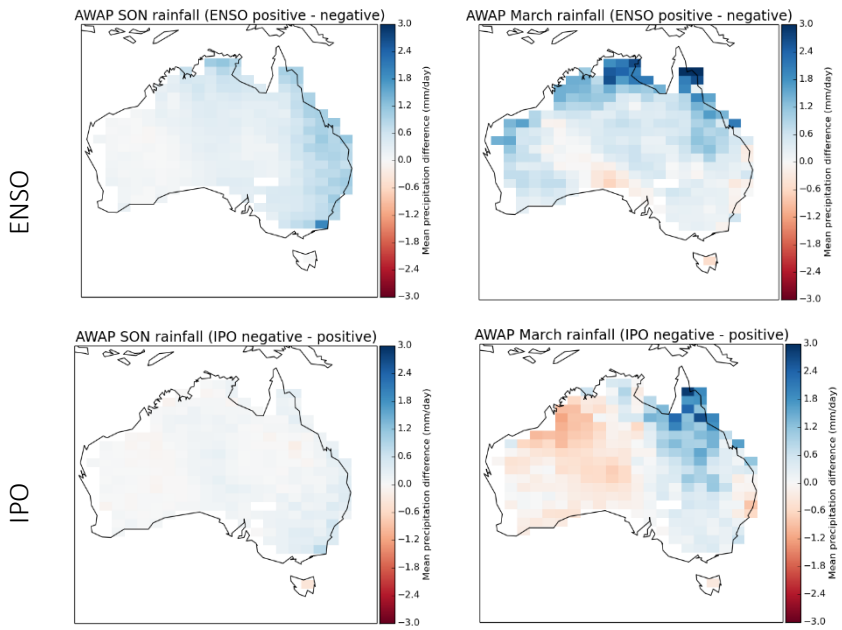

Figure 4.4: Differences in mean rainfall (mm day^{-1}) between the wet and dry states of ENSO (*upper images*) and the IPO (*lower images*). The left-hand images show these relationships in spring, and the right-hand images show these relationships in March (exemplifying the autumn relationship). Blue (positive) regions show areas in which the typical wet state (La Niña, IPO negative) produces more rain than the dry state. Red (negative) regions show areas in which the typical dry state (El Niño, IPO positive) produces more rain than the wet state.

[13] Neither of these correlation coefficients is statistically significant at the 95 per cent level; however, this does not mean a relationship is not exhibited between rainfall and the oscillations. Observe autumn in Figure 4.3.d—although it is not widespread, regions of Australia *do* show statistically significant relationships at the 95 per cent level. It is likely that these regions would be broader if the significance level was lowered (e.g. say, to 80 per cent—e.g. Risbey *et al.* (2011)), and would be more likely to reflect the lower-left (March) image in Figure 4.4.

4.3 Observations of ENSO, the IPO, and rainfall

There is a direct relationship between Niño 3.4 and the TPI (r = 0.34) that links El Niño (La Niña) events with positive (negative) phases of the IPO. Given the relationships between rainfall and the two indices explored in Sections 4.1 and 4.2, this suggests that both El Niño (La Niña) and the IPO negative (positive) states are associated with below-average (above-average) rainfall in eastern Australia. This correlation is moderate when compared with other relationships between climate drivers (e.g. ENSO and the IOD: r = 0.7; ENSO and SAM: r = –0.3; the IOD and blocking: r = –0.2) (Risbey *et al.* 2011). This may reflect the fact that the IPO is a secondary mode of low-frequency SST fluctuation in the tropical Pacific Ocean, whilst ENSO is the dominant mode (e.g. Power *et al.* 1999b; Arblaster *et al.* 2002; Parker *et al.* 2007). This study suggests that the Niño 3.4–TPI relationship may be stronger than was reported by Parker *et al.* (2007) (r = 0.22).

The Niño 3.4–TPI correlation peaks in May–July (r = 0.33–0.35) and is weakest in spring (r = 0.23). However, the joint Niño 3.4–TPI interaction has its strongest influence on rainfall between December and March (see Figure B in Appendix 2) (Klingaman *et al.* 2013). This suggests that some aspect of the relationship between ENSO, the IPO and rainfall is lagged by a period of approximately seven months. No lag is observed between Niño 3.4 and the TPI (see Figure C in Appendix 2), and as discussed in Sections 4.1 and 4.2, the Niño 3.4–rainfall (Australia-wide) and TPI–rainfall (eastern Australia) relationships are non-lagged. Thus the delay between the peak Niño 3.4–TPI correlation and peak rainfall is likely to be due to a lag in their joint relationship with rainfall.

The relationship between ENSO, the IPO, and rainfall reflects the interplay between the inter-annual and inter-decadal scales of the two oscillations, and is presented schematically in Figure 4.5; its nuances will be discussed for the remained of this chapter. When rainfall is stratified according to the states of ENSO and the IPO as defined by Trenberth (1997) and Henley *et al.* (2015), rainfall variability is influenced most strongly by the seasonally varying, inter-annual, higher-frequency ENSO. When rainfall is stratified according to states of ENSO and the IPO that are defined as ±2σ and ±3σ above the Niño 3.4 and TPI means, rainfall variability is influenced most strongly by the inter-decadal, lower-frequency IPO. This relationship suggests that the ENSO–IPO relationship *with rainfall* is non-linear.

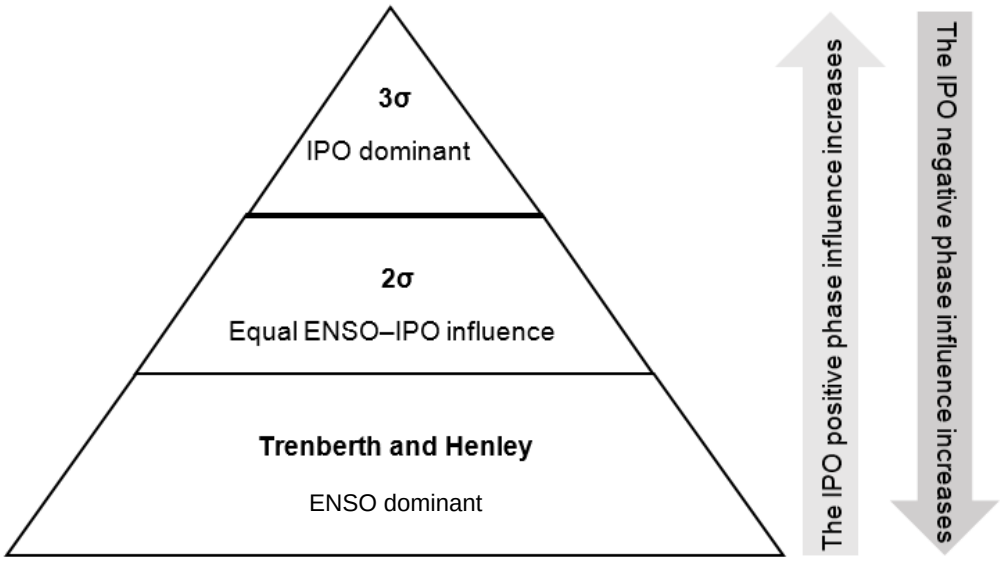

Figure 4.5: The relative impact of ENSO and IPO on rainfall. ENSO and IPO states are defined as more extreme at the top of the triangle, and as less extreme at the base of the triangle. In the case of 'Trenberth and Henley' rainfall (the base of the triangle; usually the least extreme rainfall), the states of the IPO and ENSO are defined according to Trenberth (1997) and Henley *et al.* (2015), and ENSO influences rainfall the most. The states for '2σ' rainfall (the middle of the triangle) are defined as ±2σ in relation to the mean of the Niño 3.4 and TPI indices. The states for '3σ' rainfall (the top of the triangle; usually the most extreme rainfall) are defined as ±3σ in relation to the mean of the two indices. '3σ' rainfall is influenced most by the IPO.

Variability in rainfall that tends to be less extreme—that is, rainfall stratified according to the ENSO and IPO states defined by Trenberth (1997) and Henley *et al.* (2015)—is influenced most strongly by ENSO. The clear ENSO signal is apparent in Figure 4.6.a: the ENSO negative state (El Niño) is associated with anomalously low rainfall and the ENSO positive state (La Niña) is associated with anomalously high rainfall. This is particularly clear in spring, the season of the strongest Niño 3.4–rainfall relationship (see Figure D1 in Appendix 2). The IPO negative state amplifies rainfall associated with the prevailing ENSO state; that is, the IPO tends to enhance rainfall (dryness) during La Niña (El Niño) years (see Figure 4.6.a). This relationship has been previously identified, and is particularly strong in La Niña years (Power *et al.* 1999a; Arblaster *et al.* 2002; Power *et al.* 2006; Parker *et al.* 2007; Cai and van Rensch 2012; King *et al.* 2013a). In contrast, the IPO positive state tends to moderate the effects of the dominant ENSO state; this effect has not been identified in the literature. The neutral state of the IPO shows the tendency of the IPO 'base' state to produce below-average rainfall. This predisposition to cause dryness has not yet been acknowledged, although the findings of this study support those of Kiem and

Franks (2004).[14] It is possible that the dryness associated with the IPO neutral state is associated with a weaker Pacific Ocean thermocline (see Section 5.5 for a discussion of this mechanism). These relationships are clearest in summer and autumn (see Figures D3 and D4 in Appendix 2), the seasons in which the TPI–rainfall correlation is strongest. Despite this, the stratification of rainfall according to ENSO states is the clearest rainfall pattern in the composite maps, and occurs in all seasons, which suggests that variability in ENSO (rather than variability in the IPO) affects rainfall variability the most.

Table 4.2.a presents the years in the study period stratified according to the nine combinations of the three ENSO and IPO states. Years stratified into the ENSO states align with those identified by Meyers *et al.* (2007). It is clear that the twentieth century was dominated by IPO positive years, suggesting that, overall, the IPO contributed to a reduction in mean Australian precipitation in the twentieth century. This is particularly likely as, of the 62 years identified as IPO positive, 49 were either ENSO neutral (in which the drying tendency of the IPO emerges) or negative ENSO (El Niño) events (characterised by drying). Note that some combinations of oscillation states occurred more frequently than others (e.g. maximum = 28 years (positive IPO–neutral ENSO), minimum = 4 (neutral IPO–positive ENSO combination)).

Fig. 4.6.a

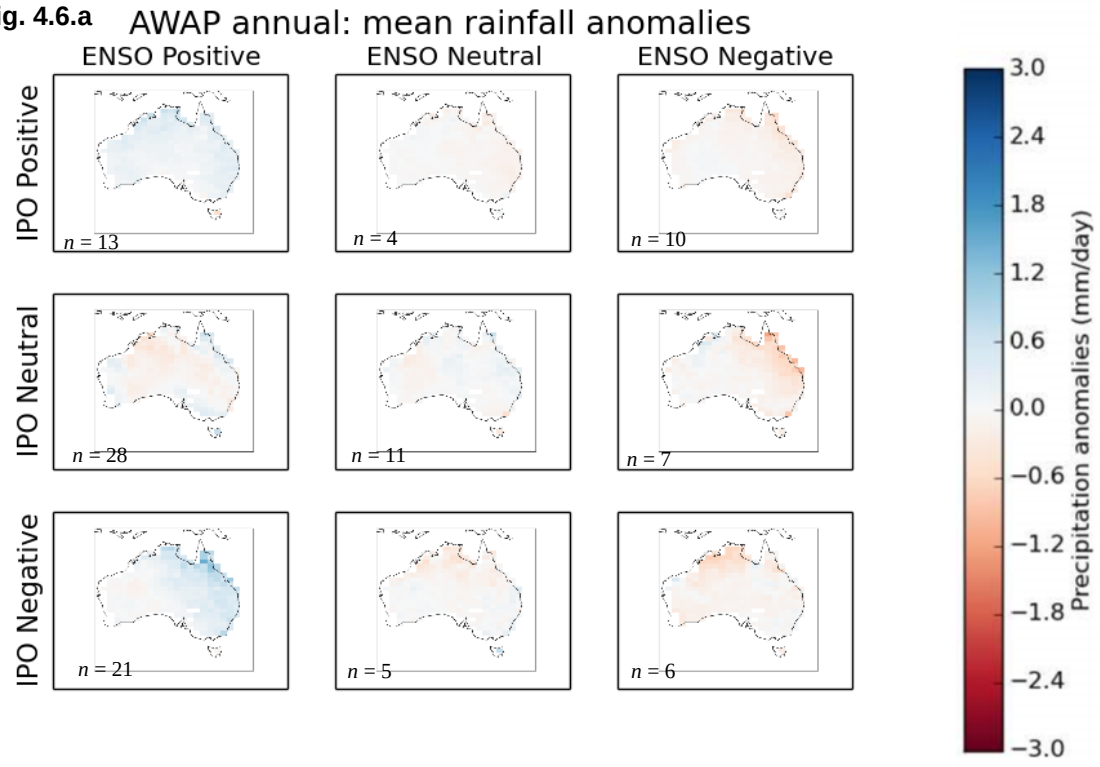

See overleaf for caption

[14] Kiem and Franks (2004) suggested that El Niño years that correspond with IPO positive years are less dry than El Niño years that correspond with IPO neutral and negative years (no comment was made on La Niña years).

Fig. 4.6.b

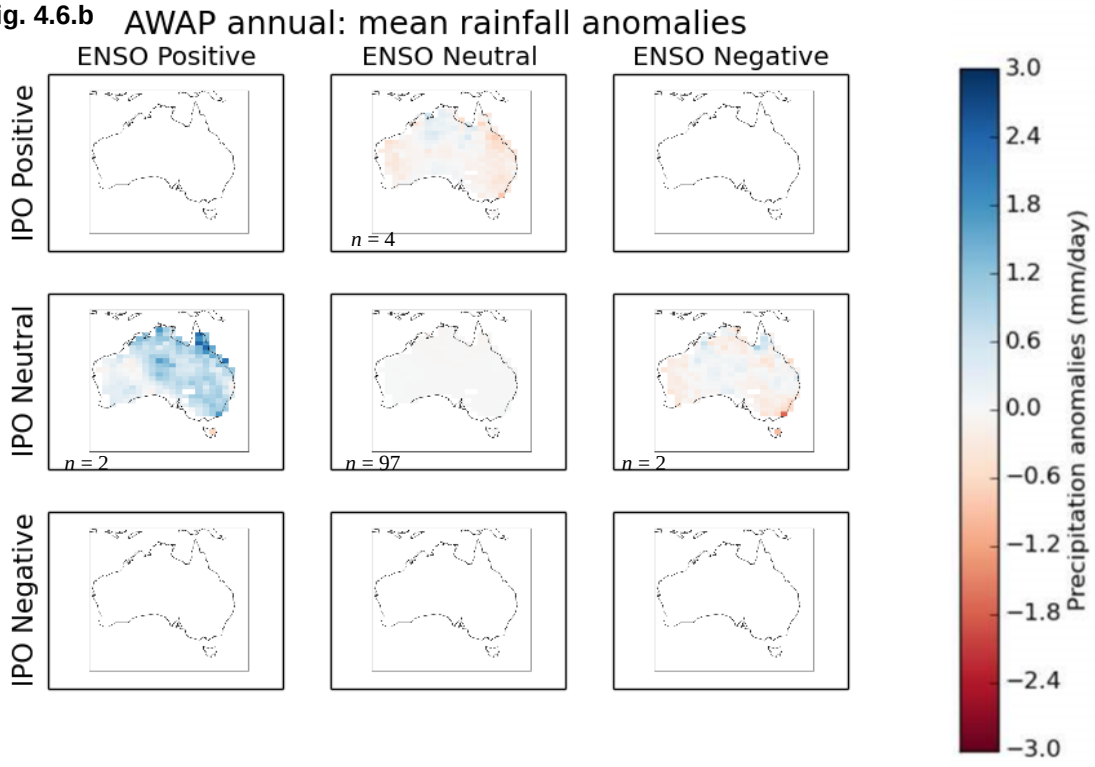

Fig. 4.6.c

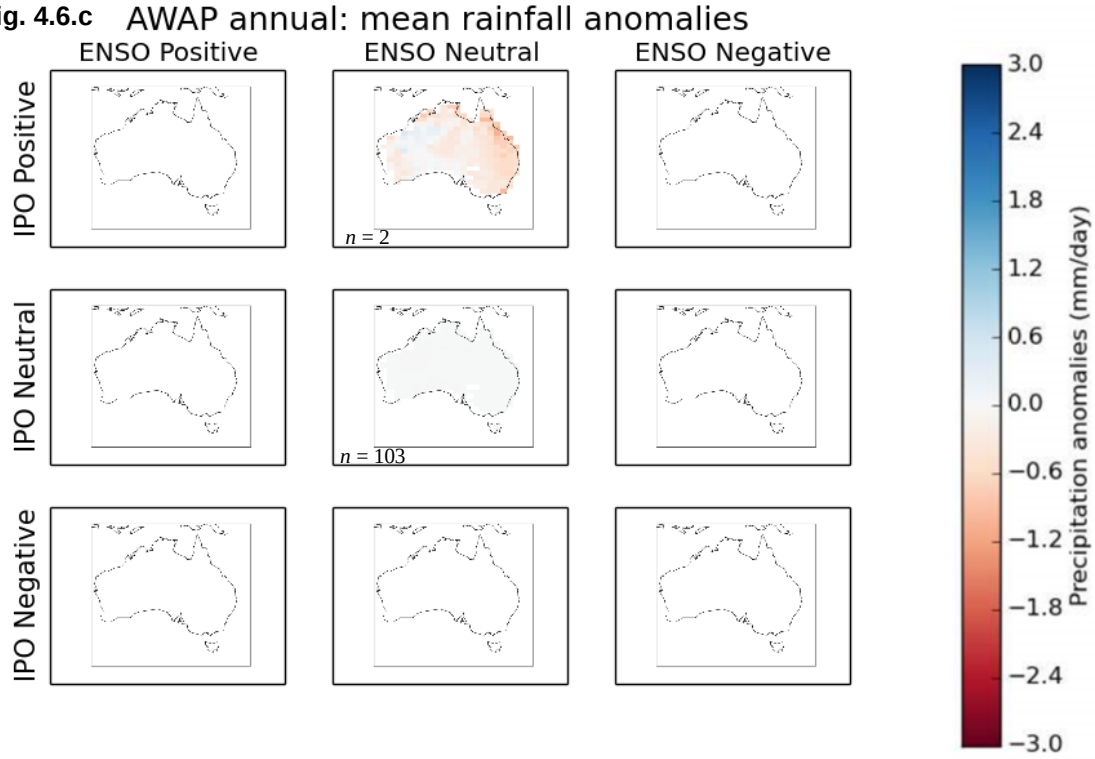

Figure 4.6: Mean annual precipitation anomalies (mm day^{-1}) for the nine combinations of the three ENSO and IPO states. *4.6.a* presents the results for ENSO and IPO states as defined by Trenberth (1997) and Henley *et al.* (2015). *4.6.b* presents results for ENSO and IPO states that have been defined according to ±2σ in relation to the mean of Niño 3.4 and the TPI, and *4.6.c* presents the similar results, but for ±3σ. '*n*' indicates the number of years in each stratification.

Whilst categories with fewer years may not yield statistically significant results (especially in the case of oscillation states defined as ±2σ or ±3σ above the index means) insights into the physical mechanisms underlying the ENSO–IPO interaction can still be proposed (in a similar manner to Meyers *et al.* (2007)).

Table 4.2: Years in the 1900–2005 study period corresponding with the nine combinations of the three ENSO and IPO states. *4.2.a* presents ENSO and IPO states as defined by Trenberth (1997) and Henley *et al.* (2015). *4.2.b* shows ENSO and IPO states that have been defined according to ±2σ ('moderately extreme' events: bold and non-bold entries) and ±3σ ('extreme' events: bold entries only) above the mean of the Niño 3.4 and TPI datasets. This reveals characteristics of the ENSO–IPO interaction in the strongest ENSO and IPO years.

Whilst the ±3σ IPO positive events occurred early in the observation record, and may therefore be influenced by data quality issues, it seems unlikely that this is the case, as Vance *et al.* (2015) show that the beginning of the twentieth century was characterised by a particularly strong IPO positive phase.

Table 4.2.a

Trenberth (1997) and Henley *et al.* (2015)	*Positive IPO*	*Neutral IPO*	*Negative IPO*
Positive ENSO	1903,1916, 1924, 1933, 1938,1942, 1983, 1984, 1985,1988, 1998, 1999, 2000	1908, 1909, 1910, 1964	1949,1950, 1954, 1955, 1956,1970, 1971, 1973, 1974, 1975
Neutral ENSO	1901,1906, 1915, 1917, 1919,1922, 1926, 1927, 1928,1929, 1931, 1932, 1934,1935, 1936, 1937, 1978,1979, 1980, 1981, 1989,1990, 1992, 1993, 1995, 1996, 2001, 2003	1907,1920, 1921, 1943, 1944,1945, 1960, 1961, 1962, 1966, 1967,	1946,1947, 1948, 1952, 1953, 1958, 1959
Negative ENSO	1900,1902, 1904, 1905, 1913,1914, 1918, 1923, 1925,1930, 1939, 1940, 1941,1982, 1986, 1987, 1991,1994, 1997, 2002, 2004	1911,1963, 1965, 1968, 1977	1951,1957, 1969, 1970, 1972, 1976

Table 4.2.b

±2σ and ±3σ	*Positive IPO*	*Neutral IPO*	*Negative IPO*
Positive ENSO	–	1973, 1988	–
Neutral ENSO	**1900, 1901,** 1902, 1903	**Remaining years**	–
Negative ENSO	–	1982, 1997	–

An interesting relationship is observed between ENSO, the IPO and precipitation anomalies that tend to be more extreme (both extreme dry and wet). In this case, 'extreme' rainfall is identified by defining ENSO and IPO events as two ('moderately extreme') and three ('extreme') standard deviations above the index means, and stratifying rainfall into the nine possible state-combinations (see Figures 4.6.b (±2σ) and 4.6.c (±3σ)). Rainfall in these categories is generally, but not always, more anomalous than rainfall stratified according to the definitions of Trenberth (1997) and Henley *et al.* (2015).

In the moderately extreme case, eight of the 105 study years were categorised as neither ENSO neutral nor IPO neutral, and in the extreme case, this number is reduced to two years. These are small sample sizes and inferences made here may be shown to not hold if, for example,

a longer rainfall record is examined; however, the observations made here may still represent real physical mechanisms and should be considered a useful preliminary analysis for further studies. Interpretation must be limited to less nuanced elements of the relationship amongst ENSO, the IPO, and rainfall. For example, in the case of moderately extreme ENSO and IPO events (the ±2σ case), rainfall is not influenced by ENSO in the IPO negative state. This contradicts the findings of King *et al.* (2013a), who concluded that it was *only* in the negative state of the IPO that ENSO exhibited a relationship with extreme rainfall. King *et al.* (2013a) seem to have identified the tendency of the IPO to amplify the effects of ENSO when rainfall is stratified according to less extreme ENSO and IPO states (discussed above); their study did not analyse details of how the relationship between ENSO, the IPO, and rainfall change as ENSO and IPO events become more extreme, and so the decreased influence of the IPO negative state on rainfall was not apparent. The ENSO–IPO interaction with rainfall variability is not apparent in the most extreme states (the ±3σ case). Figure 4.6.c and Table 4.2.b show that only the positive state of the IPO influences rainfall variability; there is no influence from ENSO.

The stratification of ENSO into El Niño and La Niña states is particularly clear in the moderately extreme (±3σ) case (e.g. Figure 4.6.b), and particularly so in summer, the season in which the strongest relationship between Niño 3.4, the TPI, and rainfall is observed (Figure 4.7; compare this with Figure 4.6.a). This suggests that the ENSO–IPO interaction with rainfall may be particularly clear in the moderately extreme (±3σ) case. All moderately extreme events in Table 4.2.b were identified by Reason *et al.* (2000) as 'protracted' ENSO events (except for 1997, which was outside of the study period, and 1901). Allan *et al.* (2003) linked protracted ENSO events with a quasi-decadal (9–13 year) signal, resulting from quasi-biennial, ENSO, and decadal signals. Meinke *et al.* (2005) suggest that this quasi-decadal signal may be affected by modulations within the IPO; therefore, it is possible that this is the same intra-decadal eight-year signal identified in the IPO–rainfall cross correlation analysis (see Section 4.2 and Figure 4.2). If this is so, this suggests that the strongest relationship between ENSO and the IPO might be observed at this quasi-decadal scale; this appears to be supported by the disappearance of the ENSO influence in the most extreme events (i.e. the ±3σ case). Note, however, that whilst all moderately extreme or extreme ENSO events are 'protracted' ENSO events, not all 'protracted' ENSO events are moderately extreme or extreme ENSO events. Analysis of the results of Reason *et al.* (2000) suggests that the 'missing' protracted ENSO events which are *not* moderately extreme or extreme occur during the IPO negative state. This suggests that the role of the negative IPO state in modulating rainfall associated with ENSO becomes increasingly weak as rainfall becomes more extreme (as presented schematically in Figure 4.5).

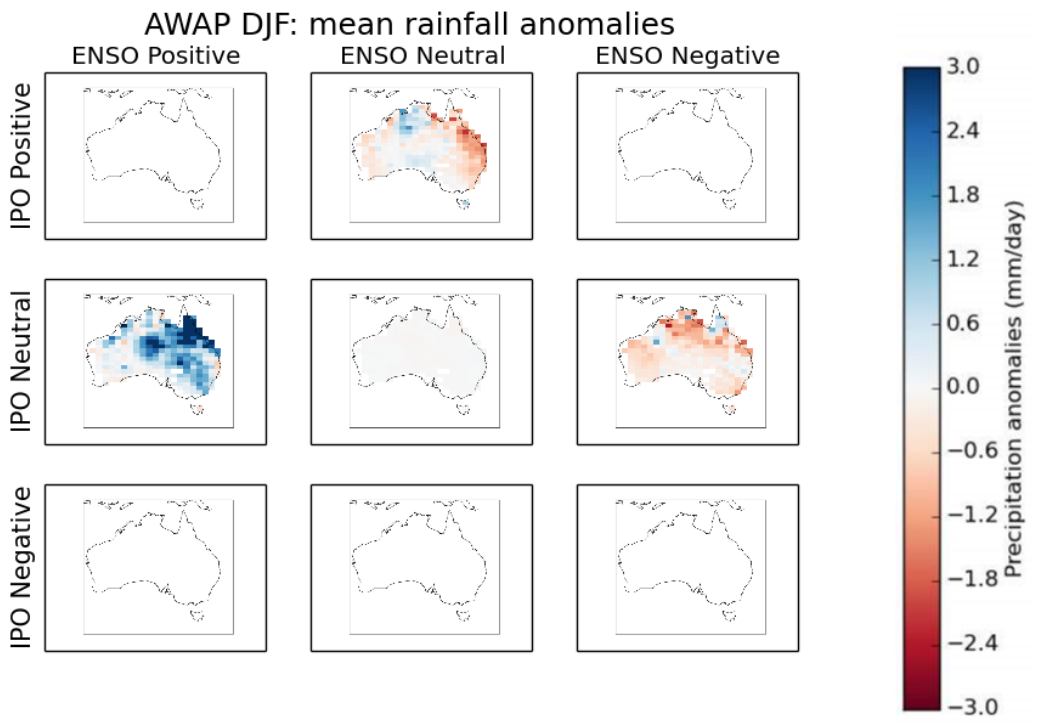

Figure 4.7: Mean summer precipitation anomalies (mm day^{-1}) for the nine combinations of the three ENSO and IPO states, where states have been defined according to ±2σ above the means of Niño 3.4 and the TPI.

4.4 Chapter summary

The relationship identified in this study between ENSO and rainfall corresponds with the conclusions of past studies. The strongest correlation between ENSO and rainfall is in spring; this relationship extends across eastern and central Australia. The relationship is strongest in coastal areas and in lower-latitude areas (e.g. Queensland). At the regional scale, differences in seasonality and the strength of the ENSO–rainfall relationship suggest that as the influence of ENSO decreases, and the influence of synoptic-scale features increases.

The correlations between IPO and rainfall are not as strong as those between ENSO and rainfall. The seasonality of the IPO and the region of its influence on rainfall is distinct from that of ENSO. The IPO–rainfall teleconnection is limited much more clearly to eastern Australia, although it appears to also exert influence on rainfall over northern-central Australia. The IPO influences rainfall in higher-latitude, coastal regions, and exhibits its strongest and broadest correlation with rainfall in summer, yet has a greater relative influence on autumn rainfall (when the ENSO teleconnection is weakest). When the IPO neutral state is accounted for, the number of phases in the twentieth century increases; it is possible that this is a result of an intra-decadal component of the IPO that appears to cycle every eight years, and which may be a mechanism through which the IPO and ENSO interact. The IPO appears to cycle every 60–80 years, which is longer than previously identified.

The relationship between ENSO, the IPO and rainfall reflects the interplay between the inter-annual and inter-decadal properties of the two oscillations. ENSO influences rainfall most

strongly that has been stratified according to the ENSO and IPO states identified by Trenberth (1997) and Henley *et al*. (2015). The negative state of the IPO amplifies ENSO rainfall variability, and the positive state of the IPO attenuates ENSO rainfall variability. The neutral state of the IPO leads to an overall reduction in rainfall. The negative state of the IPO does not influence rainfall when oscillation states are stratified as ±2σ in relation to the index means. Only the IPO positive state influences rainfall when oscillation states stratified as ±3σ above the index means. In contrast to prior thinking, these findings show that the IPO positive state affects both the ENSO relationship with rainfall, and influences rainfall in its own right. The ENSO–IPO relationship is nuanced; the following chapter will examine how well the ACCESS model captures these complexities.

Chapter 5: Simulations of ENSO, the IPO, and Rainfall Variability

This chapter investigates how well ACCESS1.3 simulates the relationships identified in Chapter 4 amongst ENSO, the IPO, and rainfall variability. To assess how well ACCESS1.3 simulates the long-term drivers of rainfall variability the analysis largely follows the same structure as the previous chapter, but begins with a discussion of current knowledge of precipitation simulation in the ACCESS1.3 GCM. This is followed by an analysis of the simulated relationship between ENSO and rainfall, and between the IPO and rainfall. The accuracy with which the ACCESS1.3 GCM simulates rainfall variability associated with the ENSO–IPO interaction is explored.

5.1 Current knowledge of ACCESS1.3 rainfall variability simulations

Throughout this chapter the three ensemble members of the ACCESS1.3 historical experiment are referred to as ACCESS R1 (r1i1p1), ACCESS R2 (r2i1p1) and ACCESS R3 (r3i1p1). The ensemble members are examined individually, as the ensemble size is not large enough to perform a statistically meaningful joint analysis. The historical ensemble mimics atmospheric and oceanic conditions of the twentieth century, but does not attempt to *match* unforced variability detected in observations (Taylor *et al.* 2012). This means that the model attempts to simulate the observed properties of unforced variability (returning, say, an equivalent number of ENSO positive and negative years to observations) but will not simulate the timing of observed events.

Research by Lewis and Karoly (2014) concluded that ACCESS1.3 simulations of historical average rainfall trends are comparable with those of other CMIP5 models. All ensemble members simulated the observed decrease in global land surface mean precipitation from 1950–2005. However, observed rainfall variability is slightly higher in observations (σ = 0.05–0.06 mm day^{-1}) than in ACCESS1.3 (σ = 0.045 to 0.05 mm day^{-1}), which further suggests that ACCESS1.3 is not detecting all elements affecting rainfall variability. The greatest uncertainty in ACCESS1.3 is in simulated rainfall variability at the regional and local scales (Lewis and Karoly 2014). Early studies of the (pre-ACCESS1.0) ACCESS model found that it performed poorly in simulating some aspects of Australian regional climate, such as winter rainfall caused by fronts, leading to dry biases of up to 2 mm day^{-1} during winter and spring (Brown *et al.* 2010). Risbey *et al.* (2011) identified that ACCESS–AMIP runs under-represented eastern Australian summer rainfall; this may reflect poor incorporation of the summer ENSO–IPO interaction. More recently, Bi *et al.* (2013) found that ACCESS1.3 overestimates mean precipitation over eastern and central Australia (by approximately 0.4 mm day^{-1}), and underestimates tropical and Tasmanian mean rainfall (by approximately –1.0 mm day^{-1}). Coastal eastern Australian mean rainfall is also underestimated (by approximately –0.2 mm day^{-1}). These differences are thought to be due to suboptimal simulations of oceanic SSTs, suggesting that some elements of the ENSO or IPO

(oscillations that are tightly coupled to changes in SSTs) may be misrepresented (Bi *et al.* 2013; Dix *et al.* 2013).

The limitations of the rainfall and rainfall variability simulations produced by ACCESS1.3 are foreshadowed by its inability to correctly simulate the observed non-normal statistical distribution of rainfall (see Table 5.1). All three ACCESS1.3 ensemble members consistently fail to capture the observed distribution at annual and seasonal scales, except in spring. Whilst the model reproduces the skewed distribution of rainfall in some months, it does not do so for the February–May period (in which the IPO signal and the ENSO–IPO interaction are strongest). Additionally, ACCESS1.3 successfully captures the normality of Niño 3.4, and largely captures the normality of the TPI, except for in ACCESS R3 in the February–May period (see Table C in Appendix 2).

Table 5.1: The p-values associated with the normality of each rainfall dataset (observed = AWAP, r1i1p1 = ACCESS R1, r1i1p1 = ACCESS R2, r1i1p1 = ACCESS R3). P-values that are statistically significantly non-normal ($p \leq 0.05$) are presented in bold.

	AWAP	***ACCESS R1***	***ACCESS R2***	***ACCESS R3***
Annual	**0.00**	0.95	0.58	0.66
JJA	0.18	0.32	0.16	**0.00**
SON	**0.01**	**0.01**	**0.00**	**0.00**
DJF	**0.00**	0.91	0.14	**0.02**
MAM	**0.00**	0.83	0.35	0.84
June	**0.03**	**0.02**	**0.01**	**0.02**
July	**0.00**	**0.00**	**0.04**	**0.00**
August	**0.00**	0.21	0.05	0.06
September	**0.00**	0.11	0.08	**0.03**
October	**0.00**	**0.00**	**0.00**	**0.00**
November	**0.01**	**0.02**	**0.00**	**0.00**
December	0.17	**0.00**	**0.00**	**0.00**
January	**0.00**	**0.00**	0.54	**0.02**
February	**0.03**	0.32	0.82	0.74
March	0.32	0.87	0.88	0.82
April	**0.00**	0.99	0.34	0.25
May	**0.00**	0.33	0.74	0.18

5.2 Simulation of ENSO and rainfall

In previous work, ACCESS1.0 and ACCESS1.3 were assessed for their representation of ENSO, and it was concluded that both versions of the model adequately simulated key components of ENSO (such as SST and wind stress) (Rashid *et al.* 2013). It is unsurprising that ACCESS1.3 simulates a continent-wide teleconnection between Niño 3.4 and rainfall: annual correlation coefficients for the Niño 3.4–rainfall relationship are comparable (observed: $r = –0.53$; modelled: $r = –0.52$ to $–0.69$). However, the modelled teleconnection becomes less strong when analysed at smaller temporal or spatial scales. A comparison of Tables A1 and D (in Appendix 2) shows that ACCESS R2 and ACCESS R3 have difficulty modelling Niño 3.4 seasonality and regional teleconnections with rainfall. Regional variability within ACCESS1.3 appears to be random. For

example, all three ensemble runs show no consistent pattern in their attribution of stronger or weaker correlations to different climate zones (see Table D in Appendix 2). Figure 5.1 shows differences in rainfall across Australia between La Niña and El Niño years, for observations and simulations; the simulated rainfall is clearly less variable and less-well represented in eastern Australia than in observations. This conforms with the research of Rashid *et al.* (2013), who concluded that the greatest limitation of ACCESS1.3 is the weakness of its rainfall teleconnection over eastern Australia. However, it appears that rainfall variability in Australia is also inadequately simulated over the remainder of the continent, as ACCESS1.3 overestimates the extent of ENSO's influence on rainfall (e.g. Figure 5.2). ACCESS1.3 does not appear to fully capture the processes driving the relationship between ENSO and Australian rainfall.

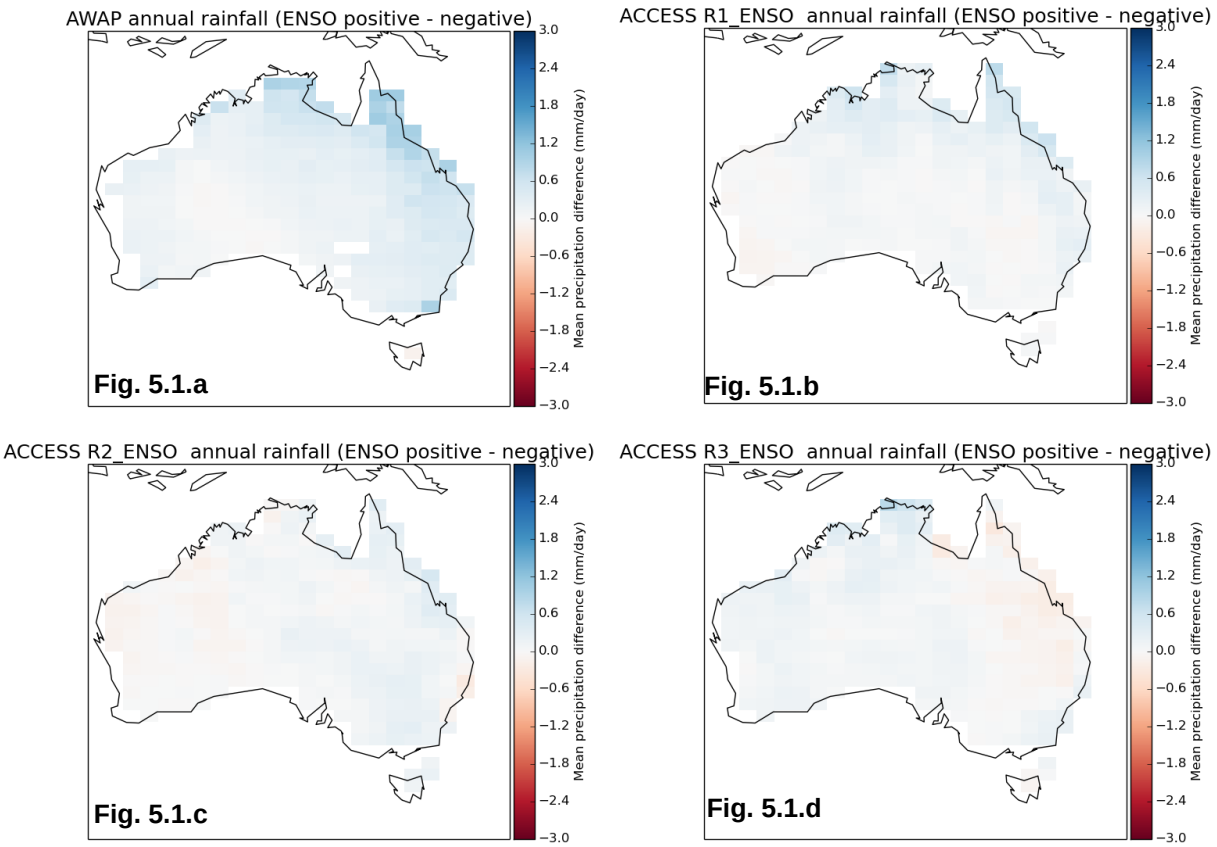

Figure 5.1: Differences between mean annual precipitation (mm day^{-1}) in El Niño years and La Niña years (as defined by Trenberth (1997)). *5.1.a*: observations (AWAP); *5.1.b*: ACCESS R1; *5.1.c*: ACCESS R2; *5.1.d*: ACCESS R3.

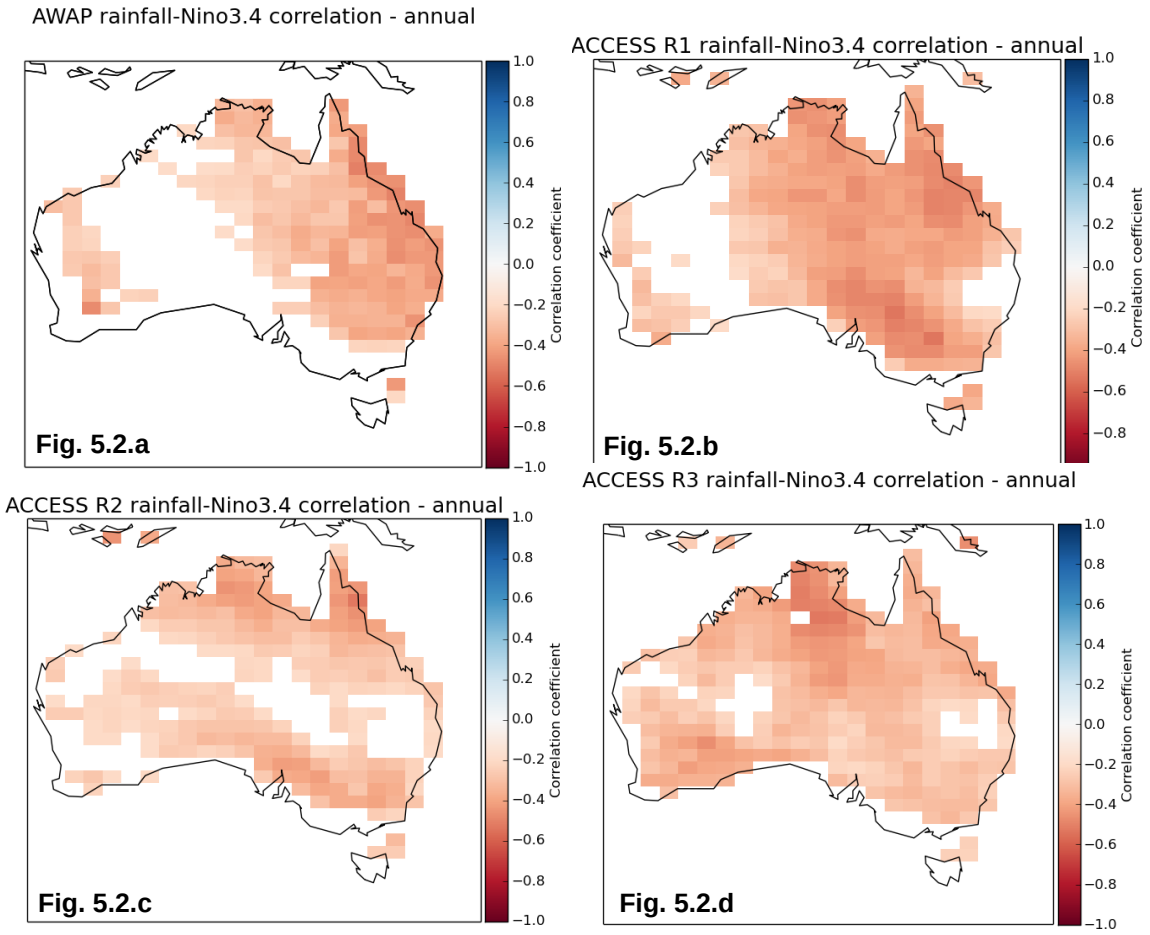

Figure 5.2: Annual correlation coefficients (*r*) for the relationship between Niño 3.4 and mean rainfall. *5.1.a*: observations (AWAP); *5.1.b*: ACCESS R1; *5.1.c*: ACCESS R2; *5.1.d*: ACCESS R3.

Observations of the Niño 3.4 index show increases in its variability towards the end of the twentieth century, when more frequent and extreme ENSO events occurred, particularly in spring and summer (see Figure 5.3.a). These findings support those of Cai *et al.* (2014), who attribute the recent changes in ENSO variability to greenhouse warming-induced changes to the centres of atmospheric convection. However, these increases are not apparent in the ACCESS1.3 simulations (see Figure 5.3.b). It may be that ACCESS1.3 does not simulate these convection changes adequately, which could be contributing to poor simulations of ENSO-related rainfall variability.

None of the simulated cross correlations between Niño 3.4 and rainfall exhibit the same lag pattern as that found in observations (compare Figures 5.4.a and 5.4.b). In observations, an underlying lag of 60–70 years is observed, which may signal the IPO. However, the ensemble runs falsely identify a lag of 25 years between ENSO and rainfall. It is possible that ACCESS1.3 is attributing shifts in rainfall variability to this false 25-year cycle, rather than the IPO.

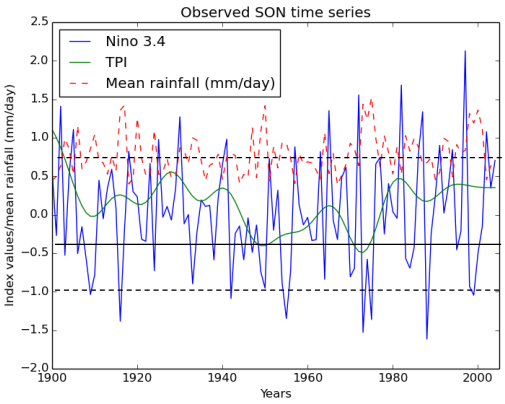

Fig. 5.3.a

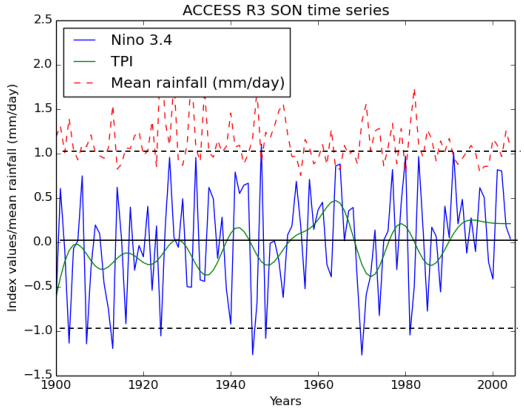

Fig. 5.3.b

Figure 5.3: These time-series figures present Niño 3.4 values (blue) throughout the study period. The TPI is shown in green, and mean rainfall (mm day^{-1}) is shown in dashed red. The observed spring time-series is presented in *5.3.a*, and the simulated time-series (ACCESS R3) is presented in *5.3.b*. The time-series show how observed Niño 3.4 values are increasing and becoming more frequent with time (in relation to the dashed lines at ±1.0), whereas modelled time-series values are not.

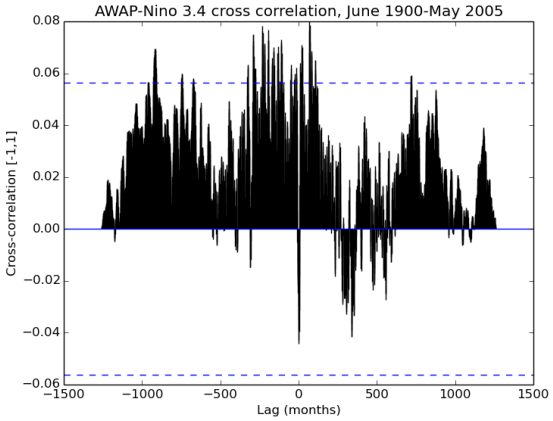

Fig. 5.4.a

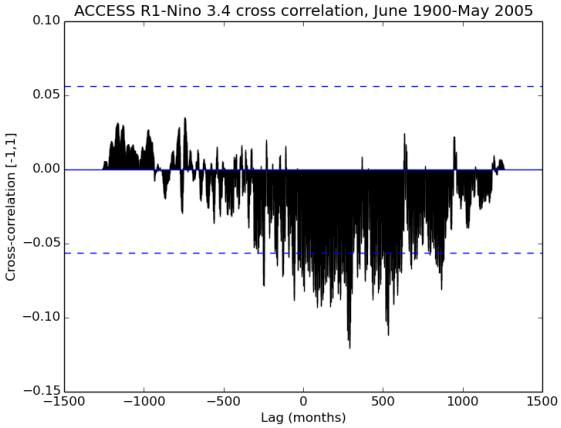

Fig. 5.4.b

Figure 5.4: Cross correlation between observed (*5.4.a*) and modelled (ACCESS R1) (*5.4.b*) Australia-wide average monthly rainfall and Niño 3.4. The lagged correlation between each of the 1260 months in the study (June 1900 to May 2005) is presented. The 95 per cent confidence interval is indicated by the dashed blue lines. Although the observed lag correlations are very small, a clear negative correlation is visible at time zero (suggesting there is no lag between rainfall and Niño 3.4). For all other times, a positive correlation exists, which appears cyclical and seems to repeat every 60–70 years. It is likely that this is an expression of the inter-decadal modulation of ENSO by the IPO. This is not replicated in ACCESS1.3.

5.3 Simulation of the IPO and rainfall

ACCESS1.3 'captures' elements of the IPO signal, in as much as IPO indices can be generated from its SST values, and analyses can be performed on such an index that show apparent relationships with rainfall or ENSO. However, it appears that, in actuality, ACCESS1.3 simulates the IPO poorly.

For example, Figure 5.5.a shows that ACCESS1.3 produces a clear TPI signal, which appears to have desired characteristics: it cycles on decadal to multi-decadal scales, and shows both positive and negative phases of reasonably comparable magnitude to those in observations (Figure 5.5.b). However, closer inspection reveals that the frequency of IPO events is higher in ACCESS1.3 (ten positive and negative phases) than in observations (five positive and negative phases), and the variance of the events is reduced. ACCESS1.3 consistently produces far more negative than positive IPO years compared to observations (observations: positive = 62 years, negative = 22 years; simulations: positive = 13–32 years, negative = 47–65 years) (see Table E in Appendix 2). It appears that ACCESS1.3 is only simulating the ENSO-like component of the IPO—its negative state.

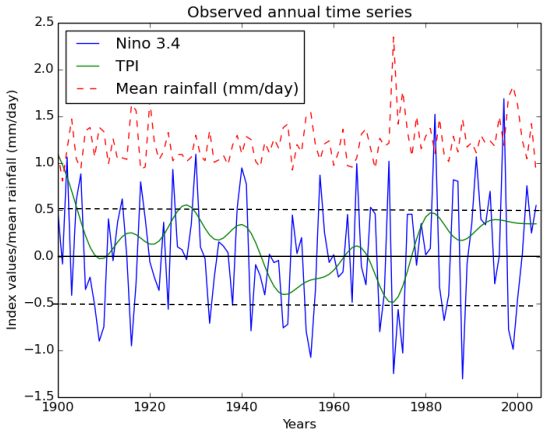

Fig. 5.5.a

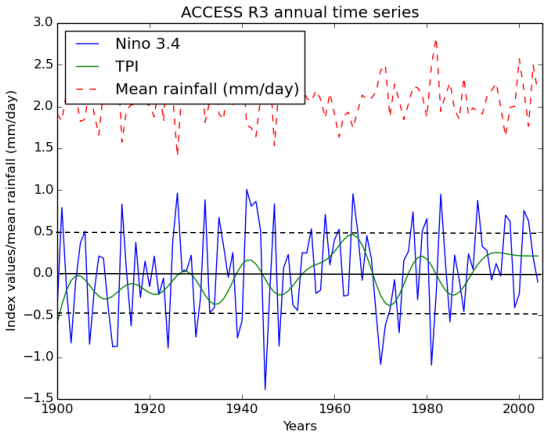

Fig. 5.5.b

Figure 5.5: Values for the TPI (green) in observations (*5.5.a*) and in ACCESS R3 (*5.5.b*). Niño 3.4 values are shown in blue, and mean rainfall (mm day^{-1}) is shown in dashed red. The observed TPI values show three (or five, if counting conservatively) distinct phase shifts around zero (solid line), whereas the modelled TPI values show eight (or ten, if counting conservatively) phase shifts. The observed TPI values show greater variance; they more frequently approach the ±0.5 lines (dotted).

The ACCESS1.3 ensemble members do not correctly simulate the observed cross correlation relationship between rainfall and the TPI (compare Figure 4.2 with Figure H in Appendix 2). The model simulates cross correlations as negative, and overestimates their magnitudes. The simulations detect neither the underlying eight-year quasi-decadal cycle identified in Figure 4.2, nor the underlying inter-decadal cycle. It appears that ACCESS1.3 is not simulating the processes driving changes in the TPI.

The strength of the annual eastern Australian correlation between the TPI and rainfall is underestimated in simulations (observations: r = –0.35; simulations: r = –0.13 to –0.23), and only ACCESS R1 detects this correlation as statistically significant. Additionally, although ACCESS1.3 simulates a stronger relationship between the TPI and rainfall in eastern Australia than in Australia, it is still weaker than the observed relationship (difference between Australian and eastern Australian observations: +0.16; ACCESS1.3: +0.02 to +0.07; compare Tables A2 and

F in Appendix 2). The strength of the spring TPI–rainfall correlation is overestimated in ACCESS R2 and R3, and the summer and autumn relationship (which shows a particularly strong negative correlation in observations) is underestimated (compare Tables A2 and F in Appendix 2). ACCESS1.3 seems unable to simulate the TPI. ACCESS1.3 has difficulty in replicating the distribution of TPI-influenced rainfall in the various climatic zones. ACCESS1.3 overestimates the influence of the TPI in lower latitudes (Table F in Appendix), and does not replicate the influence of the TPI on eastern Australian coastal, higher-latitude rainfall (e.g. Figure 5.6). ACCESS1.3 struggles to correctly capture the interaction between the TPI and rainfall.

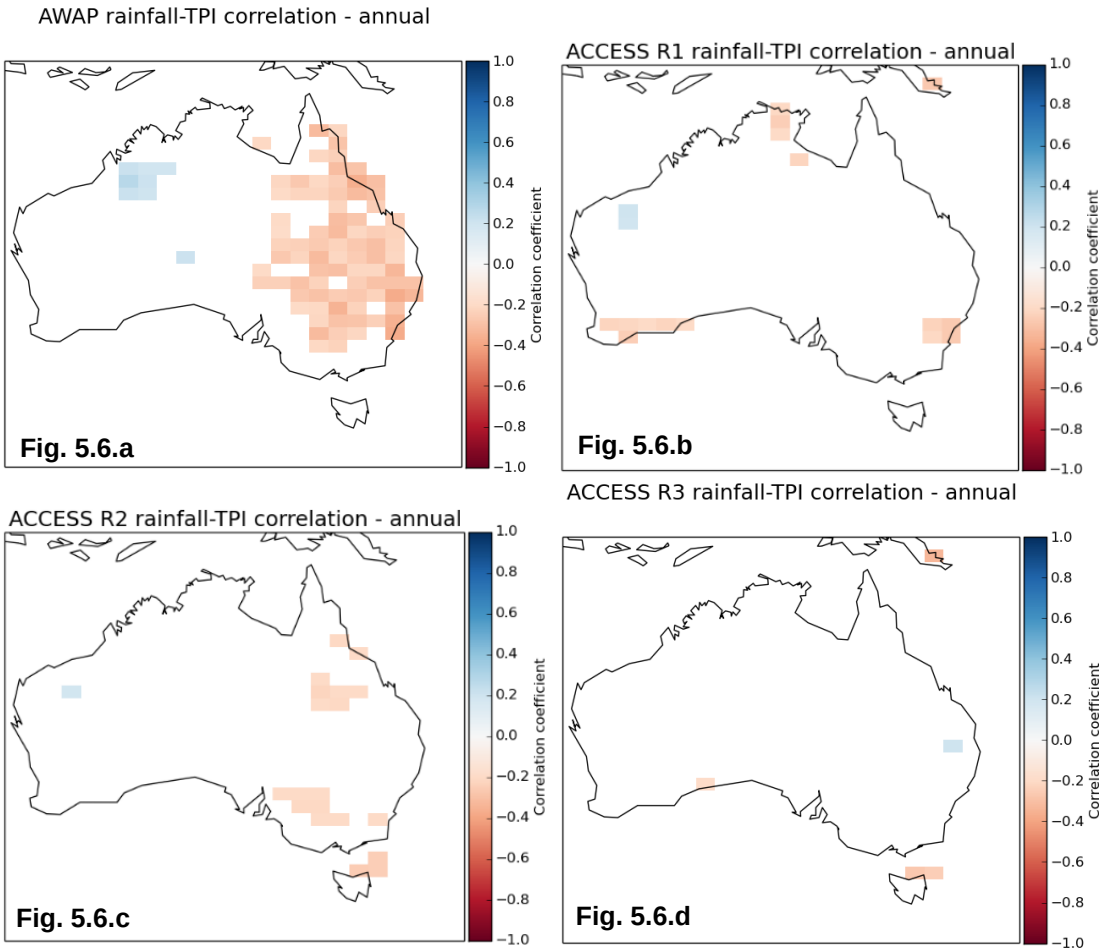

Figure 5.6: Correlation coefficients (*r*) for the annual relationship between the TPI and mean rainfall. *5.6.a*: observations (AWAP); *5.6.b*: ACCESS R1; *5.6.c*: ACCESS R2; *5.6.d*: ACCESS R3.

5.4 Simulations of ENSO, the IPO, and rainfall

ACCESS1.3 appears to simulate the Niño 3.4–TPI relationship at the annual and continental scales. For example, annual correlations between Niño 3.4 and the TPI are weaker than observed, yet still reasonable (observed: $r = 0.34$; simulated: $r = 0.23$–0.28). However, further examination of this relationship in the model simulations at the seasonal scale shows that the strongest correlations in ACCESS1.3 occur in spring, the season in which observed Niño 3.4–rainfall correlations are strongest, and that the correlations are lowest in summer and autumn, the season

of observed peak Niño 3.4–TPI interaction (see Figure 5.7; compare Figures 5.8 and 5.9). This suggests that ACCESS1.3 is not, in fact, modelling the Niño 3.4–TPI relationship with rainfall; rather, it simulates the IPO as an ENSO-like phenomenon which also peaks in spring.

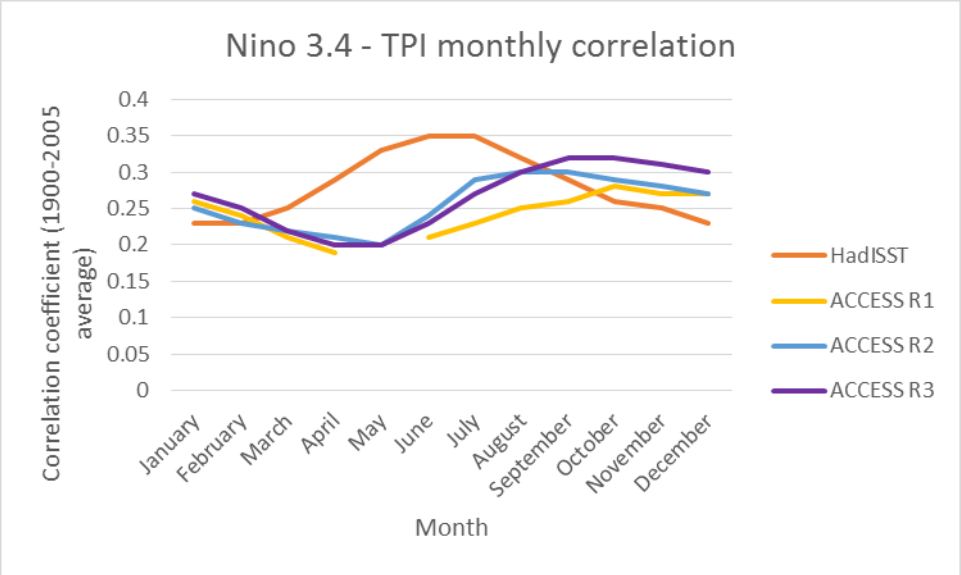

Figure 5.7: Monthly correlation coefficients (*r*) of the relationship between Niño 3.4 and the TPI, for both observed SST data (HadISST), and the three rounds of modelled SST data (ACCESS R1, ACCESS R2 and ACCESS R3). The exact monthly values, as well as the seasonal and annual correlation coefficients, can be viewed in Table B in Appendix 2.

Closer observation of Figure 5.8.b shows that ACCESS1.3 does not simulate the relationship between ENSO, the IPO, and rainfall when the oscillation states are defined according to Trenberth (1997) and Henley *et al.* (2015). Neither the observed amplification of ENSO in the IPO negative state, nor the observed attenuation of ENSO in the IPO positive state, is simulated. The neutral IPO state does not exhibit the observed decrease in precipitation. In fact, ACCESS1.3 does not appear to be discriminating the differences in rainfall between the IPO states. Once again, in summer (the peak season of the observed ENSO–IPO interaction), these relationships are visible in observations but not in the model (compare Figures 5.9.a and 5.9.b). ACCESS1.3 appears to be substituting the IPO interaction with ENSO with random synoptic elements (e.g. an increase in simulated rainfall in northern Australia, which ACCESS1.3 appears to be attributing to the monsoon (Figure 5.9.a)). Although ACCESS1.3 simulates Niño 3.4 reasonably well (see Section 5.2), it does not appear to simulate differences in rainfall during the different Niño 3.4 states, such as the tendency of La Niña extremes to be more pronounced than El Niño extremes (e.g. Power *et al.* 2006; King *et al.* 2013a). It is possible that nonlinearities within ENSO may be more closely influenced by the IPO than previously recognised.

Whilst the number of simulated extreme events is low (see '11. Count of years in ENSO and IPO stratifications' in Appendix 3) and conclusions therefore cannot be drawn with statistical certainty, it appears that the simulation by ACCESS1.3 of rainfall stratified according to extreme

Fig. 5.8.a AWAP SON: mean rainfall anomalies

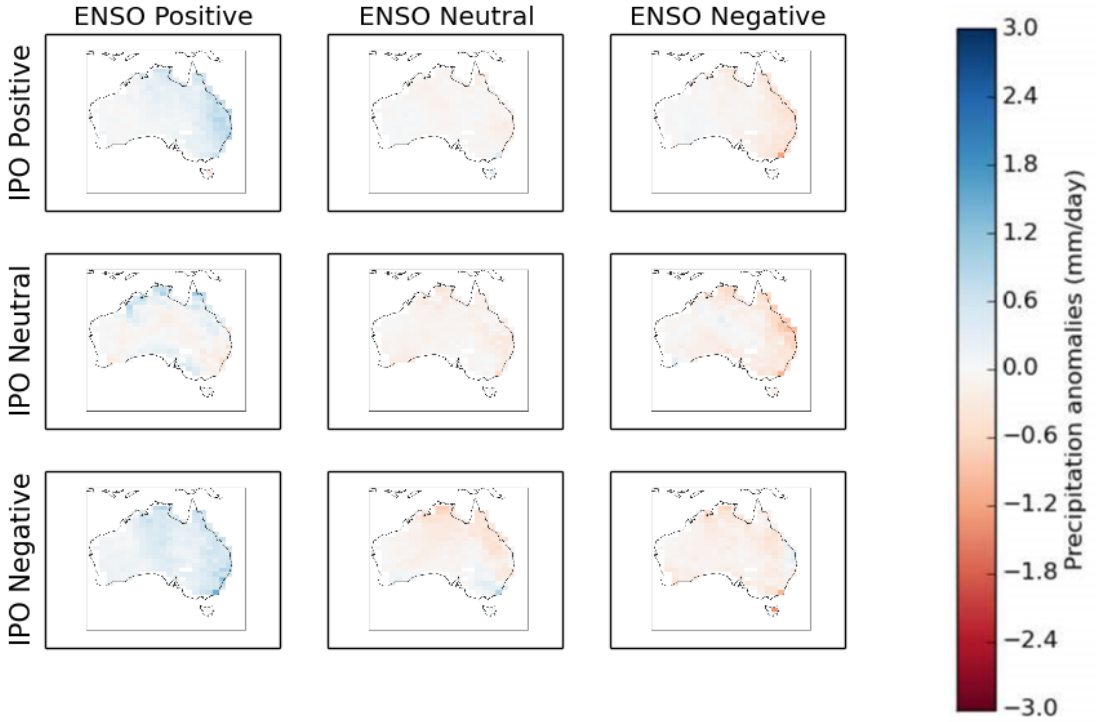

Fig. 5.8.b ACCESS1.3 R1 SON: mean rainfall anomalies

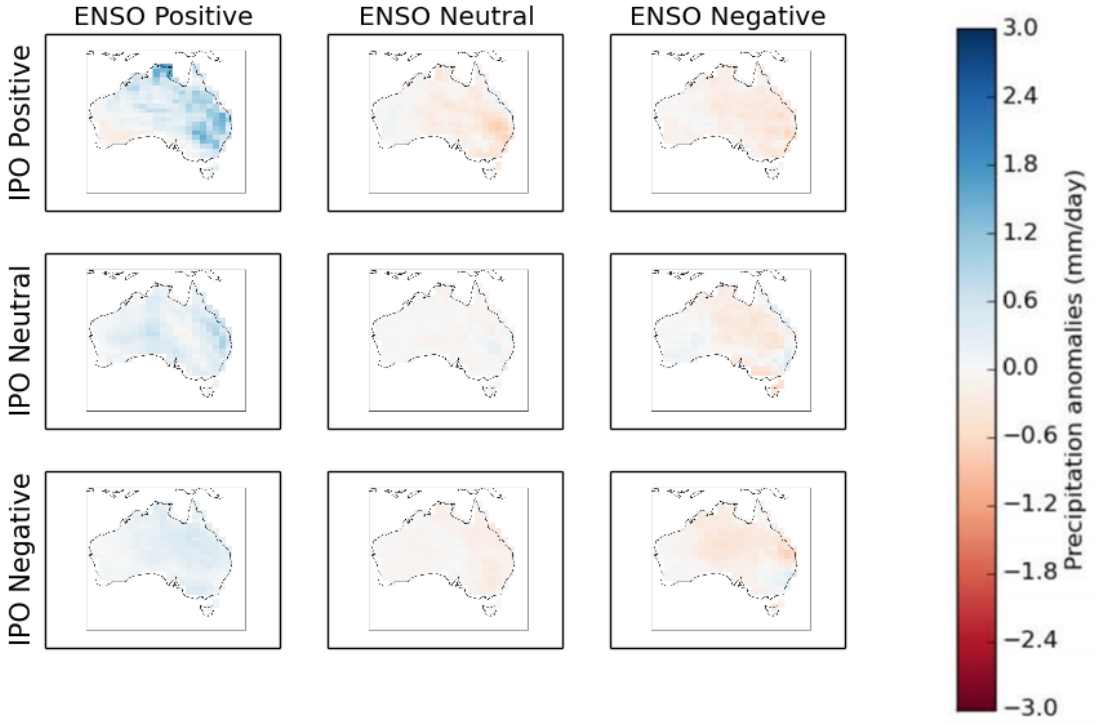

Figure 5.8: Composite maps of spring precipitation anomalies (mm day^{-1}) stratified according to the states of ENSO and the IPO (states defined by Trenberth (1997) and Henley *et al.* (2015)). *5.8.a* shows the composite map for observations, and *5.8.b* shows the composite map for ACCESS R1.

Fig. 5.9.a AWAP DJF: mean rainfall anomalies

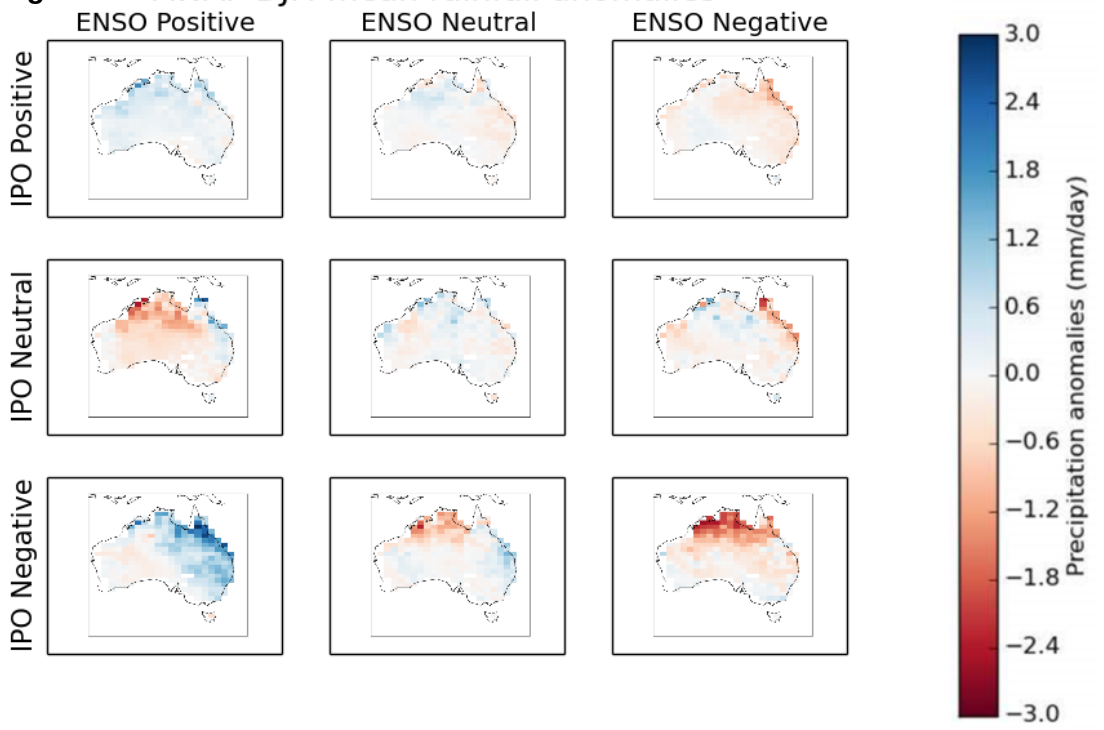

Fig. 5.9.b ACCESS1.3 R1 DJF: mean rainfall anomalies

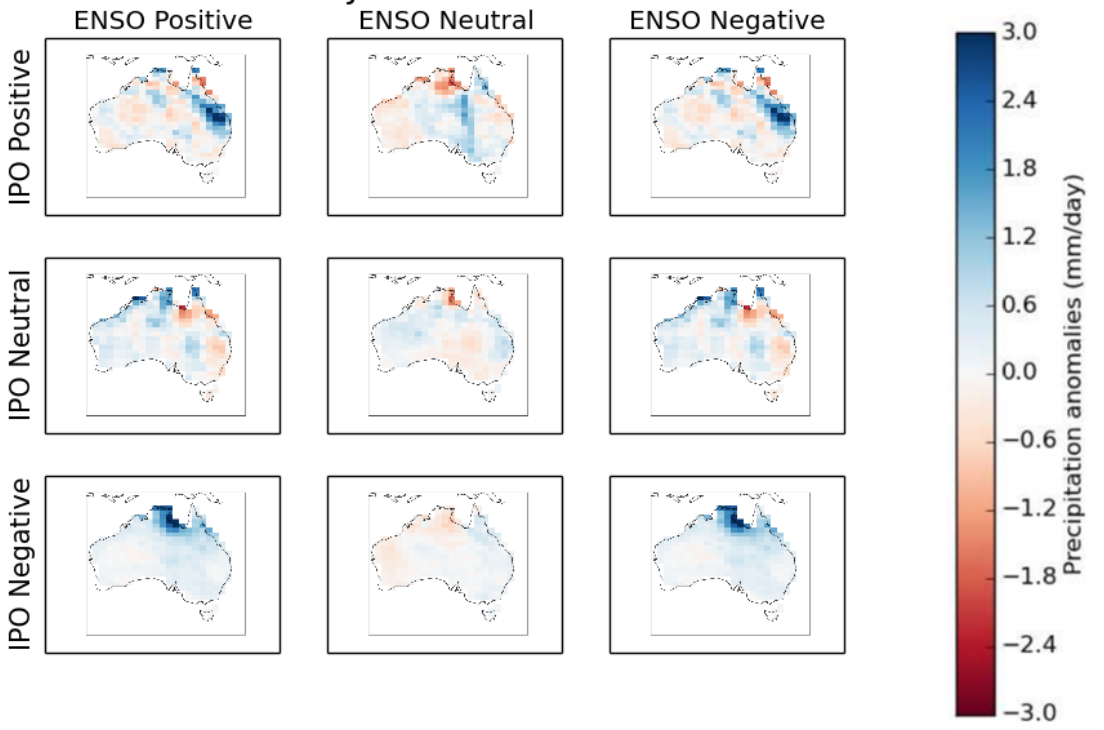

Figure 5.9: As for Figure 5.8, but for summer. *5.9.a* shows the composite map for observations, and *5.9.b* shows the composite map for ACCESS R1.

ENSO and IPO states is poor. All ensemble members falsely identify a relationship between rainfall and the negative state of the IPO in the moderately extreme (±2σ) case (e.g. Figure G in Appendix 2). Overall, ACCESS1.3 underestimates the frequency of moderately extreme IPO positive events, and overestimate the frequency of moderately extreme negative events (Table E in Appendix 2). Attribution of rainfall to the extreme (±3σ) ENSO and IPO states appears to be largely random (compare images for the ±3σ case in '14. Composite maps' in Appendix 3). In the cases where ACCESS1.3 does simulate rainfall in the extreme ENSO and IPO states, it is attributed solely to ENSO, contradicting observations (Table E in Appendix 2). The tendency of ACCESS1.3 to overestimate the frequency of rainfall occurring in the moderately extreme case and attribute it to non-positive IPO states further suggests that the model can only simulate IPO states which resemble ENSO, as does the fact that none of the ensemble members capture any of the most extreme (±3σ) IPO events which, in observations, occur in IPO positive years.

5.5 An assessment of the simulation by ACCESS1.3 of ENSO–IPO related rainfall variability

Results from the previous sections suggest that if simulations of rainfall variability are to improve, ACCESS1.3 must improve its representation of the ENSO–IPO relationship. This is particularly important given that the seasonality of climate oscillations is shifting and rainfall regimes are changing in summer and autumn (e.g. the impact of SAM on summer rainfall extremes (Min *et al.* 2013), autumn rainfall in south-east Australia (Cai and Cowan 2013)), the seasons of the ENSO–IPO interaction. It is particularly important to be able to simulate the summer and autumn ENSO–IPO interaction, so that one can identify how much *this* interaction contributes to observed changes. This is especially the case in autumn, when multiple factors contribute to changes in rainfall.

Whilst ACCESS1.3 poorly simulates the ENSO–IPO interaction, it seems that this weakness (or at least, some elements of this) are not unique to this model. Cai *et al.* (2010) identified that an aggregation of 24 CMIP3 models failed to identify asymmetry within ENSO; as foreshadowed by past research (e.g. Power *et al.* 2006; King *et al.* 2013a) and investigated in detail in this research, the ENSO–IPO interaction is at the core of this asymmetry. Failure to reproduce this asymmetry suggests other models also do not simulate the ENSO–IPO interaction. Simulations by Parker *et al.* (2007) of the observed correlation between ENSO and the IPO vary widely from observations; Parker *et al.* (2007) attribute this to the weakness of the secondary SST signal (i.e. the IPO), which is deemed to be particularly difficult to detect within GCMs. Dai (2013) examined the correlation between the IPO and US rainfall; whilst the AMIP model simulates this correlation well, like ACCESS1.3, it has difficulty in accounting for interactions with ENSO extremes. However, unlike ACCESS1.3, the model used by Dai (2013) incorporates observed twentieth century SST values, leading to improved simulations. Arblaster *et al.* (2002) use the Parallel Climate Model (PCM) to simulate Australian rainfall on inter-decadal timescales. This

is the only model which has so far simulated the observed stronger (weaker) correlations between rainfall and the IPO negative (positive) state.

In order to improve the simulation of rainfall seasonality, distribution, and strength, improvements need to be made to the way in which ACCESS1.3 simulates the IPO interaction with rainfall. It is likely that once this improves, so too will the simulation of the ENSO–IPO relationship with rainfall. It is possible that the failure of ACCESS1.3 to simulate the multi-decadal oscillation *and* the identified eight-year quasi-decadal IPO oscillations has led to the poor simulation of the ENSO–IPO relationship with rainfall. Moderately extreme events often correspond with 'protracted' ENSO events (see Section 4.3), which might be influenced by the ENSO–IPO interaction. It is possible that a mechanism that facilitates this interaction may be related to the quasi-decadal signal apparent in the IPO, which could be influenced both by the thermocline and the SPCZ, which will be discussed next.

ENSO extremes are underpinned by the eastward propagation of thermocline depth anomalies in the equatorial Pacific Ocean (i.e. El Niño conditions in Figure 2.2); for example, this occurred in the strong 1997 El Niño (Webster and Palmer 1997; McPhaden 1999). Arblaster *et al.* (2002) observed that the thermocline weakens during the IPO positive state, in a similar manner to an El Niño event, and that this reduces variability associated with ENSO (e.g. Figure 4.6.a). It is possible that ENSO and IPO are interacting through the thermocline. This interaction would explain the slight decrease in precipitation observed in IPO neutral years, when the thermocline is steeper than in IPO positive years, and SSTs are elevated slightly in the eastern Pacific (similar to the thermocline and SST structure depicted during neutral conditions in Figure 2.2). The PCM adequately captures changes in the thermocline and the resulting ENSO–IPO interaction (Arblaster *et al.* 2002). However, ACCESS1.3 simulates a more diffuse thermocline; it is possible that this is inhibiting the simulation of the ENSO–IPO interaction (Marsland *et al.* 2013; Rashid *et al.* 2013).

It is possible that interactions with the thermocline also affect the quasi-decadal interaction with rainfall in the moderately extreme ENSO and IPO states. Kim and Cai (2006) note that strong ENSO events (i.e. 'protracted' ENSO events) are associated with a 'meridional swing' of the South Pacific convergence zone (SPCZ). The SPCZ is known to interact with both ENSO and the IPO; it shifts south in La Niña and negative IPO states (Folland 2002; Salinger *et al.* 2014), and north in El Niño years (further analysis should investigate whether this is also true in positive IPO years). The 'swing' in the SPCZ is associated with a 'flattening' of the thermocline (i.e. similar to the neutral conditions of Figure 2.2), which produces anomalously warm SSTs in the eastern Pacific—the conditions associated with a positive IPO state. Protracted ENSO events have been identified alongside the 'flattening' of the thermocline (Vecchi and Harrison 2006; Kim and Cai 2006). It is possible that changes in the thermocline, associated with changes in the SPCZ, are leading to the quasi-decadal signal observed in the interaction with rainfall in the moderately extreme ENSO and IPO states. Although ACCESS1.3 adequately simulates SPCZ

cloud cover (Franklin *et al.* 2013), its south-west orientation is particularly shallow and its correlation with summer Niño 3.4 SST anomalies is weak (Brown *et al.* 2013). This suggests that potential interactions between the thermocline, the SPCZ, ENSO, and IPO may not be accurately simulated in ACCESS1.3, and may be leading to the poor simulation of both the IPO and the ENSO–IPO relationship with rainfall. The quasi-decadal phenomenon must be investigated further, and, if this mechanism proves to be critical, its representation should be improved in GCMs that aim to simulate the Australian climate (through parameterisation, increasing the resolution of SSTs in the equatorial and mid-latitudinal Pacific Ocean, improving the representation of the thermocline, and so on).

5.6 Chapter summary

ACCESS1.3 captures the ENSO teleconnection with rainfall with partial accuracy. Overall, ACCESS1.3 overestimates the area of the Niño 3.4–rainfall relationship, and has difficulty capturing changes in its seasonality. Increases towards the end of the century in the variability of Niño 3.4 appear not to be simulated. ACCESS1.3 simulates the teleconnection between rainfall and the IPO less well. It does not simulate the region or the seasonality of this relationship. It appears to simulate the IPO as a variant of ENSO (in winter and spring) or as generic synoptic-scale features (in summer and autumn).

ACCESS1.3 does not simulate the relationship between ENSO, the IPO and rainfall. It poorly simulates the nonlinear response of the different states of ENSO to precipitation, which suggests that the IPO may contribute more strongly than previously thought to the nonlinear ENSO–rainfall relationship. ACCESS1.3 fails to simulate the multi-decadal oscillation that characterises the IPO. Additionally, its inability to capture the quasi-decadal signal apparent in the IPO (which may be related to the thermocline and SPCZ) may be contributing to the poor simulations of the ENSO–IPO relationship and rainfall variability. The implications of these findings will be discussed in the final chapter.

Chapter 6: Conclusions

GCMs are commonly used as tools to understand rainfall variability, including for societal decision-making (e.g. resource management). Knowing how well a given GCM simulates past rainfall variability tells us how accurate simulations of future rainfall variability are likely to be, which improves decision-making. However, ACCESS1.3, a GCM used to simulate rainfall in the Australian region, has not been tested for the accuracy with which it simulates the interactions between ENSO and the IPO, which impact rainfall variability in eastern Australia. Given that interactions amongst multiple climate drivers impact variability the most, this omission is significant. This thesis used correlation and composite analysis to investigate the observed interaction between ENSO and the IPO and its influence on rainfall variability in eastern Australia. These results were then used to determine how well ACCESS1.3 simulated this relationship.

The relationship observed between ENSO and rainfall aligns with past research. ENSO demonstrates a negative correlation with rainfall, which is strongest in eastern and central Australia, particularly in equatorial and coastal regions. Temporally, the relationship is strongest in spring and weakest in autumn. Correlations between ENSO and rainfall remain consistently stronger than those between the IPO and rainfall. As identified in past research, the IPO exhibits a negative correlation with rainfall. The multi-decadal cycle underpinning the IPO has a period of 60–80 years, which is longer than previously identified. This study is the first to comprehensively show the extent of its influence on Australian rainfall. The IPO tends to influence higher-latitude, coastal areas of eastern Australia most strongly; it also exhibits a positive correlation with northern Australian rainfall in summer. The strongest correlation between the IPO and rainfall occurs in summer, but the oscillation influences autumn rainfall the most, when the ENSO relationship with rainfall is weakest.

The joint influence that ENSO and the IPO have on rainfall variability reflects the interplay between the inter-annual and inter-decadal scales of the two oscillations. ENSO exerts the largest influence on rainfall variability. However, the state of the IPO modifies the strength of this relationship. The IPO positive phase amplifies the ENSO–rainfall relationship, and the IPO negative phase moderates the ENSO–rainfall relationship. This study also examined the influence of the IPO neutral state on rainfall, which produces slightly anomalous decreases in precipitation. It is hypothesised that this is due to a weakened Pacific Ocean thermocline.

When the same relationship is examined but the oscillation states are defined as $\pm 2\sigma$ and $\pm 3\sigma$ in relation to the index means (the ‘moderately extreme’ and ‘extreme’ cases, respectively), additional nuances of the inter-annual–inter-decadal interplay emerge (although conclusions must be treated cautiously due to small sample sizes). Rainfall that occurs in the moderately extreme case is not influenced by the IPO neutral and positive phases, and rainfall that occurs in the extreme case is influenced only by the positive phase of the IPO. This shows that as the indices

become more extreme—and so too, generally, do the increases and decreases in precipitation—the IPO increasingly influences rainfall, and the ENSO decreasingly influences rainfall. This relationship is represented diagrammatically in Figure 4.5. In contrast to past research, this study finds that the IPO positive phase influences rainfall variability.

Although the physical processes through which the ENSO and IPO interact to influence rainfall variability have not been identified, such mechanisms may be related to an underlying quasi-decadal cycle (with a cycle of approximately eight years) within the broader, multi-decadal IPO. The mechanism may be related to changes in the Pacific Ocean thermocline, which strengthens and weakens when the SPCZ shifts meridionally, and may be the same process contributing to 'protracted' ENSO events (Reason *et al.* 2000; Allan *et al.* 2003).

Other aspects of the influence of the ENSO–IPO interaction on rainfall are yet to be investigated. The composite analysis method used in this study is a relatively simple approach that provides useful insights into the oscillations' interaction with rainfall while overcoming difficulties associated with accommodating the nonlinear nature of the interaction. However, this method does not quantify which portion of rainfall-variability is due *solely* to the ENSO–IPO interaction; the influence of other climate oscillations cannot be removed. It would be useful to quantify rainfall variability caused by the interaction between two oscillations alone, as this offers potential for improving the identification of the physical parameters underpinning the teleconnection amongst ENSO, the IPO, and rainfall variability. An approach involving artificial neural networks may provide a solution to this problem (e.g. Brown *et al.* 2010; Mekanik and Imteaz 2012; Tozer 2014; Whan *et al.* 2014).

ACCESS1.3 simulates the Australia-wide ENSO–rainfall interaction with reasonable success; it correctly identifies a negative correlation between ENSO and rainfall with a comparable magnitude to observations. However, the spatial extent of the ENSO influence is overestimated, and the model does not capture the regional differences in the ENSO–rainfall relationship. Although ACCESS1.3 largely simulates the negative correlation between Australia-wide rainfall and the IPO with a comparable strength to observations, it fails to simulate the spatial and temporal elements of the IPO–rainfall interaction, both at the Australia-wide and regional scales. ACCESS1.3 appears to be simulating the IPO as an ENSO-like mechanism. Consequently, ACCESS1.3 simulates peak correlations between IPO and rainfall in spring (not summer, as in observations). In summer and autumn, the peak period of the IPO–rainfall and ENSO–IPO interactions, IPO-influenced precipitation is represented as seemingly random synoptic-scale noise. When the oscillation states are defined with increasing extremeness (i.e. the $\pm 2\sigma$ and $\pm 3\sigma$ cases), ACCESS1.3 does not simulate the shift in influence on rainfall from ENSO to the IPO. The 60–80 year inter-decadal cycle underpinning the IPO is not simulated, and neither is its eight-year quasi-decadal cycle. It is essential that the mechanism through which ENSO and the IPO interact to influence rainfall is investigated further so that its presence or absence in GCMs can be ascertained. Even if ACCESS1.3 were to be compared with an ensemble of

observational datasets to remove the tendency of AWAP to underestimate heavy precipitation events and overestimate low precipitation events, it is likely that it would still produce poor simulations of the ENSO–IPO relationship with rainfall.

The inability of ACCESS1.3 to accurately simulate the ENSO–IPO relationship seems to be contributing to the model's underestimation of the variance of precipitation, as well as its poor simulation of regional and local precipitation. It is likely that the poor simulation by ACCESS1.3 of regional and local scale climate is also due to the failure to incorporate interactions between global-scale and smaller-scale drivers, as well as global-scale and multi-millennial climate cycles (e.g. Milankovitch cycles and the SAM (Hall and Visbeck 2002)). Likewise, until it is known whether the interactions between other global-scale oscillations, such as the MJO and the IOD, are represented within GCMs, interactions between other global-scale oscillations cannot be ignored as potential contributors to poor rainfall variability simulations.

Regardless of the exact contribution made by the ENSO–IPO interaction and of the possible impact of other inter-oscillation interactions on rainfall, ACCESS1.3 does not adequately simulate the ENSO–IPO interaction and its influence on rainfall, which contributes to poor simulations of rainfall variability. Incorporating the physical mechanisms through which climate oscillations interact into GCMs will improve the simulation of rainfall variability. If GCMs are continued to be relied on as a tool for understanding past and future changes in rainfall variability, and if this tool is to be used for the formulation of societal, economic and environmental decision-making, the important role that inter-oscillation interactions play in rainfall variability must be acknowledged, and a focus needs to be placed on improving GCM simulations of interactions amongst climate drivers.

Appendix 1: Dataset Interpolation

This appendix discusses the creation of a common grid to compare the AWAP and ACCESS1.3 datasets (as introduced in Section 3.1.4). The AWAP dataset has a higher resolution ($0.05^o \times 0.05^o$) than the ACCESS1.3 dataset ($1.25^o \times 1.875^o$), and was re-gridded to the same scale as ACCESS1.3 (to avoid downscaling ACCESS1.3 to the resolution of AWAP). The interpolation algorithm is based on that used by Hirsch (2010), who compared the AWAP dataset with several modelled datasets (including an early version of the ACCESS model). Hirsch interpolated the AWAP dataset from a resolution of $0.05^o \times 0.05^o$ to a lower-resolution grid of $1.0^o \times 1.0^o$. The interpolation algorithm used by Hirsch was developed by Peter Briggs of the CSIRO. Linearly weighted averages were used to approximate the values of the larger, new grid cells (as depicted visually in Figure I and expressed in Equation I).

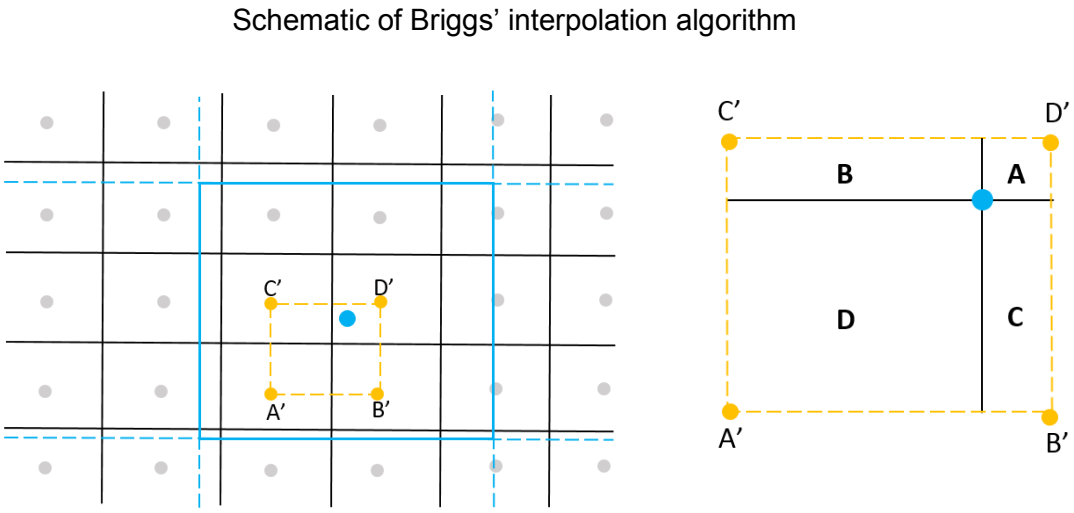

Figure I: A depiction (not to scale) of Briggs' interpolation algorithm. ***Left:*** The original $0.05^o \times 0.05^o$ AWAP dataset is shown as the black underlying grid; the centre-points of each cell are depicted as grey dots. The interpolated $1.0^o \times 1.0^o$ grid is depicted in blue. One grid cell of the interpolated grid is shown as a solid blue box; its centre-point is the blue circle. The value assigned to this cell by the Briggs interpolation algorithm is a weighted average of the four cells in the $0.05^o \times 0.05^o$ dataset that are closest to the blue dot; the centres of these four cells are shown in yellow (A′, B′, C′, D′). Note that only these four cells contribute to the value of the interpolated grid cell. ***Right:*** This is the region of the AWAP dataset that contributes to the value of the interpolated grid cell. AWAP grid cells with vertices furthest from the central blue dot (e.g. A′) contribute least to the final grid cell (see Equation I). If the underlying AWAP data is not valid (see Equation I) the interpolated grid cell has no value.

Equation II: The value of a grid cell interpolated from AWAP data to the 1.0° × 1.0° resolution. A′, B′, C′ and D′ represent the centre-points of the four 0.05° × 0.05° grid cells from which the value of the 1.0° × 1.0° interpolated grid cell is derived. These points have the values of the AWAP grid cells that they are the centre-points of. A, B, C and D represent the fraction of the new grid cell that the values of A′, B′, C′ and D′ contribute to the interpolated grid cell. All sums are taken only over input grid cells that contain valid data.

$$Interpolated\ cell\ value = \left[\frac{AA'}{(A+B+C+D)}\right] + \left[\frac{BB'}{(A+B+C+D)}\right] + \left[\frac{CC'}{(A+B+C+D)}\right] + \left[\frac{DD'}{(A+B+C+D)}\right]$$

$$If: \frac{\sum_{valid} A+B+C+D}{A+B+C+D} \leq 0.5, output\ cell\ is\ not\ valid$$

However, the scale of Hirch's interpolated grid (1.0° × 1.0°) neither matches the original AWAP grid scale (0.05° × 0.05°) nor the ACCESS1.3 grid scale (1.25° × 1.875°). Interpolating both AWAP and ACCESS1.3 data onto the 1.0° × 1.0° grid increases the risk that the interpolated data is not representative of precipitation at a given location. Consequently, the algorithm used by Hirsch (2010) has been modified by Associate Professor Franklin Mills of the Australian National University (personal communication, 20 August 2015). The modified interpolation algorithm takes the original AWAP data (which has *square* grid cells) and interpolates it onto a lower-resolution grid with *rectangular* cells, with the same dimensions as the ACCESS1.3 grid. The value assigned to the new, lower-resolution grid cell was determined by using a weighted average of the underlying AWAP grid cell values (see Figure II).

Schematic of Mills' spatial averaging algorithm

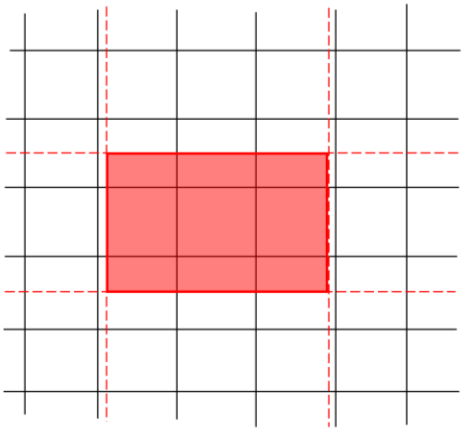

Figure II: A depiction (not to scale) of Mills' spatial averaging algorithm, used to re-grid the 0.05° × 0.05° AWAP dataset to the resolution of the ACCESS1.3 dataset (1.25° × 1.875°). The AWAP grid is shown in black; the ACCESS1.3 grid is shown in red. The value of the lower-resolution interpolated grid cell (shown here in solid red) is determined by (a) the value of the underlying AWAP grid-cells, and (b) what fraction of the interpolated grid cell each AWAP grid cell comprises (see Equation II). If the underlying AWAP data is not valid (see Equation II) the interpolated grid cell has no value. All sums are taken only over input grid cells that contain valid data.

Equation II: The value of a grid cell interpolated from AWAP data to the 1.25º × 1.875º resolution. 'i' refers to each AWAP grid cell that underlies the lower-resolution grid cell. 'Input overlap area' refers to the area that each AWAP grid cell (i) comprises of the new, lower-resolution cell ('output area'). 'Input value' refers to the precipitation value assigned to each AWAP grid cell ($valid$).

$$Spatially\ averaged\ cell\ value = \frac{\sum_{valid}(input\ overlap\ area)_{valid}(input\ value)_{valid}}{output\ area}$$

$$If: \frac{\sum_{valid}(input\ overlap\ area)_{valid}}{output\ area} < 0.5, output\ cell\ is\ not\ valid$$

Where a grid cell has no associated data (e.g. over water bodies), the remaining grid cells (if they are numerous enough) contribute to the value of the new, lower-resolution grid cell (see Equations I and II). This means that grid-cells near the coast must be interpreted cautiously, as their values may be comprised of data from less than four grid vertices.

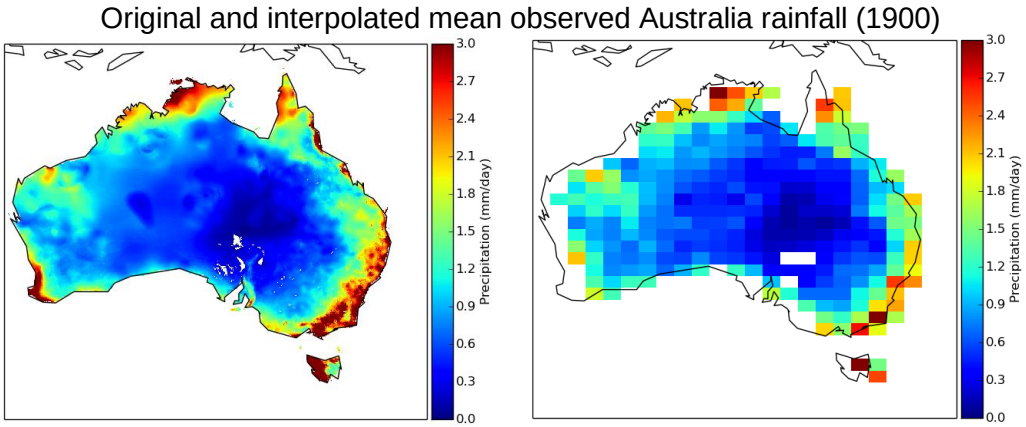

Figure III: Both images show mean AWAP precipitation data (mm day^{-1}) for 1900 (January–December). The left-hand figure shows the original dataset, with a resolution of 0.05º × 0.05º. The right-hand figure shows AWAP data that has been interpolated with the Briggs' algorithm modified by Mills to the 1.25º × 1.875º resolution.

Appendix 2: Additional Figures and Tables

This appendix contains additional figures and tables referenced throughout this thesis that were not included directly in the text itself. Throughout this appendix, seasons are referred to as: 'JJA' (austral winter), 'SON' (austral spring), 'DJF' (austral summer), 'MAM' (austral autumn).

Additional figures

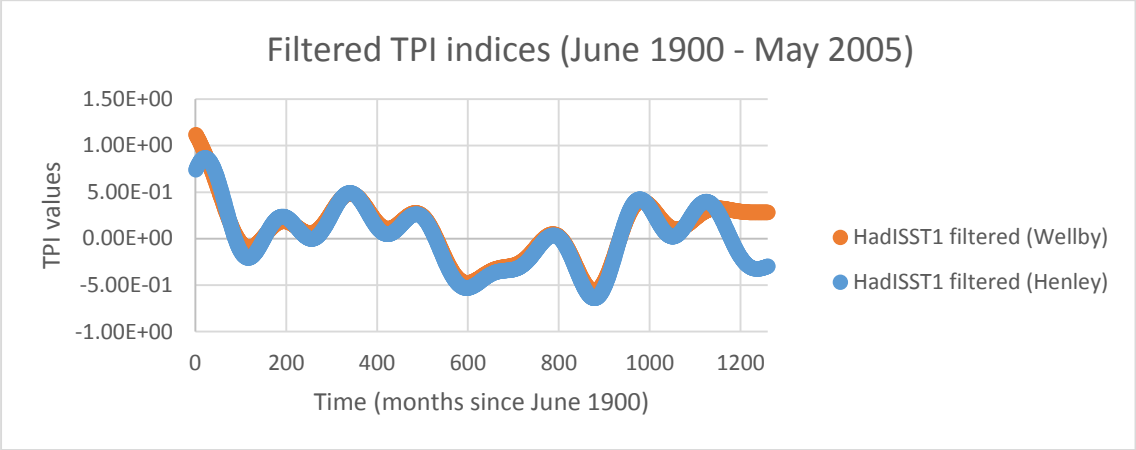

Figure A: This figure presents values of the TPI, as computed by Henley *et al.* (2015) and Wellby (this study), for the 1260 months between June 1900 and May 2005. Differences between the two realisations of the index occur at the beginning and end of the study period; these discrepancies are likely to be due to the low-pass filter algorithm, which will produce slightly erroneous values at the beginning and end of the dataset used. Because the Henley *et al.* study period (1870–2013) was longer than this study period (1900–2005), this issue is not apparent in this graph for the Henley *et al.* (2015) TPI.

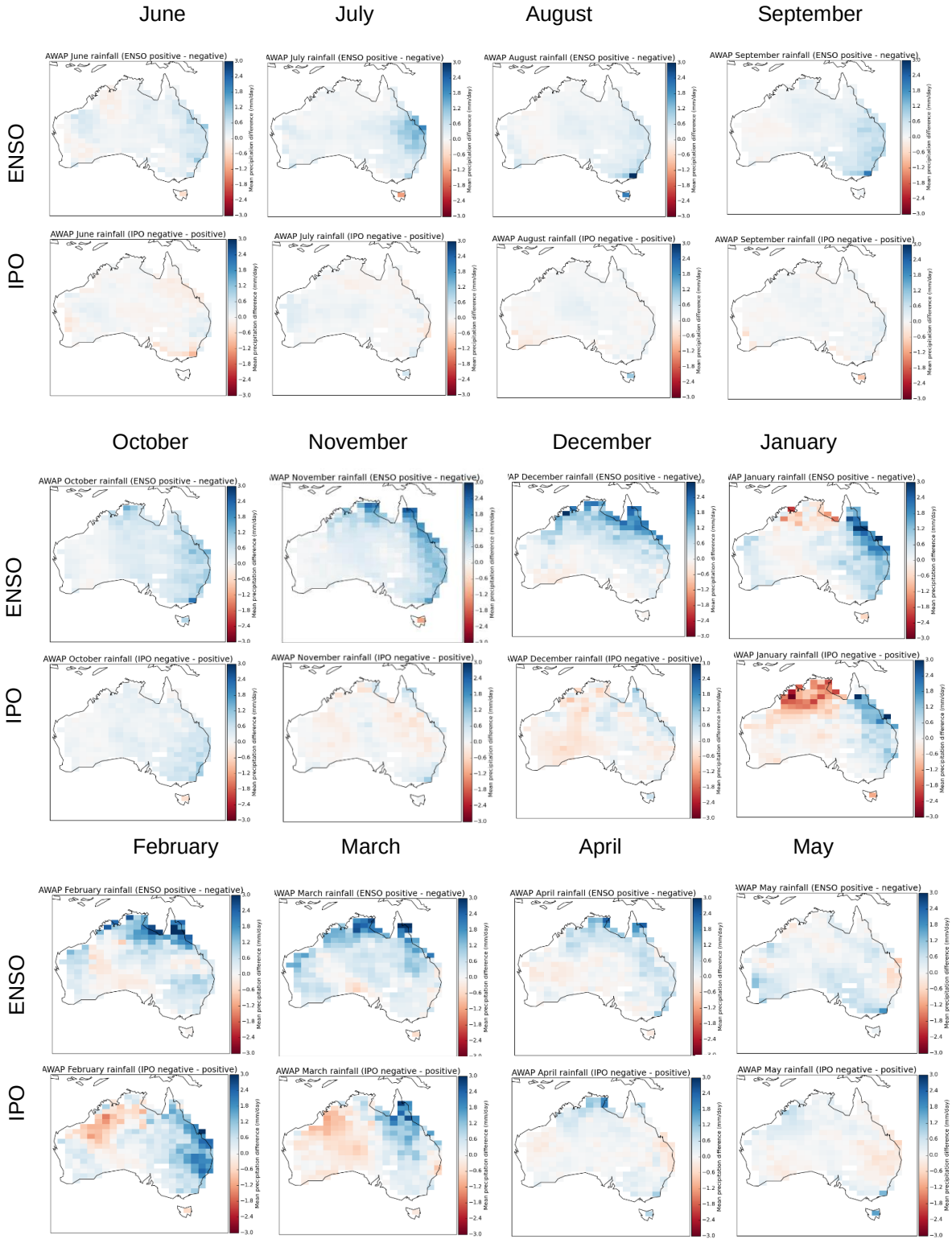

Figure B: These figures show differences in observed mean rainfall (mm day^{-1}) between the wet and dry phases of the ENSO and the IPO, for all months. It is clear that the greatest differences in rainfall in both indices occur between December and March, indicating that this is the time in which the ENSO and IPO interaction affects rainfall most strongly.

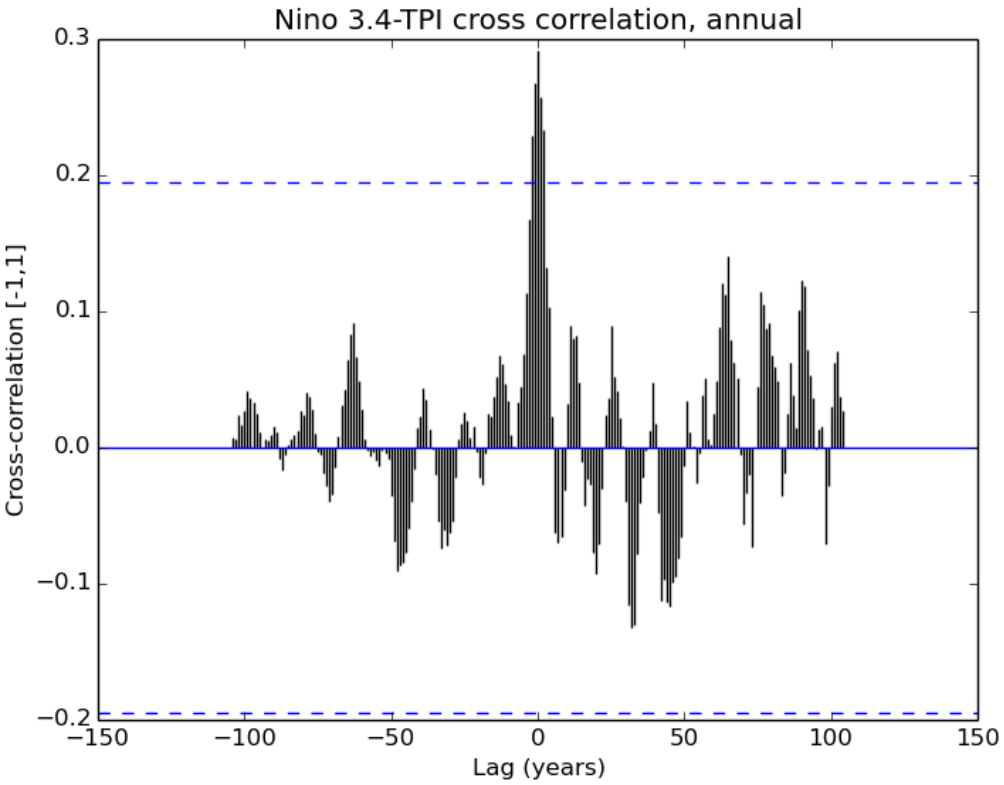

Figure C: This figure shows the cross-correlation between Niño 3.4 and the TPI, for all 105 years in the study. The strongest correlation is observed at time zero, indicating that the correlation between the two indices is simultaneous. The dashed blue lines indicate the 95 per cent confidence interval.

Fig. D1 AWAP JJA: mean rainfall anomalies

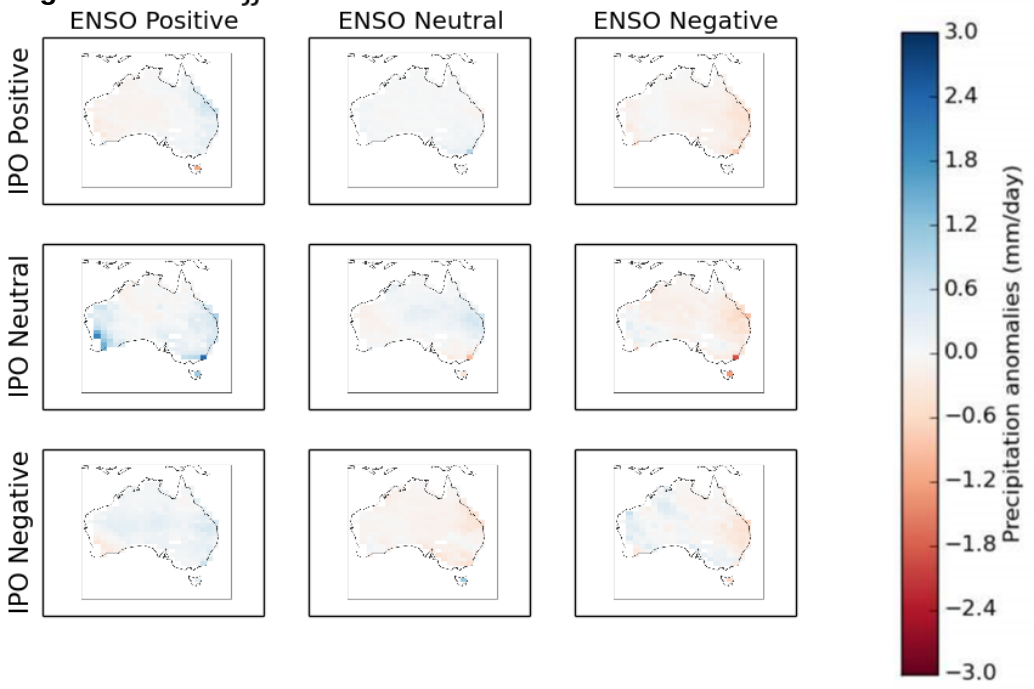

Fig. D2 AWAP SON: mean rainfall anomalies

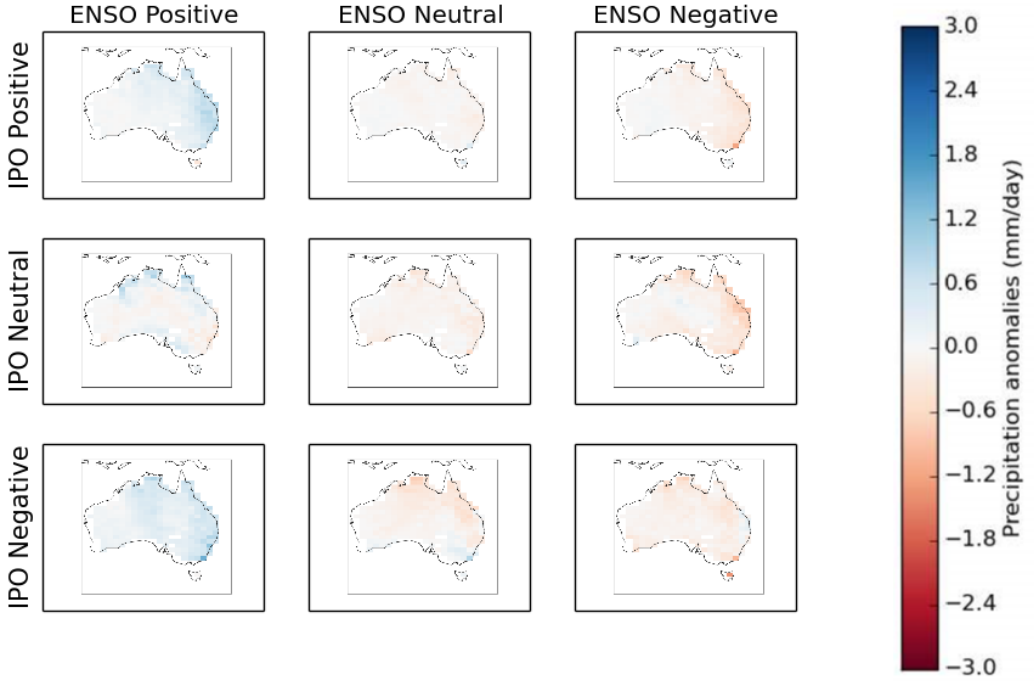

Fig. D3 AWAP DJF: mean rainfall anomalies

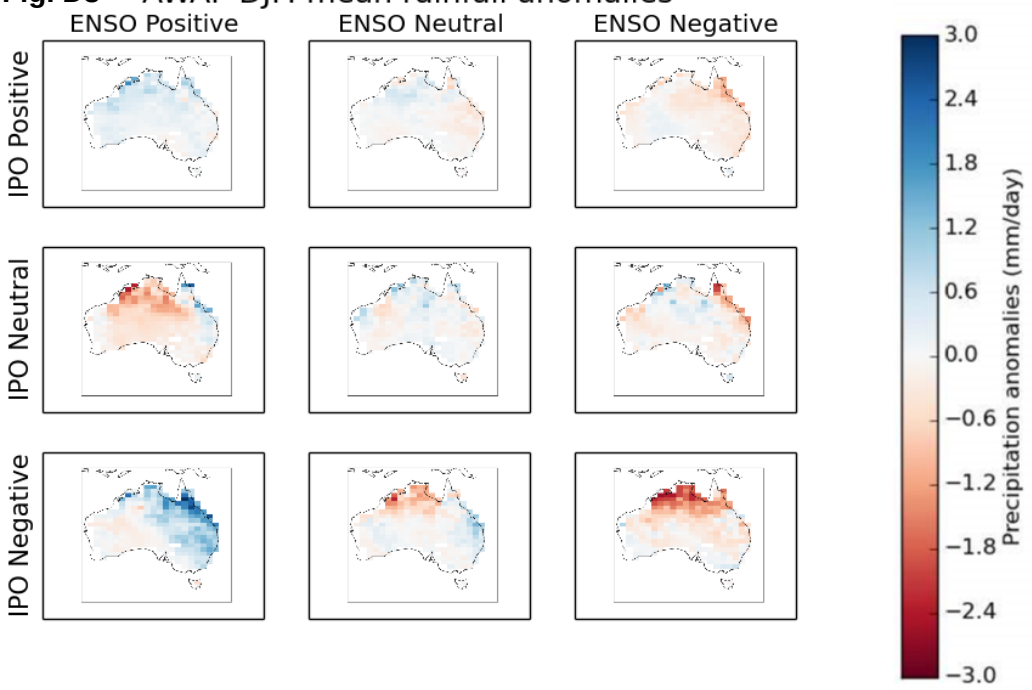

Fig. D4 AWAP MAM: mean rainfall anomalies

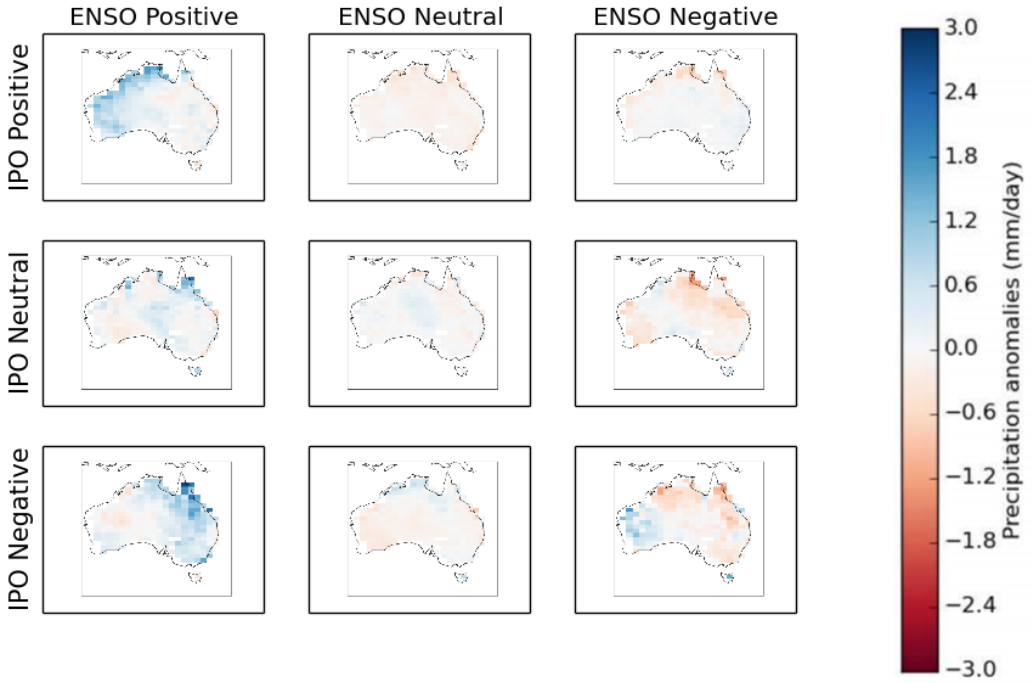

Figure D: This figure presents observed mean annual precipitation anomalies (mm day^{-1}) for the nine combinations of the three ENSO and IPO phases, as defined by Trenberth (1997) and Henley *et al.* (2015). Results for winter (*Fig. D1*), spring (*Fig. D2*), summer (*Fig. D3*), and autumn (*Fig. D4*) are presented.

Fig. E1 AWAP annual: standardised mean rainfall

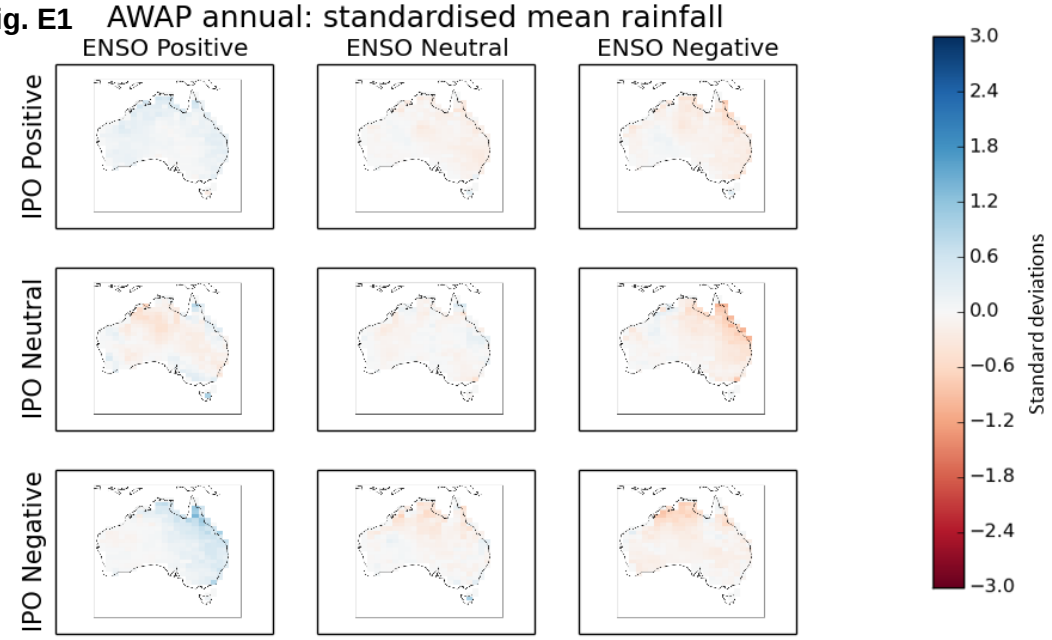

Fig. E2 AWAP annual: standardised mean rainfall (2 σ)

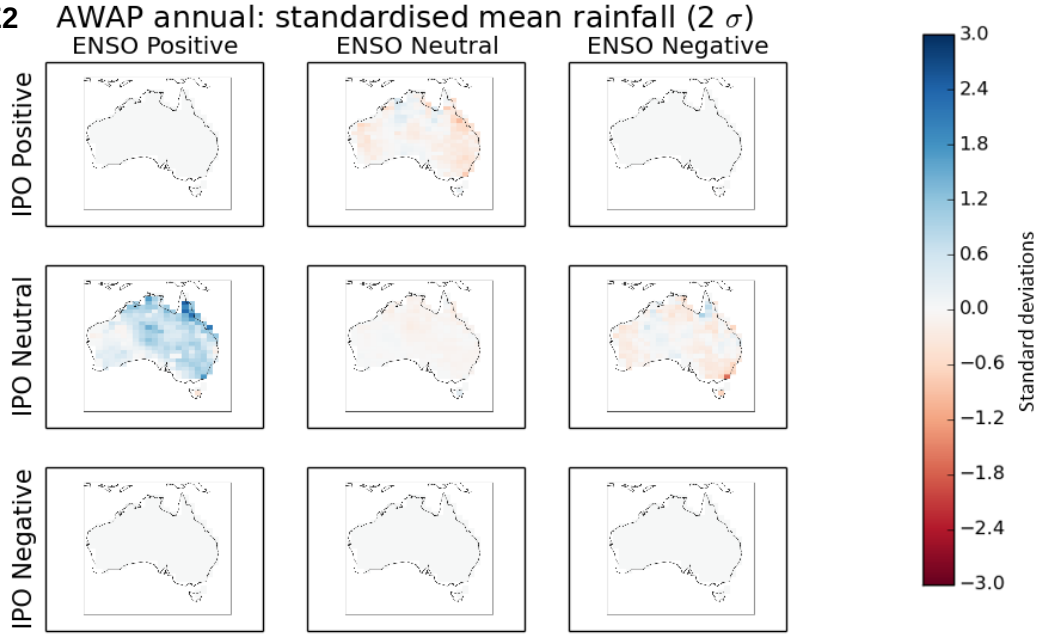

Fig. E3

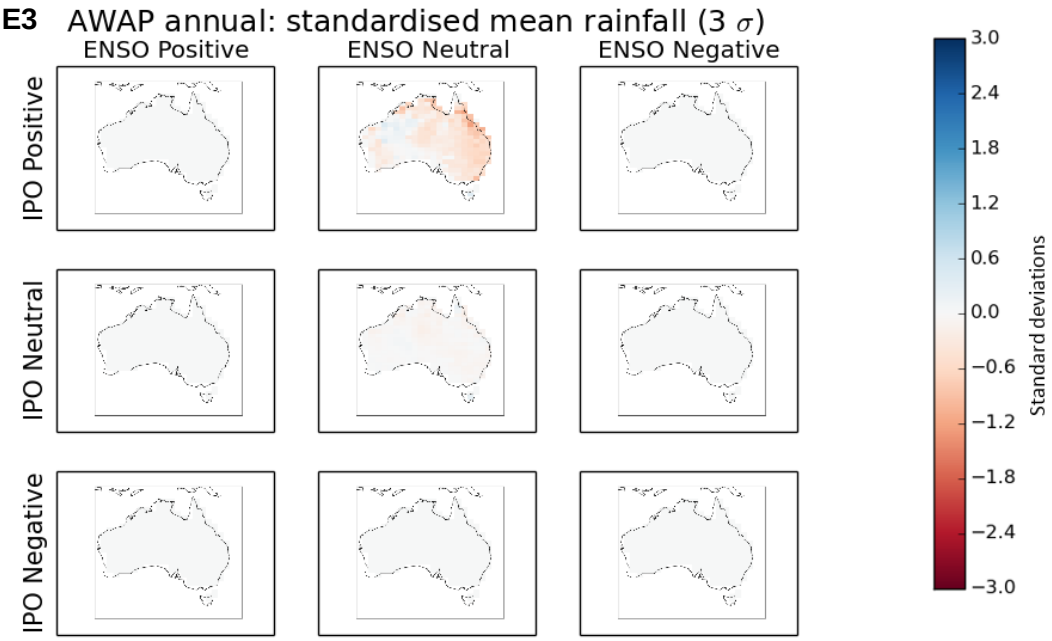

Figure E: This figure presents annual composite maps of standardised mean rainfall anomalies (σ), for the nine combinations of the three ENSO and IPO phases, as defined (*Fig. E1*) by Trenberth (1997) and Henley *et al.* (2015), (*Fig. E2*) as ±2σ above the index means, and (*Fig. E3*) as ±3σ above the index means.

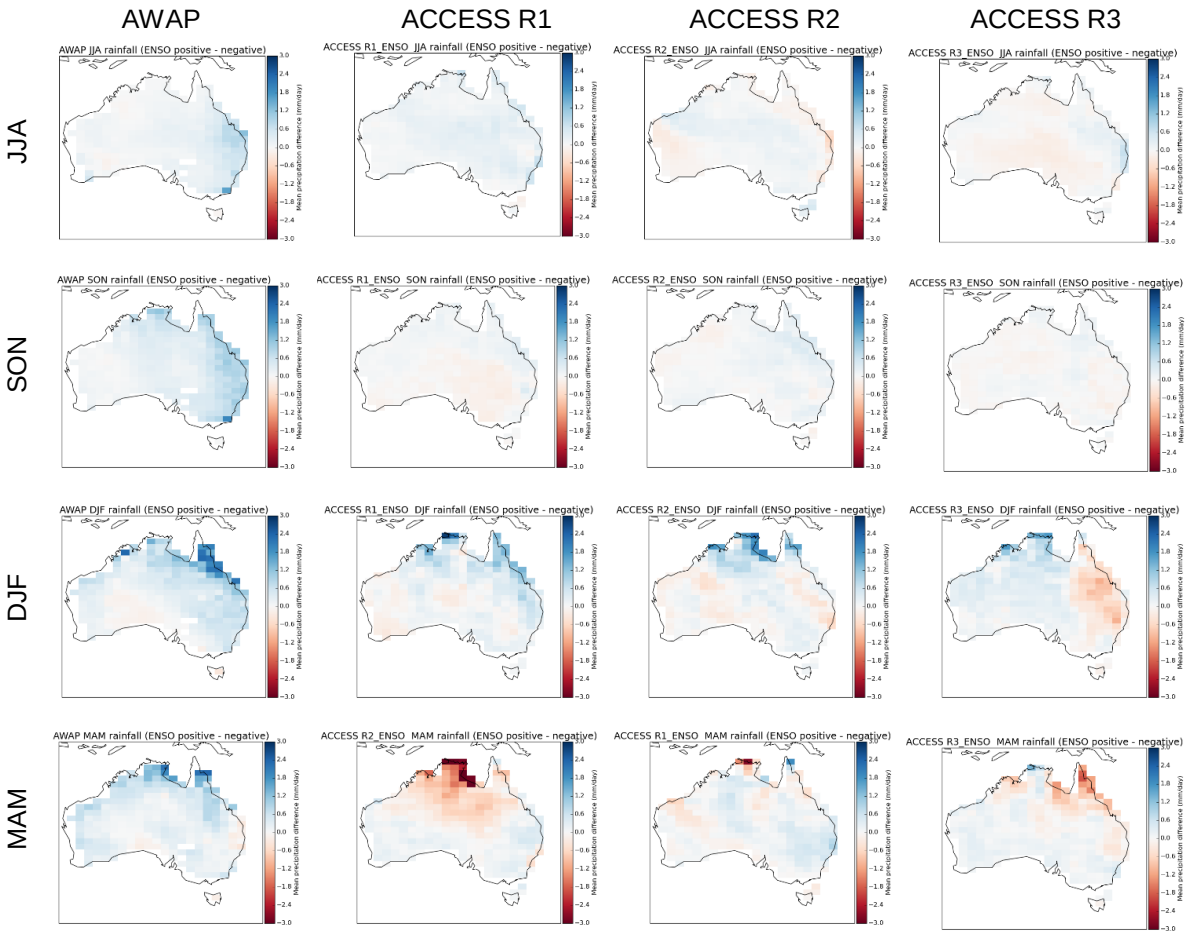

Figure F: This figure shows differences in El Niño and La Niña rainfall (mm day^{-1}) for observations, ACCESS R1, ACCESS R2, and ACCESS R3. Difference maps are presented for winter, spring, summer, and autumn.

Fig. G1 ACCESS1.3 R1 annual: mean rainfall anomalies

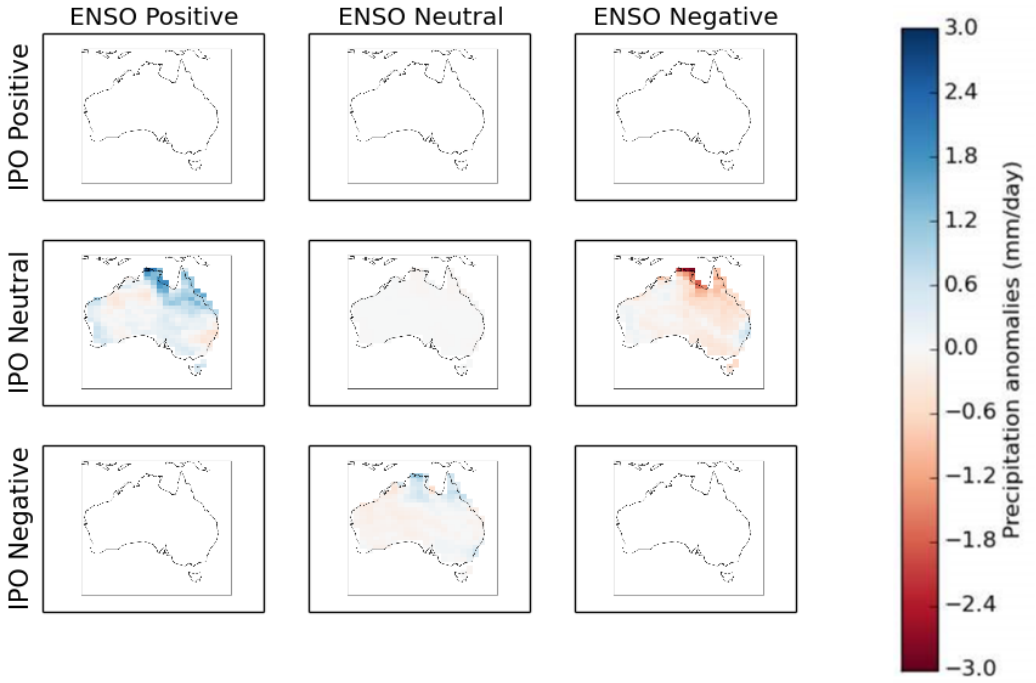

Fig. G2 ACCESS1.3 R3 annual: mean rainfall anomalies

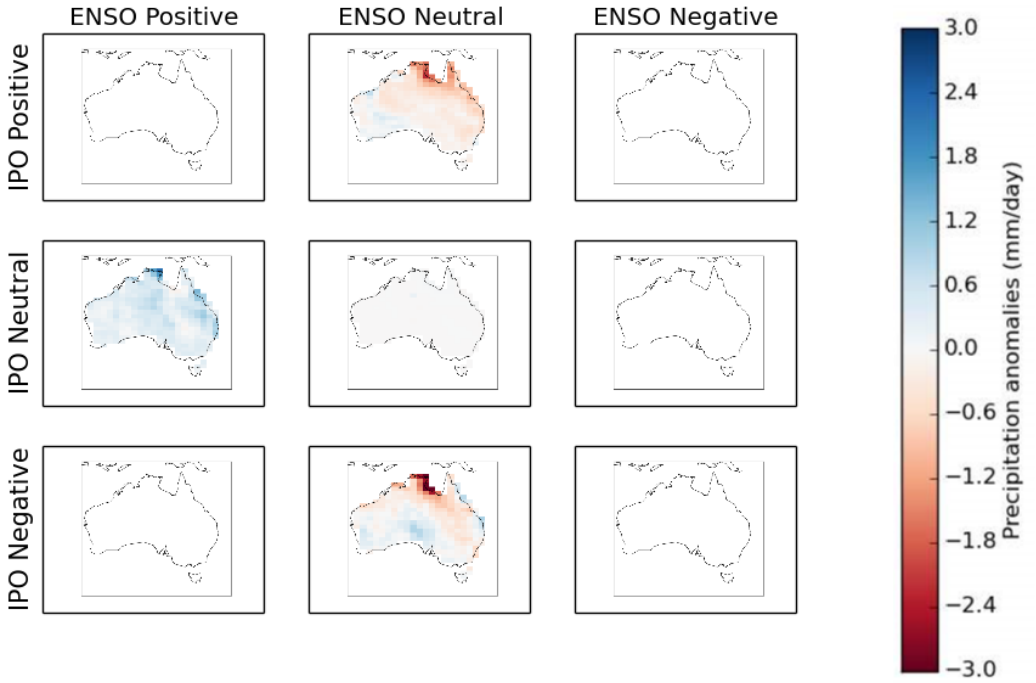

Figure G: This figure shows composite maps of simulated precipitation anomalies (mm day^{-1}), stratified according to the ENSO and IPO phases (defined as ±2σ above the index means). *Fig. G1* shows simulations produced by ACCESS R1 (similar results are produced by ACCESS R2), and *Fig. G2* shows simulations produced by ACCESS R3.

Fig. H1

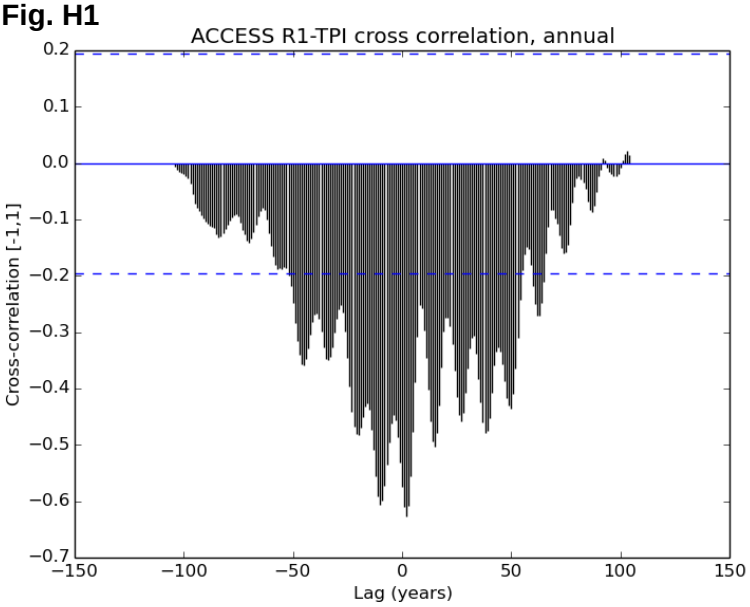

Fig. H2

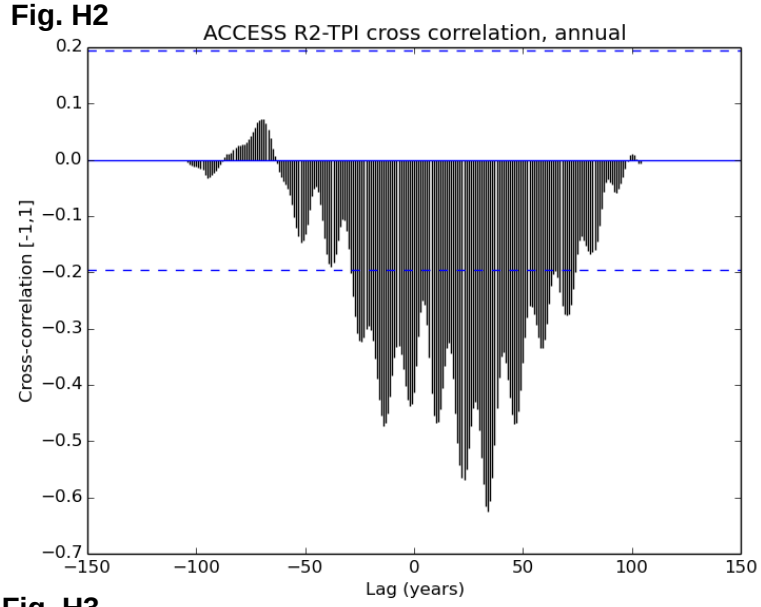

Fig. H3

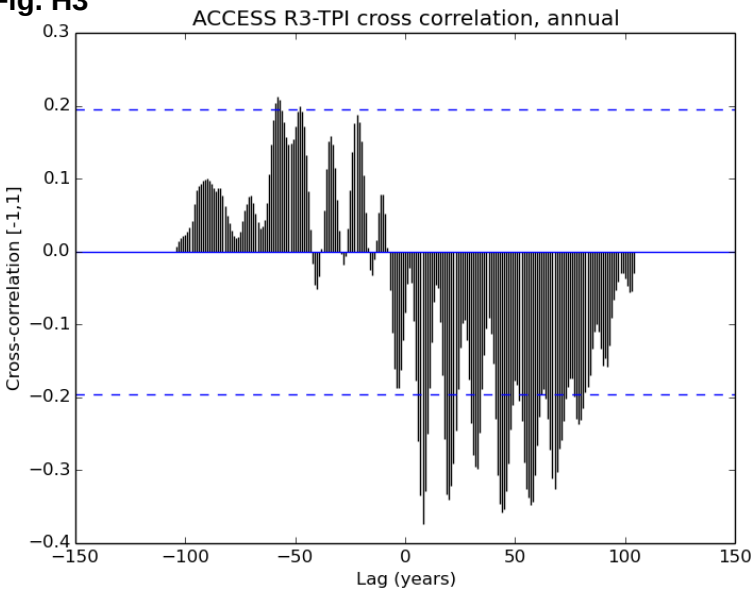

Figure H: This figure shows simulated cross correlations between rainfall and the TPI for ACCESS R1 (*Fig. H1*), ACCESS R2 (*Fig. H2*) and ACCESS R3 (*Fig. H3*). The dashed blue lines indicate the 95 per cent confidence interval.

Additional tables

Table A: This table presents correlation coefficients (*r*) between Niño 3.4 and rainfall (*Table A1*) and the TPI and rainfall (*Table A2*), for the observational AWAP dataset. Correlation coefficients that are statistically significant at the 95 percent level are presented in boldface. P-values are presented for significant difference ($p \leq 0.05$; boldface) between (a) eastern Australia and broader Australia, and (b) significant difference between the climate zones' correlation coefficients and eastern Australia.

Table A1

Niño 3.4 and AWAP	*Australia*	*Eastern Australia*	*Equatorial*	*Tropical*	*Sub-tropical*	*Desert*	*Grassland*	*Temperate*
Annual	**-0.53**	**-0.60**	**-0.50**	**-0.48**	**-0.57**	**-0.38**	**-0.40**	**-0.38**
JJA	**-0.39**	**-0.48**	-0.18	**-0.28**	**-0.45**	**-0.36**	**-0.28**	**-0.28**
SON	**-0.54**	**-0.55**	**-0.56**	**-0.54**	**-0.48**	**-0.35**	**-0.41**	**-0.39**
DJF	**-0.38**	**-0.42**	**-0.34**	**-0.39**	**-0.37**	**-0.30**	**-0.25**	**-0.21**
MAM	**-0.25**	-0.18	**-0.37**	**-0.21**	-0.11	**-0.19**	-0.17	-0.06
June	**-0.21**	**-0.24**	-0.09	-0.16	**-0.21**	-0.18	-0.14	-0.11
July	**-0.39**	**-0.46**	-0.17	**-0.20**	**-0.48**	**-0.28**	**-0.23**	-0.10
August	**-0.29**	**-0.35**	-0.13	**-0.23**	**-0.24**	**-0.27**	**-0.28**	**-0.30**
September	**-0.31**	**-0.38**	**-0.22**	**-0.31**	**-0.34**	**-0.26**	**-0.28**	-0.15
October	**-0.44**	**-0.45**	**-0.32**	**-0.38**	**-0.36**	**-0.34**	**-0.33**	**-0.44**
November	**-0.45**	**-0.44**	**-0.50**	**-0.43**	**-0.36**	-0.10	**-0.22**	**-0.20**
December	**-0.35**	**-0.38**	**-0.35**	**-0.37**	**-0.31**	**-0.29**	**-0.23**	-0.15
January	-0.17	**-0.28**	-0.10	-0.17	**-0.30**	**-0.20**	-0.13	-0.16
February	**-0.27**	**-0.22**	**-0.21**	**-0.31**	-0.12	-0.12	-0.15	-0.10
March	**-0.27**	**-0.20**	**-0.26**	-0.16	-0.17	-0.19	-0.13	0.05
April	-0.14	-0.16	**-0.30**	-0.16	-0.11	0.01	-0.05	-0.08
May	-0.05	0.03	-0.02	0.01	0.12	-0.12	-0.14	-0.07
P-value (diff. from 'Australia'/'E. Aus.')		0.71	0.23	0.27	0.36	**0.03**	**0.02**	**0.00**

Table A2

TPI and AWAP	Australia	*Eastern Australia*	*Equatorial*	*Tropical*	*Sub-tropical*	*Desert*	*Grassland*	*Temperate*
Annual	-0.19	**-0.35**	-0.14	**-0.24**	**-0.34**	**-0.25**	**-0.28**	**-0.24**
JJA	-0.10	-0.10	-0.14	-0.03	-0.09	-0.10	-0.02	-0.10
SON	-0.17	**-0.19**	-0.16	-0.15	-0.15	-0.10	-0.13	-0.12
DJF	-0.13	**-0.36**	-0.03	**-0.20**	**-0.42**	**-0.21**	**-0.19**	-0.13
MAM	-0.07	-0.12	-0.14	-0.14	-0.02	**-0.20**	**-0.26**	-0.18
June	-0.05	-0.07	-0.08	-0.02	-0.08	-0.10	0.02	-0.01
July	-0.05	-0.04	-0.14	0.05	-0.04	-0.01	-0.01	-0.08
August	-0.13	-0.11	-0.03	-0.10	-0.07	-0.11	-0.08	-0.12
September	-0.05	-0.07	**-0.27**	-0.15	-0.06	-0.07	-0.02	0.09
October	**-0.23**	**-0.26**	0.05	-0.09	**-0.26**	-0.16	**-0.23**	-0.12
November	-0.10	-0.12	-0.18	-0.11	-0.05	0.02	0.00	**-0.22**
December	-0.04	-0.10	-0.10	-0.08	-0.08	-0.07	0.00	-0.15
January	-0.04	**-0.21**	0.01	-0.11	**-0.26**	-0.14	-0.13	0.09
February	-0.16	**-0.36**	0.01	**-0.19**	**-0.37**	**-0.19**	**-0.20**	-0.14
March	-0.04	**-0.22**	-0.13	-0.19	**-0.20**	**-0.23**	-0.19	0.04
April	-0.07	0.01	-0.12	0.03	0.08	-0.07	-0.17	-0.08
May	-0.07	0.02	0.05	0.04	0.14	-0.05	-0.15	**-0.24**
P-value (diff. from 'Australia'/'E. Aus.')		0.10	0.08	0.12	0.62	0.30	0.34	0.15

Table B: This table presents correlation coefficients (*r*) between Niño 3.4 and the TPI, for observations (HadISST) and the three ensemble members of ACCESS1.3. Correlation coefficients that are not statistically significant at the 95 percent level are presented as in italics. P-values are presented for significant difference ($p \leq 0.05$; boldface) between observed data and ACCESS1.3 ensemble members.

	HadISST	**ACCESS1.3 R1 SST**	**ACCESS1.3 R2 SST**	**ACCESS1.3 R3 SST**
Annual	0.34	0.23	0.28	0.27
JJA	0.27	0.27	0.29	0.32
SON	0.23	0.26	0.25	0.28
DJF	0.29	0.20	0.21	0.21
MAM	0.29	0.26	0.29	0.31
June	0.35	0.21	0.24	0.23
July	0.35	0.23	0.29	0.27
August	0.32	0.25	0.30	0.30
September	0.29	0.26	0.30	0.32
October	0.26	0.28	0.29	0.32
November	0.25	0.27	0.28	0.31
December	0.23	0.27	0.27	0.30
January	0.23	0.26	0.25	0.27
February	0.23	0.24	0.23	0.25
March	0.25	0.21	0.22	0.22
April	0.29	0.19	0.21	0.20
May	0.33	*0.18*	0.20	0.20
P-value (difference from HadISST1)		**0.00**	0.09	0.43

Table C: This table presents the p-values associated with the normality of each index dataset (observed = HadISST, r1i1p1 = ACCESS R1, r1i1p1 = ACCESS R2, r1i1p1 = ACCESS R3). P-values that are statistically significantly non-normal ($p \leq 0.05$) are presented in boldface.

	Niño 3.4 (ENSO)				**TPI (IPO)**			
	HadISST	**ACCESS R1**	**ACCESS R2**	**ACCESS R3**	**HadISST**	**ACCESS R1**	**ACCESS R2**	**ACCESS R3**
Annual	0.78	0.34	0.54	0.27	0.74	0.21	0.15	0.11
JJA	0.71	0.84	0.23	0.08	0.55	0.21	0.14	0.49
SON	0.54	0.11	0.74	0.10	0.69	0.21	0.15	0.19
DJF	0.63	0.41	0.72	0.38	0.78	0.21	0.15	0.06
MAM	0.54	0.90	0.31	0.57	0.81	0.22	0.15	**0.02**
June	0.54	0.65	0.09	0.29	0.51	0.21	0.14	0.63
July	0.64	0.86	0.22	0.08	0.55	0.21	0.14	0.49
August	0.54	0.65	0.66	**0.03**	0.60	0.21	0.15	0.37
September	0.44	0.22	0.99	**0.04**	0.65	0.21	0.15	0.27
October	0.49	0.11	0.75	0.10	0.69	0.21	0.15	0.19
November	0.61	0.10	0.56	0.16	0.73	0.21	0.15	0.13
December	0.66	0.20	0.50	0.16	0.76	0.21	0.15	0.09
January	0.61	0.45	0.70	0.36	0.79	0.21	0.15	0.06
February	0.58	0.62	0.99	0.64	0.80	0.22	0.15	**0.04**
March	0.46	0.76	0.78	0.68	0.81	0.22	0.15	**0.03**
April	0.52	0.90	0.30	0.58	0.81	0.22	0.15	**0.02**
May	0.55	0.84	0.10	0.48	0.80	0.23	0.15	**0.02**

Table D: These tables show correlation coefficients (*r*) for the relationship between Niño 3.4 and rainfall, for ACCESS1.3 historical experiment ensemble members (observations are shown in Table A1). All correlation coefficients in boldface are statistically significant (at the 95 per cent level). *P-value (diff. from 'Australia'/'E. Aus')*: eastern Australian correlation coefficients are tested for differences from those of Australia, and the various climate zones are tested for differences from eastern Australia. *P-value (diff. from AWAP/R1/R2/R3)*: the climate zone in question is tested for statistical difference in correlation coefficients from the same climate zone in AWAP/R1/R2/R3. Statistically significantly different correlation coefficients ($p \leq 0.05$) are presented in bold.

Table D1

ACCESS R1	Australia	*Eastern Australia*	*Equatorial*	*Tropical*	*Sub-tropical*	*Desert*	*Grass-land*	*Temp-erate*
Annual	**-0.69**	**-0.61**	**-0.46**	**-0.51**	**-0.46**	**-0.45**	**-0.54**	**-0.47**
JJA	**-0.32**	**-0.27**	**-0.28**	-0.08	-0.16	-0.12	-0.14	-0.18
SON	**-0.60**	**-0.53**	**-0.30**	**-0.39**	**-0.39**	**-0.45**	**-0.51**	**-0.33**
DJF	**-0.54**	**-0.44**	**-0.33**	**-0.38**	**-0.33**	**-0.26**	**-0.34**	**-0.26**
MAM	**-0.38**	**-0.35**	**-0.23**	**-0.25**	**-0.25**	**-0.24**	**-0.26**	-0.16
June	**-0.20**	**-0.23**	**-0.20**	-0.16	-0.07	-0.13	-0.12	-0.09
July	**-0.28**	**-0.23**	**-0.25**	-0.01	-0.14	-0.07	-0.12	-0.16
August	**-0.26**	-0.10	-0.15	0.06	-0.06	-0.08	-0.08	-0.05
September	**-0.46**	**-0.33**	-0.11	-0.08	**-0.25**	**-0.32**	**-0.38**	**-0.22**
October	**-0.47**	**-0.40**	**-0.22**	**-0.32**	**-0.22**	**-0.28**	**-0.33**	**-0.21**
November	**-0.44**	**-0.38**	**-0.33**	**-0.33**	**-0.24**	**-0.23**	**-0.33**	-0.17
December	**-0.37**	**-0.30**	**-0.31**	**-0.34**	-0.09	0.05	0.00	-0.14
January	**-0.52**	**-0.37**	**-0.24**	**-0.23**	**-0.30**	**-0.25**	**-0.32**	-0.17
February	**-0.32**	**-0.36**	-0.14	**-0.28**	**-0.23**	**-0.24**	**-0.28**	-0.17
March	**-0.36**	**-0.24**	-0.17	-0.15	-0.18	**-0.24**	**-0.25**	-0.07
April	**-0.35**	**-0.34**	-0.12	**-0.22**	-0.18	-0.18	-0.16	**-0.27**
May	-0.15	**-0.21**	-0.14	**-0.22**	-0.17	0.04	-0.05	0.01
P-value (diff. from 'Australia'/'E. Aus.')		0.19	**0.01**	**0.03**	**0.01**	**0.01**	0.08	**0.00**
P-value (diff. from AWAP)	0.12	0.93	0.40	0.30	0.19	0.52	0.61	0.99
P-value (diff. from R2)	**0.00**	**0.00**	**0.00**	**0.00**	**0.00**	**0.00**	**0.00**	**0.00**
P-value (diff. from R3)	**0.00**	**0.00**	**0.00**	**0.00**	**0.00**	**0.00**	**0.00**	**0.00**

Table D2

ACCESS R2	Australia	*Eastern Australia*	*Equatorial*	*Tropical*	*Sub-tropical*	*Desert*	*Grass-land*	*Temp-erate*
Annual	**-0.52**	**-0.41**	**-0.24**	**-0.43**	**-0.35**	**-0.23**	**-0.38**	**-0.31**
JJA	**-0.45**	**-0.39**	-0.18	**-0.31**	**-0.25**	**-0.39**	**-0.41**	**-0.20**
SON	**-0.46**	**-0.40**	-0.14	**-0.19**	**-0.37**	**-0.36**	**-0.40**	**-0.40**
DJF	**-0.40**	**-0.28**	-0.18	**-0.35**	-0.14	-0.07	-0.17	-0.16
MAM	**-0.39**	**-0.21**	-0.14	**-0.23**	-0.06	0.00	-0.17	-0.16
June	**-0.30**	**-0.21**	-0.07	-0.16	-0.15	**-0.30**	**-0.23**	-0.10
July	**-0.31**	**-0.26**	-0.13	**-0.23**	**-0.25**	**-0.22**	**-0.29**	-0.04
August	**-0.45**	**-0.34**	**-0.20**	**-0.23**	-0.07	**-0.28**	**-0.34**	**-0.30**
September	**-0.34**	**-0.28**	-0.08	-0.07	**-0.25**	**-0.26**	**-0.32**	**-0.20**
October	**-0.39**	**-0.35**	-0.10	**-0.20**	**-0.28**	**-0.27**	**-0.26**	**-0.36**
November	**-0.30**	**-0.29**	-0.16	-0.14	**-0.22**	-0.12	**-0.28**	-0.18
December	**-0.31**	**-0.25**	-0.07	**-0.27**	**-0.21**	-0.09	-0.17	-0.11
January	**-0.25**	-0.15	-0.12	-0.16	-0.01	-0.06	-0.08	-0.14
February	**-0.31**	**-0.27**	-0.12	**-0.35**	-0.13	0.00	-0.12	-0.04
March	**-0.39**	**-0.23**	**-0.23**	**-0.23**	-0.02	0.04	-0.08	-0.06
April	**-0.26**	-0.14	0.01	-0.16	-0.11	0.05	-0.17	-0.14
May	-0.13	-0.07	-0.04	-0.04	-0.03	-0.15	-0.13	-0.07
P-value (diff. from 'Australia'/'E. Aus.')		0.98	0.63	0.75	0.84	0.10	0.10	0.32
P-value (diff. from AWAP)	**0.00**	**0.00**	**0.00**	**0.00**	**0.00**	**0.00**	**0.00**	**0.00**
P-value (diff. from R1)	**0.00**	**0.00**	**0.00**	**0.00**	**0.00**	**0.00**	**0.00**	**0.00**
P-value (diff. from R3)	0.28	0.27	0.07	0.99	0.68	**0.05**	**0.02**	0.85

Table D3

ACCESS R3	Australia	*Eastern Australia*	*Equatorial*	*Tropical*	*Sub-tropical*	*Desert*	*Grass-land*	*Temp-erate*
Annual	**-0.68**	**-0.57**	**-0.52**	**-0.53**	**-0.41**	**-0.38**	**-0.40**	**-0.34**
JJA	**-0.48**	**-0.43**	-0.16	**-0.25**	**-0.35**	**-0.27**	**-0.32**	**-0.35**
SON	**-0.49**	**-0.52**	**-0.27**	**-0.42**	**-0.40**	**-0.34**	**-0.44**	**-0.40**
DJF	**-0.49**	**-0.34**	**-0.32**	**-0.35**	**-0.19**	-0.19	-0.19	-0.06
MAM	**-0.50**	**-0.36**	**-0.24**	**-0.32**	**-0.26**	**-0.21**	-0.19	-0.11
June	**-0.33**	**-0.28**	-0.12	**-0.24**	**-0.23**	-0.19	**-0.24**	-0.10
July	**-0.53**	**-0.43**	-0.08	**-0.19**	**-0.31**	**-0.30**	**-0.35**	**-0.38**
August	**-0.20**	-0.16	-0.17	0.00	-0.09	0.00	-0.02	**-0.20**
September	**-0.43**	**-0.40**	-0.14	**-0.23**	**-0.35**	**-0.40**	**-0.42**	-0.19
October	**-0.38**	**-0.42**	**-0.28**	**-0.33**	**-0.33**	-0.19	**-0.26**	**-0.25**
November	**-0.35**	**-0.32**	**-0.21**	**-0.35**	-0.11	-0.17	**-0.25**	**-0.24**
December	**-0.33**	**-0.25**	**-0.23**	**-0.31**	-0.12	-0.07	-0.13	-0.07
January	**-0.50**	**-0.31**	-0.18	**-0.32**	-0.18	**-0.27**	**-0.24**	-0.08
February	-0.16	-0.19	**-0.22**	-0.17	-0.07	0.02	0.04	0.01
March	**-0.33**	**-0.24**	-0.08	-0.14	**-0.25**	-0.15	-0.12	-0.13
April	**-0.32**	-0.15	-0.02	**-0.19**	-0.10	-0.12	-0.15	-0.03
May	**-0.38**	**-0.38**	**-0.33**	**-0.36**	**-0.20**	-0.05	0.00	-0.04
P-value (diff. from 'Australia'/'E. Aus.')		0.94	0.58	0.49	0.34	0.36	0.80	**0.03**
P-value (diff. from AWAP)	**0.00**	**0.00**	**0.00**	**0.00**	**0.00**	**0.00**	**0.00**	**0.00**
P-value (diff. from R1)	**0.00**	**0.00**	**0.00**	**0.00**	**0.00**	**0.00**	**0.00**	**0.00**
P-value (diff. from R2)	0.28	0.27	0.07	0.99	0.68	**0.05**	**0.02**	0.85

Table E: This table shows the number of years in the study period (maximum = 105) that are classed as ENSO positive, neutral and negative phases, and IPO positive, neutral and negative phases. Results are presented for simulations (HadISST) and for the three ensemble members of ACCESS1.3 (ACCESS R1, ACCESS R2, and ACCESS R3). Phases are defined as normal (i.e. Trenberth (1997) and Henley *et al.* (2015)), as well as ±2σ and ±3σ, where phases are stratified ±2σ and ±3σ above the respective index means). Only annual results are presented here; seasonal and monthly values are also viewable in the electronic appendix.

	Normal				**±2σ**				**±3σ**			
	HadISST	***ACCESS R1***	***ACCESS R2***	***ACCESS R3***	***HadISST***	***ACCESS R1***	***ACCESS R2***	***ACCESS R3***	***HadISST***	***ACCESS R1***	***ACCESS R2***	***ACCESS R3***
ENSO positive	28	34	27	31	2	2	1	3	0	1	0	0
ENSO neutral	46	48	52	44	101	100	99	102	105	104	105	105
ENSO negative	31	23	26	30	2	3	5	0	0	0	0	0
IPO positive	62	13	17	32	4	0	0	2	2	0	0	0
IPO neutral	21	27	28	26	101	96	99	102	103	105	105	105
IPO negative	22	65	60	47	0	9	6	1	0	0	0	0

Table F: These tables show correlation coefficients (*r*) for the relationship between the TPI and rainfall, for ACCESS1.3 historical experiment ensemble members (observations are shown in Table A2). All correlation coefficients shown in boldface are significant (at the 95 per cent level). *P-value (diff. from 'Australia'/'E. Aus')*: eastern Australian correlation coefficients are tested for differences from those of Australia, and the various climate zones are tested for differences from eastern Australia. *P-value (diff. from AWAP/R1/R2/R3)*: the climate zone in question is tested for statistical difference in correlation coefficients from the same climate zone in AWAP/R1/R2/R3. Statistically significantly different correlation coefficients ($p \leq 0.05$) are presented in bold.

Table F1

ACCESS R1	Australia	*Eastern Australia*	*Equatorial*	*Tropical*	*Sub-tropical*	*Desert*	*Grass-land*	*Temp-erate*
Annual	**-0.20**	**-0.23**	**-0.36**	**-0.20**	-0.01	-0.06	-0.08	-0.17
JJA	-0.13	-0.12	-0.18	0.13	0.06	-0.02	-0.01	**-0.30**
SON	-0.14	-0.14	**-0.34**	-0.06	0.08	0.00	-0.01	-0.07
DJF	**-0.23**	**-0.23**	-0.18	**-0.27**	-0.13	-0.06	-0.15	-0.09
MAM	-0.06	-0.16	**-0.34**	-0.13	0.05	-0.03	0.04	0.04
June	0.04	-0.02	-0.05	0.13	0.10	0.01	0.03	**-0.22**
July	-0.13	-0.08	**-0.21**	0.09	0.03	0.00	-0.02	-0.11
August	**-0.28**	-0.19	**-0.26**	0.00	-0.02	-0.04	-0.02	**-0.25**
September	-0.01	0.04	**-0.32**	-0.03	**0.19**	0.09	0.12	0.04
October	-0.17	-0.18	**-0.28**	-0.08	-0.04	-0.08	-0.08	-0.01
November	-0.15	-0.13	**-0.21**	0.00	0.02	-0.04	-0.08	-0.15
December	-0.14	**-0.24**	**-0.25**	-0.17	-0.05	-0.01	-0.08	-0.18
January	-0.15	-0.16	-0.09	-0.15	-0.11	-0.07	-0.15	-0.07
February	**-0.23**	-0.18	-0.07	**-0.25**	-0.10	-0.04	-0.08	0.05
March	-0.13	-0.18	**-0.23**	-0.16	-0.10	-0.04	-0.03	0.05
April	-0.05	-0.18	**-0.30**	-0.14	0.07	0.00	0.15	0.00
May	0.08	0.05	-0.12	0.16	0.14	-0.01	-0.06	0.05
P-value (diff. from 'Australia'/'E. Aus.')		0.63	**0.01**	0.07	**0.00**	**0.00**	**0.00**	0.11
P-value (diff. from AWAP)	0.41	0.61	**0.00**	0.40	**0.00**	**0.00**	**0.01**	0.61
P-value (diff. from R2)	**0.00**	**0.00**	**0.00**	**0.00**	0.24	0.11	**0.01**	**0.00**
P-value (diff. from R3)	**0.00**	**0.00**	**0.00**	**0.01**	0.12	**0.03**	0.10	0.14

Table F2

ACCESS R2	Australia	*Eastern Australia*	*Equatorial*	*Tropical*	*Sub-tropical*	*Desert*	*Grass-land*	*Temp-erate*
Annual	-0.06	-0.13	-0.07	-0.08	-0.13	-0.15	-0.16	-0.16
JJA	-0.02	-0.08	0.02	-0.02	-0.09	-0.04	-0.07	-0.11
SON	**-0.23**	**-0.25**	**-0.21**	-0.13	-0.17	**-0.25**	**-0.24**	-0.17
DJF	-0.10	-0.07	-0.04	-0.05	-0.01	-0.07	-0.09	-0.15
MAM	0.06	-0.05	-0.02	-0.05	-0.09	-0.04	-0.05	0.06
June	0.02	-0.05	-0.01	0.02	-0.10	-0.01	-0.03	-0.01
July	0.02	-0.05	0.06	-0.03	-0.10	0.09	-0.01	-0.08
August	-0.12	-0.07	-0.03	-0.05	0.07	-0.14	-0.09	-0.15
September	**-0.23**	**-0.23**	-0.04	-0.10	**-0.23**	**-0.19**	**-0.25**	-0.15
October	-0.19	-0.18	**-0.19**	-0.10	-0.10	**-0.20**	-0.16	-0.06
November	-0.10	-0.15	**-0.23**	-0.08	0.01	-0.08	-0.06	-0.11
December	-0.10	-0.11	-0.14	-0.14	-0.05	0.10	0.05	-0.04
January	-0.03	-0.02	-0.02	0.00	0.05	-0.03	-0.01	-0.11
February	-0.10	-0.07	0.03	-0.04	-0.04	-0.15	-0.16	-0.14
March	-0.08	-0.08	-0.03	-0.11	-0.08	-0.09	-0.09	0.11
April	0.12	-0.01	0.03	-0.02	-0.10	0.03	0.01	0.05
May	0.11	-0.01	-0.05	0.11	0.00	0.01	0.00	-0.06
P-value (diff. from 'Australia'/'E. Aus.')		0.34	0.66	0.94	0.49	0.09	0.55	0.16
P-value (diff. from AWAP)	**0.00**	**0.00**	**0.00**	**0.00**	**0.00**	**0.00**	**0.00**	**0.00**
P-value (diff. from R1)	**0.00**	**0.00**	**0.00**	**0.00**	0.24	0.11	**0.01**	**0.00**
P-value (diff. from R3)	0.33	0.23	0.21	0.36	**0.00**	0.64	0.31	**0.05**

Table F3

ACCESS R3	Australia	*Eastern Australia*	*Equator-ial*	*Tropical*	*Sub-tropical*	*Desert*	*Grass-land*	*Temp-erate*
Annual	-0.14	-0.16	**-0.35**	-0.14	-0.03	0.01	0.00	-0.06
JJA	-0.18	-0.18	**-0.27**	0.02	-0.02	-0.04	-0.07	-0.19
SON	**-0.27**	**-0.33**	**-0.35**	-0.19	-0.16	**-0.20**	**-0.24**	**-0.22**
DJF	-0.09	-0.09	**-0.26**	-0.16	0.05	0.04	0.06	0.12
MAM	0.02	-0.01	-0.06	-0.02	-0.02	0.16	0.18	0.03
June	-0.11	-0.08	-0.18	-0.02	0.04	-0.08	-0.05	0.00
July	**-0.25**	-0.16	**-0.24**	0.04	0.02	-0.07	-0.12	**-0.26**
August	-0.04	-0.13	**-0.20**	0.04	-0.10	0.07	0.02	-0.11
September	**-0.24**	**-0.30**	-0.17	-0.11	**-0.26**	**-0.19**	**-0.26**	-0.14
October	-0.19	**-0.21**	**-0.33**	-0.18	-0.08	-0.15	-0.11	-0.06
November	**-0.22**	**-0.23**	**-0.30**	-0.13	0.00	-0.10	-0.15	-0.19
December	0.03	-0.02	-0.15	-0.13	0.12	0.02	0.03	0.06
January	-0.14	-0.10	**-0.22**	-0.18	0.05	-0.06	0.03	0.08
February	-0.04	-0.08	-0.15	-0.08	-0.04	0.11	0.05	0.09
March	0.04	0.02	-0.06	0.06	0.01	0.05	0.12	0.00
April	0.10	0.12	0.01	-0.04	0.10	**0.22**	0.18	**0.22**
May	-0.11	-0.18	-0.05	-0.13	-0.18	0.00	-0.02	**-0.19**
P-value (diff. from 'Australia'/'E. Aus.')		0.22	**0.03**	0.72	**0.03**	0.94	0.74	**0.04**
P-value (diff. from AWAP)	**0.00**	**0.00**	**0.00**	**0.00**	**0.00**	**0.00**	**0.00**	**0.00**
P-value (diff. from R1)	**0.00**	**0.00**	**0.00**	**0.01**	0.12	**0.03**	0.10	0.14
P-value (diff. from R2)	0.33	0.23	0.21	0.36	**0.00**	0.64	0.31	**0.05**

References

Alexander, L. V., Hope, P., Collins, D., Trewin, B., Lynch, A., and Nicholls, N. 2007. Trends in Australia's climate means and extremes: a global context. *Australian Meteorological Magazine*, 56(1), 1–18.

Alexander, L.V. and Arblaster, J.M., 2009. Assessing trends in observed and modelled climate extremes over Australia in relation to future projections. *International Journal of Climatology*, 29(3), 417–35.

Allan, R.J., Reason, C. J. C., Lindesay, J. A., and Ansell, T. J., 2003. "Protracted" ENSO episodes and their impacts in the Indian Ocean region. *Deep Sea Research Part II: Topical Studies in Oceanography*, 50(12-13), 2331–2347.

Arblaster, J., Meehl, G. and Moore, A., 2002. Interdecadal modulation of Australian rainfall. *Climate Dynamics*, 18(6), 519–531.

Ashok, K., Guan, Z. and Yamagata, T., 2003. Influence of the Indian Ocean Dipole on the Australian winter rainfall. *Geophysical Research Letters*, 30(15), 3–6.

Australian Bureau of Meteorology, 2010. *Australian climate influences*. Available at: http://www.bom.gov.au/watl/about-weather-and-climate/australian-climate-influences.shtml [Accessed October 29, 2015].

Bi, D., Dix, M., Marsland, S. J., O'Farrell, S., Rashid, H. A., Uotila, P., Hirst, A. C., Kowalczyk, E., Golebiewski, M., Sullivan, A., Yan, H., Hannah, N., Franklin, C., Sun, Z., Vohralik, P., Watterson, I., Zhou, X., Fiedler, R., Collier, M., Ma, Y., Noonan, J., Stevens, L., Uhe, P., Zhu, H., Griffies, S. M., Hill, R., Harris, C. and Puri, K., 2013. The ACCESS coupled model: description, control climate and evaluation. *Australian Meteorological and Oceanographic Journal*, 63(1), 41–64.

Brown, J.N., McIntosh, P. C., Pook, Michael J., Risbey, J. S., 2009. An Investigation of the Links between ENSO Flavors and Rainfall Processes in Southeastern Australia. *Monthly Weather Review*, 137(11), 3786–3795.

Brown, J.R., Jakob, C. and Haynes, J.M., 2010. An evaluation of rainfall frequency and intensity over the Australian region in a global climate model. *Journal of Climate*, 23(24), 6504–6525.

Brown, J.R., Moise, A.F. and Colman, R. A., 2013. The South Pacific Convergence Zone in CMIP5 simulations of historical and future climate. *Climate Dynamics*, 41(7), 2179–2197.

Cai, W., van Rensch, P., Cowan, T., Hendon, H. H., 2012. An Asymmetry in the IOD and ENSO Teleconnection Pathway and Its Impact on Australian Climate. *Journal of Climate*, 25(18), pp.6318–6329.

Cai, W. *et al.*, van Rensch, P., Cowan, T., Sullivan, A., 2010. Asymmetry in ENSO teleconnection with regional rainfall, its multidecadal variability, and impact. *Journal of Climate*, 23(18), 4944–4955.

Cai, W., Borlace, S., Lengaigne, M., van Rensch, P., Collins, M., Vecchi, G., Timmermann, A., Santoso, A., McPhaden, M. J., Wu, L., England, M. H., Wang, G., Guilyardi, E., Jin, F., 2014. Increasing frequency of extreme El Niño events due to greenhouse warming. *Nature Climate Change*, 5(1), 1–6.

Cai, W., Collier, Mark A., Gordon, H. B., Waterman, L. J., 2003. Strong ENSO Variability and a Super-ENSO Pair in the CSIRO Mark 3 Coupled Climate Model. *Monthly Weather Review*, 131(7), 1189–1210.

Cai, W. and Cowan, T., 2013. Southeast Australia autumn rainfall reduction: A climate-change-induced poleward shift of ocean-atmosphere circulation. *Journal of Climate*, 26(1), 189–205.

Cai, W. and van Rensch, P., 2012. The 2011 southeast Queensland extreme summer rainfall: A confirmation of a negative Pacific Decadal Oscillation phase? *Geophysical Research Letters*, 39(8), 1–6.

Cai, W., Sullivan, A. and Cowan, T., 2009. Rainfall teleconnections with Indo-Pacific variability in the WCRP CMIP3 models. *Journal of Climate*, 22(19), 5046–5071.

Chakraborty, A. and Krishnamurti, T.N., 2003. A coupled model study on ENSO, MJO and Indian summer monsoon rainfall relationships. *Meteorology and Atmospheric Physics*, 84(3-4), 243–254.

Chen, H., Sun, J. and Chen, X., 2014. Projection and uncertainty analysis of global precipitation-related extremes using CMIP5 models. *International Journal of Climatology*, 34(8), 2730–2748.

Collier, M. and Uhe, P., 2012. *CMIP5 datasets from the ACCESS1.0 and ACCESS1.3 coupled climate models*, CAWCR Technical Report No. 059, CSIRO and the Bureau of Meteorology.

Conrad, V., 1941. The Variability of Precipitation. *Monthly Weather Review*, 69(1), 5–11.

Contractor, S., Alexander, L. V., Donat, M. G., Herold, N., 2015. How Well Do Gridded Datasets of Observed Daily Precipitation Compare over Australia? *Advances in Meteorology*, 2015, 1–15.

CSIRO, 2014. *CSIRO-Mk3.6.0*. Available at: https://wiki.csiro.au/display/CSIROMk360/Home [Accessed October 30, 2015].

Dai, A., 2013. The influence of the inter-decadal Pacific oscillation on US precipitation during 1923–2010. *Climate Dynamics*, 41(3), 633–646.

Davidson, B.R., 1969. *Australia wet or dry? The physical and economic limits to the expansion of irrigation*, Carlton, Melbourne: Melbourne University Press.

Dix, M., Vohralik, P., Bi, D., Rashid, H., Marsland, S., O'Farrell, S., Uotila, P., Hirst, T., Kowalczyk, E., Sullivan, A., Yan, H., Franklin, C., Sun, Z., Watterson, I., Collier, M., Noonan, J., Rotstayn, L., Stevens, L., Uhe, P., Puri, K., 2013. The ACCESS coupled model: documentation of core CMIP5 simulations and initial results. *Australian Meteorological and Oceanographic Journal*, 63(1), pp.83–99.

Dong, B. and Dai, A., 2015. The influence of the Interdecadal Pacific Oscillation on Temperature and Precipitation over the Globe. *Climate Dynamics*, 45(9), 2667–2681.

Eden, J.M., Widmann, M., Grawe, D., Rast, S., 2012. Skill, correction, and downscaling of GCM-simulated precipitation. *Journal of Climate*, 25(11), 3970–3984.

Folland, C.K., 2002. Relative influences of the Interdecadal Pacific Oscillation and ENSO on the South Pacific Convergence Zone. *Geophysical Research Letters*, 29(13), 2–5.

Franklin, C.N., Sun, Z., Bi, D., Dix, M., Yan, H., Bodas-Salcedo, A., 2013. Evaluation of clouds in ACCESS using the satellite simulator package COSP: Global, seasonal, and regional cloud properties. *Journal of Geophysical Research: Atmospheres*, 118(2), 732–748.

Gallant, A.J.E., Hennessy, K.J. and Risbey, J.S., 2007. Trends in rainfall indices for six Australian regions : 1910-2005. *Australian Meteorolgical Magazine*, 56(4), 223–239.

Hall, A. and Visbeck, M., 2002. Synchronous variability in the Southern Hemisphere atmosphere, sea ice, and ocean resulting from the annular mode. *Journal of Climate*, 15(21), 3043–3057.

Hanson, C.E., Palutikof, J. P., Livermore, M. T. J., Barring, L., Bindi, M., Corte-Real, J., Durao, R., Giannakopoulos, C., Good, P., Holt, T., Kundzewicz, Z., Leckebusch, G. C., Moriondo, M., Radziejewski, M., Santos, J., Schlyter, P., Schwarb, M., Stjernquist, I., Ulbrich, U., 2007. Modelling the impact of climate extremes: An overview of the MICE project. *Climatic Change*, 81, 163–177.

Hastings, P.A., 1990. Southern Oscillation influences on tropical cyclone activity in the Australian/south-west Pacific region. *International Journal of Climatology*, 10(3), 291–298.

Haylock, M. and Nicholls, N., 2000. Trends in extreme rainfall indices for an updated high quality data set for Australia, 1910-1998. *International Journal of Climatology*, 20(13), 1533–1541.

Hendon, H.H., Thompson, D.W.J. and Wheeler, M.C., 2007. Australian rainfall and surface temperature variations associated with the Southern Hemisphere annular mode. *Journal of Climate*, 20(11), 2452–2467.

Hendon, H.H., Wheeler, M.C. and Zhang, C., 2007. Seasonal dependence of the MJO-ENSO relationship. *Journal of Climate*, 20(3), 531–543.

Henley, B.J., Gergis, J., Karoly, D. J., Power, S., Kennedy, J., Folland, C. K., 2015. A Tripole Index for the Interdecadal Pacific Oscillation. *Climate Dynamics*. Available at: http://link.springer.com/10.1007/s00382-015-2525-1.

Hennessy, K.J., Suppiah, R. and Page, C.M., 1999. Australian rainfall changes, 1910-1995. *Australian Meteorological Magazine*, 48(1), 1–13.

Hirsch, A.L., 2010. *Australian Precipitation from Models and Observations*. Honours thesis, Australian National University, Canberra.

Hutchinson, M.F., 1995. Interpolating mean rainfall using thin plate smoothing splines. *International Journal of Geographical Information Systems*, 9(4), 385–403.

IPCC, 2014. Summary for Policy Makers. Field, C. B., Barros, V. R., Dokken, D. J., Mach, K. J., Mastrandrea, M. D., Bilir, T. E., Chatterjee, M., Ebi, K. L., Otsuki Estrada, Y., Genova, R. C., Girma, B., Kissel, E. S., Levy, A. N., MacCracken, S., Mastrandrea, P. R., White, L. L. (eds). *Climate Change 2014: Impacts, Adaptation and Vulnerability - Contributions of the Working Group II to the Fifth Assessment Report of the Intergovernmental Panel on Climate Change*. Cambridge, United Kingdom and New York, NY, US: Cambridge University Press.

Jeffrey, S.J., Carter, J. O., Moodie, K. B., Beswick, A. R., 2001. Using spatial interpolation to construct a comprehensive archive of Australian climate data. *Environmental Modelling and Software*, 16(4), 309–330.

Jones, D.A., Wang, W. and Fawcett, R., 2009. High-quality spatial climate data-sets for Australia. *Australian Meteorological and Oceanographic Journal*, 58(4), 233–248.

Kalnay, E., Kanamitsu, M., Kistler, R., Collins, W., Deaven, D., Gandin, L., Iredell, M., Saha, S., White, G., Woollen, J., Zhu, Y., Chelliah, M., Ebisuzaki, W., Higgins, W., Janowiak, J. E., Mo, K.C., Ropelewski, C., Wang, J., Leetmaa, A., Reynolds, R. W., Jenne, R., Joseph, D., 1996. The NCEP/NCAR 40-year reanalysis project. *Bulletin of the American Meteorological Society*, 77(3), 437–471.

Kiem, A.S. and Franks, S.W., 2004. Multi-decadal variability of drought risk, eastern Australia. *Hydrological Processes*, 18(11), 2039–2050.

Kiem, A.S. and Franks, S.W., 2001. On the identification of ENSO-induced rainfall and runoff variability: a comparison of methods and indices. *Hydrological Sciences Journal*, 46(5), 715–727.

Kiem, A.S., Franks, S.W. and Kuczera, G., 2003. Multi-decadal variability of flood risk. *Geophysical Research Letters*, 30(2), 1–4.

Kiem, A.S. and Verdon-Kidd, D.C., 2009. Climatic drivers of Victorian streamflow: Is ENSO the dominant influence? *Australian Journal of Water Resources*, 13(1), 17–29.

Kim, W. and Cai, W., 2006. Second peak in the far eastern Pacific sea surface temperature anomaly following strong El Niño events. *Journal of Climate*, 19(12), 2633–2646.

King, A.D., Alexander, L. V. and Donat, M.G., 2013a. Asymmetry in the response of eastern Australia extreme rainfall to low-frequency Pacific variability. *Geophysical Research Letters*, 40(10), 2271–2277.

King, A.D., Alexander, L. V. and Donat, M.G., 2013b. The efficacy of using gridded data to examine extreme rainfall characteristics: A case study for Australia. *International Journal of Climatology*, 33(10), 2376–2387.

Klingaman, N.P., Woolnough, S.J. and Syktus, J., 2013. On the drivers of inter-annual and decadal rainfall variability in Queensland, Australia. *International Journal of Climatology*, 33(10), 2413–2430.

Koch, S.E., Desjardins, M. and Kocin, P.J., 1983. An interactive Barnes objective map analysis scheme for use with satellite and conventional data. *Journal of Climate and Applied Meteorology*, 22(9), 1487–1503.

Köppen, W., 1923. *Die Klimate der Erde: Grundriss der Klimakunde*, Walter de Gruyter and Company.

Krishnamurti, T.N., Stefanova, L. and Misra, V., 2013. Madden Julian Oscillation. In *Tropical Meteorology*. Springer, New York, pp. 143–168.

Kuleshov, Y., Ming, F.C. and Qi, L., 2009. Tropical cyclone genesis in the Southern Hemisphere and its relationship with the ENSO. *Annales Geophysicae*, 27(6), 2523–2538.

Latif, M., Kleeman, R. and Eckert, C., 1997. Greenhouse warming, decadal variability, or El Niño? An attempt to understand the anomalous 1990s. *Journal of Climate*, 10(9), 2221–2239.

Lejenäs, H. and Økland, H., 1983. Characteristics of northern hemisphere blocking as determined from a long time series of observational data. *Tellus A*, 35A(5), 967–979.

Lewis, S.C. and Karoly, D.J., 2014. Assessment of forced responses of the Australian Community Climate and Earth System Simulator (ACCESS) 1.3 in CMIP5 historical detection and attribution experiments. *Australian Meteorological and Oceanographic Journal*, 64(2), 87–101.

Limpasuvan, V. and Hartmann, D.L., 2000. Wave-maintained annular modes of climate variability. *Journal of Climate*, 13(24), 4414–4429.

Madden, R.A. and Julian, P.R., 1971. Detection of a 40–50 Day Oscillation in the Zonal Wind in the Tropical Pacific. *Journal of the Atmospheric Sciences*, 28(5), 702–708.

Madden, R.A. and Julian, P.R., 1994. Observations of the 40–50-Day Tropical Oscillation—A Review. *Monthly Weather Review*, 122(5), 814–837.

Mantua, N.J., Hare, S. R., Zhang, Y., Wallace, J. M., Francis, R. C., 1997. A Pacific Interdecadal Climate Oscillation with Impacts on Salmon Production. *Bulletin of the American Meteorological Society*, 78(6), 1069–1079.

Marsland, S.J., Bi, D., Uotila, P., Fiedler, R., Griffies, S. M., Lorbacher, K., O'Farrell, S., Sullivan, A., Uhe, P., Zhou, X., Hirst, A. C., 2013. Evaluation of ACCESS Climate Model Ocean Diagnostics in CMIP5 Simulations. *Australian Meteorological and Oceanographic Journal*, 63(1), 101–119.

Matthews, A.J. and Meredith, M.P., 2004. Variability of Antarctic circumpolar transport and the Southern Annular Mode associated with the Madden-Julian Oscillation. *Geophysical Research Letters*, 31(24), 1–5.

McBride, J.L. and Nicholls, N., 1983. Seasonal Relationships between Australian Rainfall and the Southern Oscillation. *Monthly Weather Review*, 111(10), 1998–2004.

McMahon, T. A, Peel, M.C. and Karoly, D.J., 2015. Assessment of precipitation and temperature data from CMIP3 global climate models for hydrologic simulation. *Hydrology and Earth System Sciences*, 19(1), 361–377.

McPhaden, M.J., 1999. Genesis and Evolution of the 1997–98 El Niño. *Science*, 283(5404), 950–954.

Meehl, G. A. and Hu, A., 2006. Megadroughts in the Indian monsoon region and southwest North America and a mechanism for associated multidecadal Pacific Sea surface temperature anomalies. *Journal of Climate*, 19(9), 1605–1623.

Meinke, H., DeVoil, P., Hammer, G. L., Power, S., Allan, R., Stone, R. C., Folland, C., Potgieter, A., 2005. Rainfall variability of decadal and longer time scales: signal or noise? *Journal of Climate*, 18(1), 89–96.

Mekanik, F. and Imteaz, M.A., 2012. Forecasting Victorian spring rainfall using ENSO and IOD: A comparison of linear multiple regression and nonlinear ANN. IEEE, *Proceedings of the 2012 International Conference on Uncertainty Reasoning and Knowledge Engineering, URKE 2012*. 86–89.

Meneghini, B., Simmonds, I. and Smith, I.N., 2007. Association between Australian rainfall and the Southern Annular Mode. *International Journal of Climatology*, 27(1), 109–121.

Meyers, G., McIntosh, P., Pigot, L., Pook, M., 2007. The Years of El Niño, La Niña, and Interactions with the Tropical Indian Ocean. *Journal of Climate*, 20(13), 2872–2880.

Min, S., Cai, W. and Whetton, P., 2013. Influence of climate variability on seasonal extremes over Australia. *Journal of Geophysical Research: Atmospheres*, 118(2), 643–654.

Murphy, B.F. and Timbal, B., 2008. A review of recent climate variability and climate change in southeastern Australia. *International Journal of Climatology*, 28(7), 859–879.

Murray–Darling Basin Authority, 2010. *Guide to the proposed Basin Plan*, Canberra, Australia [electronic text]. Available at: http://www.mdba.gov.au/sites/default/files/archived/Guide-to-proposed-BP-vol2-02.pdf. [Accessed November 2, 2015].

Nakamura, N., Kayanne, H., Iijima, H., McClanahan, T. R., Behera, S. K., Yamagata, T., 2009. Mode shift in the Indian Ocean climate under global warming stress. *Geophyscal Research Letters*, 36(29).

NCAR CDC, 2012. *TNI (Trans-Niño Index) and N3.4 (Niño 3.4 Index)*. Available at: http://www.cgd.ucar.edu/cas/catalog/climind/TNI_N34/index.html#Sec5 [Accessed October 31, 2015].

Newman, M., Compo, G.P. and Alexander, M.A., 2003. ENSO-forced variability of the Pacific Decadal Oscillation. *Journal of Climate*, 16(23), 3853–3857.

Nicholls, N., 1988. El Niño–Southern Oscillation and Rainfall Variability. *Journal of Climate*, 1(4), 418–421.

Nicholls, N., 1989. Sea surface temperatures and Australian winter rainfall. *Journal of Climate*, 2(9), 965–973.

Nicholls, N., Drosdowsky, W. and Lavery, B., 1997. Australian rainfall variability and change. *Weather*, 52(3), 66–72.

Nicholls, N. and Kariko, A., 1993. East Australian rainfall events: interannual variations, trends, and relationships with the Southern Oscillation. *Journal of Climate*, 6(6), 1141–1152.

NOAA, *Equatorial Pacific Sea Surface Temperatures*. Available at: https://www.ncdc.noaa.gov/teleconnections/enso/indicators/sst.php [Accessed October 30, 2015].

NOAA, PMEL, T., *Diagrams*. Tropical Atmosphere Ocean project. Available at: http://www.pmel.noaa.gov/tao/proj_over/diagrams/index.html [Accessed October 30, 2015].

NWS CPC, 2015. *Monthly Atmospheric and SST Indices*. Available at: http://www.cpc.ncep.noaa.gov/data/indices/ [Accessed October 31, 2015].

Parker, D., Folland, C., Scaife, A., Knight, J., Colman, A., Baines, P., Dong, B., 2007. Decadal to multidecadal variability and the climate change background. *Journal of Geophysical Research: Atmospheres*, 112(D18), 1–18.

Perkins, S.E., Pitman, A. J., Holbrook, N. J., McAneney, J., 2007. Evaluation of the AR4 climate models' simulated daily maximum temperature, minimum temperature, and precipitation over Australia using probability density functions. *Journal of Climate*, 20(17), 4356–4376.

Perkins, S.E., Moise, A., Whetton, P., Katzfey, J., 2014. Regional changes of climate extremes over Australia – a comparison of regional dynamical downscaling and global climate model simulations. *International Journal of Climatology*, 34(12), pp.3456–3478.

Pielke Jr., R.A. and Landsea, C.N., 1999. La Niña, El Niño, and Atlantic Hurricane Damages in the United States. *Bulletin of the American Meteorological Society*, 80(1994), 2027–2033.

Pook, M.J., McIntosh, P.C. and Meyers, G. A., 2006. The synoptic decomposition of cool-season rainfall in the southeastern Australian cropping region. *Journal of Applied Meteorology and Climatology*, 45(8), 1156–1170.

Power, S., Casey, T., Folland, C., Colman, A., Mehta, V., 1999a. Inter-decadal modulation of the impact of ENSO on Australia. *Climate Dynamics*, 15(5), 319–324.

Power, S., Tseitkin, F., Mehta, V., Lavery, B., Torok, S., Holbrook, N., 1999b. Decadal climate variability in Australia during the twentieth century. *International Journal of Climatology*, 19(2), 169–184.

Power, S. and Colman, R., 2006. Multi-year predictability in a coupled general circulation model. *Climate Dynamics*, 26(2-3), 247–272.

Power, S.B., Haylock, M., Colman, R., Wang, X., 2006. The predictability of interdecadal changes in ENSO activity and ENSO teleconnections. *Journal of Climate*, 19(19), 4755–4771.

Puri, K., Dietachmayer, G., Steinle, P., Dix, M., Rikus, L., Logan, L., Naughton, M., Tingwell, C., Xiao, Y., Barras, V., Bermous, I., Bowen, R., Deschamps, L., Franklin, C., Fraser, J., Glowacki, T., Harris, B., Lee, J., Le, T., Roff, G., Sulaiman, A., Sims, H., Sun, X., Sun, Z., Zhu, H., Chattopadhyay, M., Engel, C., 2013. Implementation of the initial ACCESS numerical weather prediction system. *Australian Meteorological and Oceanographic Journal*, 63(2), 265–284.

Randall, D.A., Randall, D. A., Wood, R. A., Bony, S., Colman, R., Fichefet, T., Fyfe, J., Kattsov, V., Pitman, A., Shukla, J., Srinivasan, J., Stouffer, R. J., Sumi, A., Taylor, K. E., 2007. Climate Models and Their Evaluation. In S. Solomon *et al.*, eds. *Climate Change 2007: The Physical Science Basis. Contribution of Working Group I to the Fourth Assessment Report of the Intergovernmental Panel on Climate Change*. Cambridge: Cambridge University Press.

Rashid, H.A., Sullivan, A., Hirst, A. C., Bi, D., Zhou, X., Marsland, S. J., 2013. Evaluation of El Niño–Southern Oscillation in the ACCESS coupled model simulations for CMIP5. *Australian Meteorological and Oceanographic Journal*, 63(1), 161–180.

Raupach, M., Briggs, P. R., Haverd, V., King, E. A., Paget, M., Trudinger, C. M., 2012. Australian Water Availability Project. Available at: http://www.csiro.au/awap [Accessed May 19, 2012].

Raupach, M.R., Briggs, P. R., Haverd, V., King, E. A., Paget, M., Trudinger, C. M., 2009. *Australian Water Availability Project (AWAP): CSIRO Marine and Atmospheric Research Component: Final Report for Phase 3*, CAWCR Technical Report No. 013, CSIRO and the Bureau of Meteorology.

Rayner, N.A., Parker, D.E., Horton, E.B., Folland, C.K., Alexander, L.V., Rowell, D.P., Kent, E.C., Kaplan, A., 2003. Global analyses of sea surface temperature, sea ice, and night marine air temperature since the late Nineteenth Century. *Journal of Geophysical Research: Atmospheres*, 108(D14).

Reason, C.J.C., Allan, R. J., Lindesay, J. A., Ansell, T. J., 2000. ENSO and climatic signals across the Indian Ocean basin in the global context: Part I, Interannual composite patterns. *International Journal of Climatology*, 20(11), 1285–1327.

Risbey, J.S., Pook, M.J., McIntosh, P.C., Wheeler, M.C., Hendon, H. H., 2009a. On the Remote Drivers of Rainfall Variability in Australia. *Monthly Weather Review*, 137(10), 3233–3253.

Risbey, J.S., Pook, M.J., McIntosh, P.C., Ummenhofer, C.C., Meyers, G., 2009b. Characteristics and variability of synoptic features associated with cool season rainfall in southeastern Australia. *International Journal of Climatology*, 29(11), 1595–1613.

Risbey, J.S., McIntosh, P. C., Pook, M. J., Rashid, H. A., Hirst, A. C., 2011. Evaluation of rainfall drivers and teleconnections in an ACCESS AMIP run. *Australian Meteorological and Oceanographic Journal*, 61(2), 91–105.

Rocheta, E. Sugiyanto, M., Johnson, F., Evans, J., Sharma, A., 2014. How well do general circulation models represent low frequency rainfall variability? *Water Resources Research*, 50(3), 2108–2123.

Ropelewski, C.F. and Halpert, M.S., 1987. Global and Regional Scale Precipitation Patterns Associated with the El Niño/Southern Oscillation. *Monthly Weather Review*, 115(8), 1606–1626.

Rotstayn, L.D., Cai, W., Dix, M. R., Farquhar, G. D., Feng, Y., Ginoux, P., Herzog, M., Ito, A., Penner, J. E., Roderick, M. L., Wang, M., 2007. Have Australian rainfall and cloudiness increased due to the remote effects of Asian anthropogenic aerosols? *Journal of Geophysical Research: Atmospheres*, 112(12), 1–28.

Rotstayn, L.D., Collier, M. A., Dix, M. R., Feng, Y., Gordon, H. B., O'Farrell, S. P., Smith, I. N., Syktus, J., 2010. Improved simulation of Australian climate and ENSO-related rainfall variability in a global climate model with an interactive aerosol treatment. *International Journal of Climatology*, 30(7), 1067–1088.

Saji, N.H. and Vinayachandran, P.N., 1999. A dipole mode in the tropical Indian Ocean. *Nature*, 401(6751), 360–363.

Salinger, M.J., McGree, S., Beucher, F., Power, S. B., Delage, F., 2014. A new index for variations in the position of the South Pacific convergence zone 1910/11-2011/2012. *Climate Dynamics*, 43(3), 881–892.

Schneider, N. and Cornuelle, B.D., 2005. The forcing of the Pacific Decadal Oscillation. *Journal of Climate*, 18(21), 4355–4373.

Shi, G., Cai, W., Cowan, T., Ribbe, J., Rotstayn, L., Dix, M., 2008. Variability and trend of North West Australia rainfall: Observations and coupled climate modeling. *Journal of Climate*, 21(D9), 2938–2959.

Smith, I., 2004. An assessment of recent trends in Australian rainfall. *Australian Meteorological Magazine*, 53(3), 163–173.

Spencer, H. and Slingo, J.M., 2003. The simulation of peak and delayed ENSO teleconnections. *Journal of Climate*, 16(11), 1757–1774.

Sturman, A. and Tapper, N., 2009. *The Weather and Climate of Australia and New Zealand*, Second Ed., South Melbourne: Oxford University Press.

Sun, Y., Solomon, S., Dai, A., Portmann, R. W., 2006. How often does it rain? *Journal of Climate*, 19(1996), 916–934.

Suppiah, R., Hennessy, K. J., Whetton, P. H., Mcinnes, K., Macadam, I., Bathols, J., Ricketts, J., Page, C. M., 2007. Australian climate change projections derived from simulations performed for the IPCC 4th Assessment Report. *Australian Meteorolgical Magazine*, 56(3), 131–152.

Suppiah, R., 2004. Trends in the southern oscillation phenomenon and Australian rainfall and changes in their relationships. *International Journal of Climatology*, 24(3), 269–290.

Taylor, K.E., Stouffer, R.J. and Meehl, G. A., 2012. An overview of CMIP5 and the experiment design. *Bulletin of the American Meteorological Society*, 93(4), 485–498.

Tozer, C.R., 2014. *Utilising Insights into Rainfall Patterns and Climate Drivers to Inform Seasonal Rainfall Forecasting in South Australia*. PhD thesis, University of Newcastle, Australia.

Trenberth, K.E., Dai, A., Rasmussen, R. M., Parsons, D. B., 2003. The changing character of precipitation. *Bulletin of the American Meteorological Society*, 84(9), 1205–1217.

Trenberth, K.E., 1997. The Definition of El Niño. *Bulletin of the American Meteorological Society*, 78(12), 2771–2777.

Trenberth, K.E. and Hurrell, J.W., 1994. Decadal atmosphere-ocean variations in the Pacific. *Climate Dynamics*, 9(6), 303–319.

Trenberth, K.F. and Mo, K.C., 1985. Blocking in the Southern Hemisphere. *Monthly Weather Review*, 113(1), 3–21.

Vance, T.R., Roberts, J.L., Plummer, J.T., Kiem, A.S., van Ommen, T.D., 2015. Interdecadal Pacific variability and eastern Australian megadroughts over the last millennium. *Geophysical Research Letters*, 42, 129–137.

Vecchi, G. A. and Harrison, D.E., 2006. The termination of the 1997-98 El Niño. Part I: Mechanisms of oceanic change. *Journal of Climate*, 19(12), 2633–2646.

Verdon, D.C., Wyatt, A. M., Kiem, A. S., Franks, S. W., 2004. Multidecadal variability of rainfall and streamflow: Eastern Australia. *Water Resources Research*, 40(10), 1–8.

Verdon, D.C. and Franks, S.W., 2006. Long-term behaviour of ENSO: Interactions with the PDO over the past 400 years inferred from paleoclimate records. *Geophysical Research Letters*, 33(October 2005), 1–5.

von Storch, H. and Zwiers, F.W., 1999. *Statistical Analysis in Climate Research*, Cambridge: Cambridge University Press.

Wang, G. and Hendon, H.H., 2007. Sensitivity of Australian rainfall to inter-El Niño variations. *Journal of Climate*, 20(16), 4211–4226.

Webster, P.J. and Palmer, T.N., 1997. The past and the future of El Niño. *Nature*, 390, 562–564.

Westra, S., Renard, B. and Thyer, M., 2015. The ENSO–Precipitation Teleconnection and Its Modulation by the Interdecadal Pacific Oscillation. *Journal of Climate*, 28(12), 4753–4773.

Whan, K., Timbal, B. and Lindesay, J., 2014. Linear and nonlinear statistical analysis of the impact of sub-tropical ridge intensity and position on south-east Australian rainfall. *International Journal of Climatology*, 34(2), 326–342.

Wheeler, M.C., Hendon, H. H., Cleland, S., Meinke, H., Donald, A., 2009. Impacts of the Madden-Julian oscillation on Australian rainfall and circulation. *Journal of Climate*, 22(6), 1482–1498.

Wheeler, M.C. and Hendon, H.H., 2004. An All-Season Real-Time Multivariate MJO Index: Development of an Index for Monitoring and Prediction. *Monthly Weather Review*, 132(8), 1917–1932.

Williams, A.A.J. and Stone, R.C., 2009. An assessment of relationships between the Australian subtropical ridge, rainfall variability, and high-latitude circulation patterns. *International Journal of Climatology*, 29(5), 691–709.

Wilson, D.R., Bushell, A. C., Kerr-Munslow, A. M., Price, J. D., Morcrette, C. J., 2007. PC2: A prognostic cloud fraction and condensation scheme. I: Scheme description. *Quarterly Journal of the Royal Meteorological Society*, 134(637), 2093–2107.

Winderlich, S., 2010. *Kakadu National Park Landscape Symposia, Series 2007–2009*. Symposium 4: Climate change, 6–7 August 2008, Internal Report 567. Available at: http://www.environment.gov.au/system/files/resources/2d60ca79-da7a-415f-aa1c-2ef01819f630/files/ir567.pdf#page=25 [Accessed October 23, 2015].

Zhang, Y., Wallace, J.M. and Battisti, D.S., 1997. ENSO-like interdecadal variability: 1900-93. *Journal of Climate*, 10(5), 1004–1020.